

Università degli Studi di Napoli “Federico II”



Department of Pharmacy

Graduate School of Pharmaceutical Science

XXVII cycle

Angela Corvino

PhD Master Thesis

NOVEL TOOLS FOR THE ELUCIDATION OF PHYSIO-PATHOLOGICAL ROLE OF H₂S

Supervisor:

Dott.ssa Beatrice Severino

PhD Program Coordinator:

Prof.ssa Maria Valeria D'Auria

Sommario

1. Introduction	1
1.1. H₂S chemistry and biology.....	1
1.2. H₂S biosynthesis and metabolism.....	2
1.2.1. Enzymatic Production of H₂S	3
1.2.2. Non-enzymatic production of H₂S	5
1.3. Key enzymes responsible for H₂S production.....	6
1.3.1. Cystathionine beta-synthase	6
1.3.2. Cystathionine gamma-lyase	8
1.4. Biological functions of hydrogen sulfide.....	11
1.4.1. Cardiovascular system.....	12
1.4.2. Immune system and inflammation.....	13
1.4.3. Respiratory system.....	14
1.4.4. Reproductive system	15
1.4.5. Central Nervous System	16
2. Aim of project	17
3. Materials and methods	23
3.1. Chemistry	23
3.2. Experimental procedures	27
3.2.1. Cysteine surrogates: propargylamide and <i>n</i>-butylamide derivatives (Ia-IIIa and Ib-IIIb)	27
3.2.2. Synthesis of glucocorticoids-H₂S donors (FAS I-IV) ...	36

3.2.3. General procedure for the preparation of 1,2,4-thiadiazoline-3,5-diones (THIA I-VII)	39
3.3. Pharmacology	42
3.3.1. Cysteine surrogates: propargylamide and <i>n</i> -butylamide derivatives	42
3.3.2. Glucocorticoids-H ₂ S donors	45
3.3.3. 1,2,4-Thiadiazolidine-3,5-diones	46
4. Results and Discussion	48
4.1. Cysteine surrogates: propargylamide and <i>n</i> -butylamide derivatives	48
4.2. Glucocorticoids-H ₂ S donors	56
4.3. 1,2,4-Thiadiazolidine-3,5-diones	59
5. NMR-based metabolomics	65
5.1. Objectives	65
5.2. Expression and purification of recombinant CBS and CSE enzymes	65
5.2.1. Plasmids, bacterial strains and media	65
5.2.2. Bacterial expression of human CBS enzyme	65
5.2.3. Bacterial expression of human CSE enzyme	66
5.2.4. Purification of human enzymes	67
5.3. Structural characterization of recombinant enzymes	71
5.3.1. Analysis of protein secondary structure via circular dichroism (CD) measurements	71
5.3.2. UV-vis Spectroscopy Analysis of recombinant enzymes CBS and CSE	74
5.3.3. Kinetics of H ₂ S production from purified recombinant human CBS and CSE	75

5.4. Enzyme Kinetics: NMR spectroscopy	80
5.4.1. Sample preparation.....	80
5.4.2. NMR measurements	81
5.5. Results and Discussion II	82
6. Conclusion.....	98
7. Bibliografia	101

1. Introduction

Hydrogen sulfide is a chemical compound, made up of two hydrogens and one sulfide atom, hence the chemical formula H_2S . It is a colorless, flammable, water-soluble gas with the odor of rotten eggs.

The initial observations by Kimura's group suggesting hydrogen sulfide is a biologically relevant signaling molecule have been followed by a myriad of studies demonstrating some effect of this gas on virtually every organ system and tissue. Growing evidence has shown that in addition to nitric oxide (NO) and carbon monoxide (CO), H_2S is a third gasotransmitter (Wang, 2002).

Hydrogen sulfide is now recognized as a ubiquitous gaseous signaling molecule that plays important and different roles in the endocrine, neuronal and cardiovascular system (Szabo, 2007).

1.1. H_2S chemistry and biology

Hydrogen sulfide is a gas with a structure very similar to that of water, but this is where the similarity ends (**Figure 1**). The sulfur atom is not nearly as electronegative as oxygen so that hydrogen sulfide is much less polar than water.



Figure 1 - Similarity in molecular structure between water (H_2O) and hydrogen sulfide (H_2S)

Because of this, comparatively weak intermolecular forces exist for H₂S and the melting and boiling points are much lower than they are in water. The boiling temperatures of hydrogen sulfide and water are -60.7 and +100.0 °C, respectively (Caliendo, 2010).

Hydrogen sulfide is weakly acidic, dissociating in aqueous solution into hydronium cation (H₃O⁺) and hydrosulfide anion (HS⁻), which subsequently may decompose to H₃O⁺ and sulfide ion (S²⁻) (K_{a1}=1.3 x 10⁻⁷M, K_{a2}=1 x 10⁻¹⁹M).

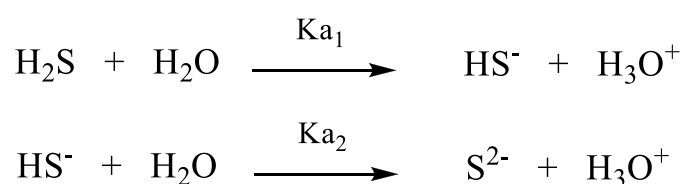


Figure 2- Chemical equilibrium of H₂S in water

Under physiological conditions, i.e., at pH 7.4, one-third of hydrogen sulfide is undissociated and present in biological fluids as H₂S.

1.2. H₂S biosynthesis and metabolism

In mammalian systems, H₂S may be produced by two pyridoxal-5'-phosphate (PLP)-dependent enzymes (vitamin B₆), cystathionine β-synthase (CBS, EC 4.2.1.22) and cystathionine γ-lyase (CSE aka CGL, EC 4.4.1.1), as well as cysteine aminotransferase (CAT, EC 2.6.1.3) and 3-mercaptopyruvate sulfurtransferase (3-MST, EC 2.8.1.2).

These enzymes are involved in transsulfuration and reverse transsulfuration pathways in different capacities and utilize specific substrates (**Figure 3**).

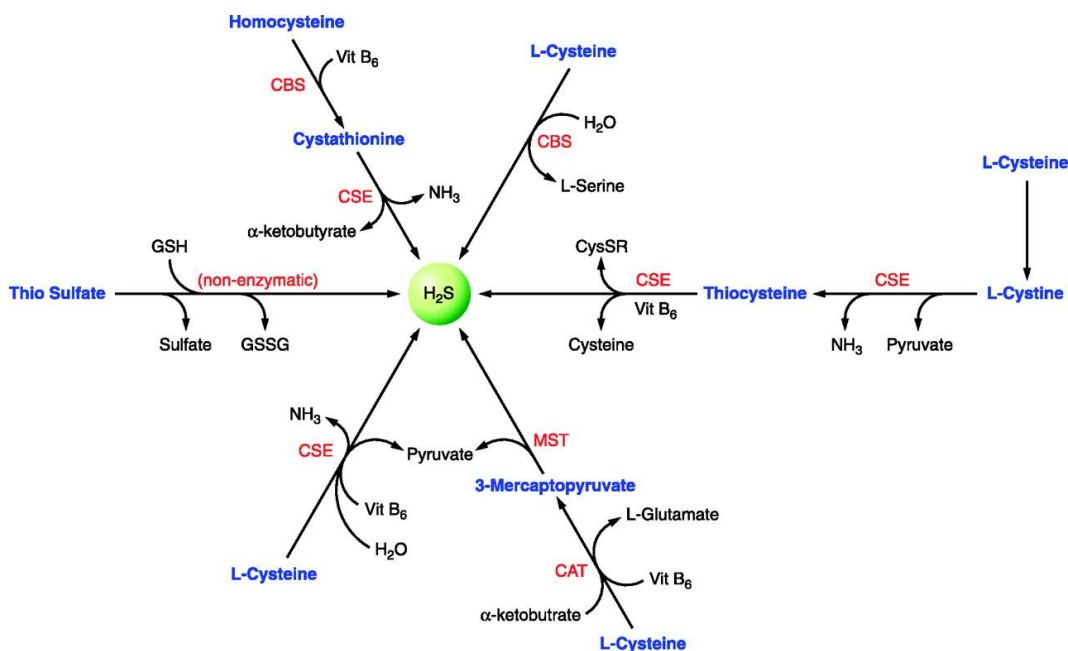


Figure 3 - Biosynthesis and transformation of H₂S in mammalian cells. CBS, cystathionine β-synthase; CSE, cystathionine γ-lyase; CAT, cysteine aminotransferase; MST, 3-mercaptopyruvate sulfurtransferase.

1.2.1. Enzymatic Production of H₂S

Initially CBS and CSE catalysed reactions were thought to be the primary pathways for H₂S production. CBS catalyzes the β-replacement reaction of homocysteine with serine to form cystathionine, thereby irreversibly committing this reaction into the transsulfuration pathway (Stipanuk, 2004).

CSE then catalyzes the α,γ-elimination of cystathionine to form cysteine, α-ketobutyrate and NH₃. Both CBS and CSE can then generate H₂S from cysteine via β-elimination reactions (Singh, 2009).

A combination of homocysteine and cysteine constitutes the optimal substrate for CBS, generating cystathionine and H₂S (**Figure 3**).

Furthermore, CSE is capable of using L-cysteine as the substrate to form two gases, H₂S and NH₃ and pyruvate. The involvement of CSE in other elimination reactions includes the catalysis of L-homoserine to form H₂O, NH₃, and 2-oxobutanoate and that of L-cystine to form thiocysteine, pyruvate, and NH₃.

CAT transfers the amine group from cysteine to a keto acid, typically α -ketoglutarate, forming 3-mercaptopyruvate. Subsequent desulfuration of 3-mercaptopyruvate by 3-MST forms the persulfide, 3-MST-SSH. MST would then transfer the sulfur from 3-mercaptopyruvate to sulfite or other sulfur acceptors or form elemental sulfur. The direct outcome of the CAT-MST pathway is the production of sulfane sulfur (or bound sulfur), not the free form of H₂S. H₂S would be consequently formed either through reduction of the atomic sulfur or released from thiosulfate or persulfides.

The former requires the presence of reductants (Kabil, 2010) and the latter, specific enzymes such as thiosulfate sulphur transferase or thiosulfate reductase (Stipanuk, 1982).

CBS and CSE are cytosolic enzymes. CBS was originally considered to be the predominant enzyme for H₂S production in the brain, whereas H₂S synthesis in the heart and vasculature was attributed to CSE (Kimura, 2011).

Recent studies with improved markers have provided a broader picture of enzyme distribution, e.g., CBS in vascular endothelium, CAT and 3-MST in vascular endothelium and brain and MST, but not CAT, in vascular smooth muscle (Olson, 2010). CAT and 3-MST have been found in both mitochondria and cytosol (Kamoun, 2004), although 3-MST may be more localized to the mitochondrial matrix (Mikami, 2011).

The most commonly used agents to inhibit H₂S biosynthesis include propargylglycine (PGG), β-cyanoalanine (BCA), aminooxyacetic acid (AOAA), trifluoroalanine and hydroxylamine (HA) (Szabo, 2007; Whiteman et al., 2011). PGG and BCA are claimed to be specific inhibitors of CSE, while AOAA is often used as a selective CBS inhibitor.

1.2.2. Non-enzymatic production of H₂S

A minor endogenous source of H₂S is the non-enzymatic reduction of elemental sulfur to H₂S using reducing equivalents obtained from the oxidation of glucose in erythrocytes (Searcy, 1998). Human erythrocytes produce H₂S when provided with elemental sulfur or inorganic polysulfides.

Sulfide, via non-enzymatic oxidation, yields thiosulfate. The latter can be converted to sulfite by thiosulfate reductase in liver, kidney, or brain tissues or by thiosulfate sulfurtransferase in the liver. H₂S can also be released from thiosulfate and persulfides. Garlic and garlic-derived organic polysulfides induce H₂S production in a thiol-dependent manner (Benavides, 2007).

Instead, while garlic has long been felt beneficial as an antioxidant, recent evidence suggests that a number of beneficial effects of garlic are derived from H₂S production.

Thus far the best characterized naturally occurring H₂S-donating compound from garlic (*Allium sativum*) is allicin (diallylthiosulfinate) which decomposes in water to a number of compounds, such as diallyldisulfide (DADS) and diallyltrisulfide (DATS).

1.3. Key enzymes responsible for H₂S production

1.3.1. Cystathionine beta-synthase

The human enzyme comprises 551 amino acids with a subunit molecular weight of ~63 kDa (Kraus, 1986). It is a tetramer, which is prone to aggregation, and binds one heme and one PLP per subunit. AdoMet functions as a V-type allosteric activator, binds stoichiometrically to each subunit (Taoka, 1999), and increases enzyme activity ~2- to 3-fold (**Figure 4**).

The catalytic core represents the conserved part of the protein and resembles other members of the β - or fold II class of PLP-dependent enzymes (Alexander, 1994). The presence of protoporphyrin IX in cystathionine β -synthase is unique in the family of PLP-dependent enzymes and is seen in only a subset of organisms.

A glycine rich loop, G256–T257–G258–G259–T260, another conserved structural feature of fold II enzymes, makes multiple electrostatic interactions with the phosphate moiety of PLP (**Figure 5**). Based on the chemical shift of the enzyme-bound PLP in yeast and human cystathionine β -synthase, the phosphate appears to be bound as a dianion (Kabil, 2001).

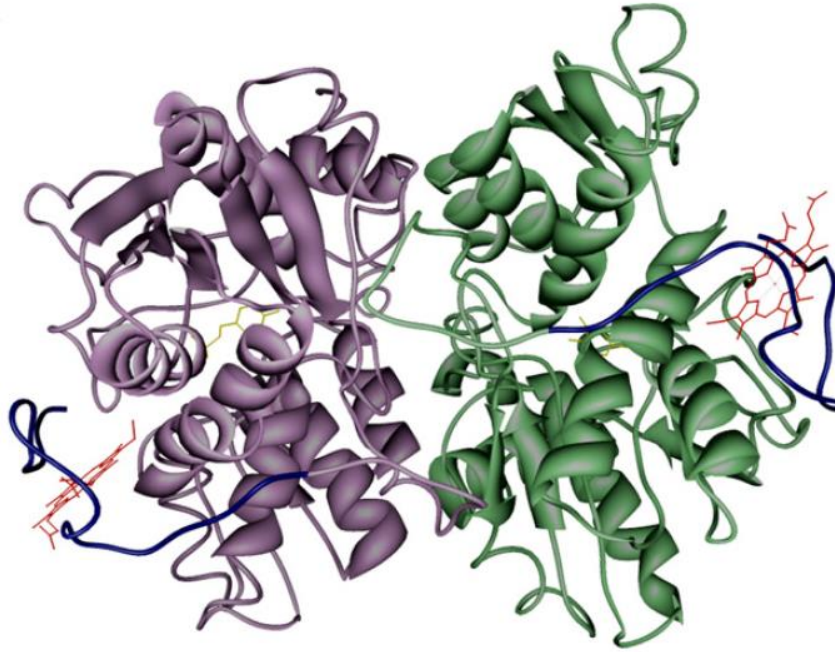


Figure 4 - Cristal structure of dimeric human cystathionine β -synthase lacking the C-terminal regulatory. The figure was generated using the PDB file 1M54. The heme is shown in red and the PLP in yellow.

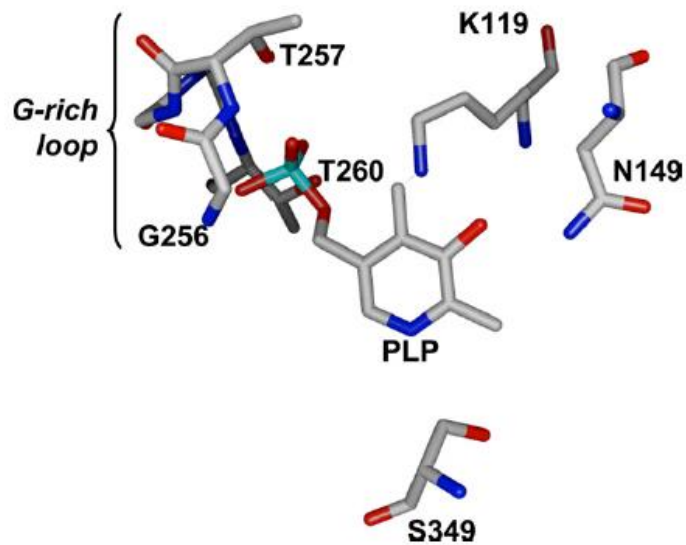


Figure 5 -Close up of the active site of human cystathionine β -synthase showing the conserved residues that interact with the PLP.

The human cystathionine β -synthase catalyzes the condensation of serine and homocysteine to give cystathionine and H_2O . Furthermore, the β -elimination reaction catalyzed by cystathionine- β -synthase has the potential for generating also H_2S , using homocysteine and cysteine as substrates (**Figure 6**).

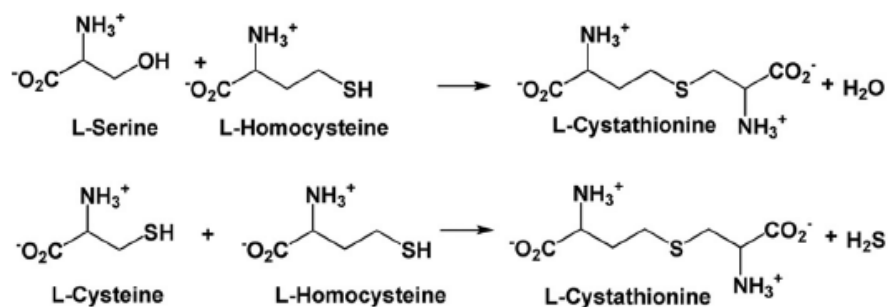


Figure 6 - Reactions catalysed by CBS.

1.3.2. Cystathionine gamma-lyase

The three-dimensional structures of human and yeast CSE have recently been elucidated via X-ray crystallography (Sun, 2009).

Structurally, the enzyme consists of four identical monomers of approximately 45 kDa, with a covalently bound pyridoxal 5'-phosphate (PLP) cofactor in each monomer (**Figure 7**). However, some studies show evidence for differential PLP binding affinities among the monomers of CSE and transient dissociation or removal of PLP from the enzyme during the catalytic process (Messerschmidt, 2003).



Figure 7 - Cristal structure of human cystathionine γ -lyase. The figure was generated using the PDB file 2NMP. The PLP is shown in pink.

Based on the crystal structures of yeast and human CSE as well as on sequence alignment with other transsulfuration enzymes, several active-site residues that could be involved in catalyzing the α,β -elimination reaction, leading to H_2S production, were identified (Huang, 2010).

In the crystal structures of yeast and human CSE, several residues were found to contribute towards the binding of the PLP cofactor. These residues include Tyr60 and Arg62 from the adjacent monomer; Tyr114, which π -stacks with the pyridoxal ring of the cofactor; Asp187, which hydrogen bonds to the pyridoxal nitrogen; and Ser209 and Thr211, which provide hydrogen-bond contacts to the phosphate group. Studies have also shown that Lys212 serves as an important catalytic residue by forming a covalent bond to the PLP cofactor and

facilitating proton transfer reactions during the α,γ -elimination reaction of L-cystathionine.

The location of the residues (only side chains shown) studied by site-directed mutagenesis is shown in **Figure 8**, and significant hydrogen bonds and polar interactions are depicted by dotted lines. Besides interacting with residues from the same subunit, the PLP cofactor is hydrogen bonded to Tyr60* and Arg62* from the adjacent subunit as well. The figure was produced by the program PyMOL (DeLano, 2002).

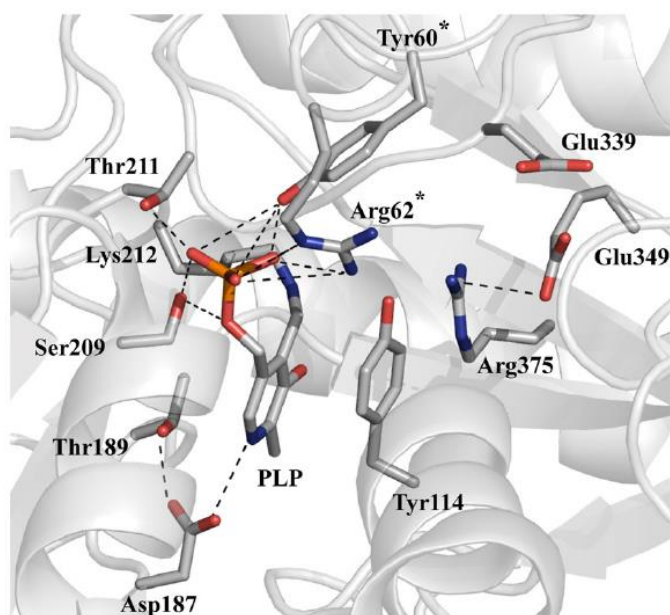


Figure 8- Active site of the human CSE enzyme.

CSE is an enzyme that is found predominantly in mammals and some fungi and is traditionally known for its role in the reverse transsulfuration pathway, where L-methionine is converted into L-cysteine through a series of metabolic interconversions.

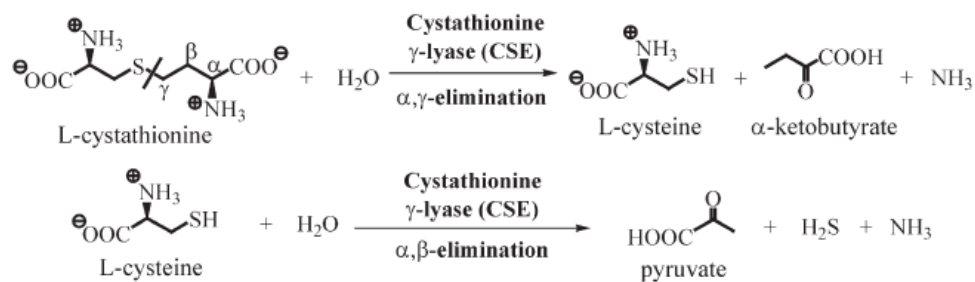


Figure 9- Reactions catalysed by CSE.

Specifically, the role of CSE in this reaction pathway is to convert L-cystathionine into L-cysteine whilst generating α -ketobutyrate and ammonia (**Figure 9**). The reaction proceeds via an α,γ -elimination mechanism where the $C-\gamma-S$ bond of L-cystathionine is specifically cleaved to yield L-cysteine.

Besides its role in the conversion of L-cystathionine into L-cysteine, studies have also shown that CSE can utilize L-cysteine as a substrate for producing H_2S via an α,β -elimination reaction (**Figure 9**).

1.4. Biological functions of hydrogen sulfide

Knowledge of the biological roles for endogenous H_2S is constantly expanding. Many studies in the literature indicate that H_2S executes physiological effects at a wide range of concentrations between 10 and 300 μM (Li, 2011).

It is clear that H_2S is involved in modulating various physiological responses including anti-inflammation (Zanardo, 2006), reducing oxidative stress (Yonezawa, 2007), neuromodulation (Abe, 1996), vasoregulation (Laggner, 2007), protection from reperfusion injury after myocardial infarction (Sivarajah, 2009), and inhibition of insulin resistance (Ali, 2007).

Moreover, many researchers continue to explore this signalling molecule for its involvement in various aspects of cell function, cytoprotection and cellular signalling.

1.4.1. Cardiovascular system

The growing knowledge about the biological significance of H₂S in the heart and blood vessels is unravelling the importance of this gaseous mediator in the control of CV homeostasis.

In particular, it is emerging that H₂S shares almost all the beneficial effects of NO, without being the source of toxic metabolites (Lefer, 2007). Recently, it has been proposed that the role of H₂S in CV homeostasis becomes more important and critical, when the NO-mediated control is compromised (for example, in the case of endothelial dysfunction). H₂S evokes relaxing responses in the vascular smooth muscle, and this action has been observed in large vessels, such as the rat thoracic aorta and portal vein, as well as (and with higher potency) in peripheral resistance vessels, which play a more significant role than large conduit arteries in the regulation of vascular resistance and blood pressure (Cheng, 2004). The vasomotor effects of H₂S are mimicked by L-cysteine and the vasorelaxing activity of L-cysteine is abolished by the CSE inhibitor PGG, thus proving that L-cysteine acts as a H₂S source. Consistently, genetic deletion of CSE in mice markedly reduces H₂S levels in the serum, heart, and aorta, and mutant mice lacking CSE develop marked hypertension and a decreased endothelium-dependent vasorelaxant effect (Yang, 2008).

It is currently acknowledged that H₂S relaxes blood vessels mainly (not exclusively) by opening the K_{ATP} channels of vascular smooth muscle cells.

Together with vasorelaxing activity, H₂S (such as NO) is endowed with a wide range of additional biological roles, which are relevant for a polyedric control of the CV system. For example, H₂S inhibits platelet aggregation/adhesion induced by ADP, collagen, epinephrine, arachidonic acid, thromboxane mimetic U46619, and thrombin.

1.4.2. Immune system and inflammation

It is well known that nonsteroidal anti-inflammatory drugs (NSAIDs) induce gastroenteropathy (Fiorucci, 2005). Research suggests that NSAIDs suppressed endogenous H₂S synthesis by reducing expression of CSE.

The accompanying reduction of H₂S synthesis may in turn contribute to an increase in leukocyte adherence resulting in gastric injury that is seen after NSAID administration (Perini, 2004).

Similarly, administration of exogenous H₂S reduced the ability of these agents to cause gastric injury. Exogenously supplied H₂S suppressed NSAID-induced granulocyte infiltration, expression of endothelial and leukocyte adhesion molecules, and expression of tumor necrosis factor α (TNF α) (Fiorucci, 2005). It was found that leukocyte adhesion to the vascular endothelium induced by aspirin injury was decreased after increasing H₂S bioavailability and that CSE inhibition with propargylglycine exacerbated aspirin mediated mucosal injury and inflammation. This study also observed that leukocyte expression of LFA-1 was suppressed by exogenous H₂S. Interestingly, this article also showed a molecular

aspect of H₂S induced anti-inflammatory effects, such that H₂S donors decreased aspirin-induced leukocyte adhesion through the activation of K_{ATP} channels and inhibition of CSE activity that promotes leukocyte adhesion. Additional studies demonstrated that co-administration of an H₂S donor with an NSAID resulted in inhibition of NSAID-induced leukocyte adherence and reduction of the severity of gastric damage (Wallace, 2007).

1.4.3. Respiratory system

The major environmental exposure to H₂S in humans is through the respiratory tract. On the basis of the H₂S relaxing action on the vascular smooth muscle, the relaxant property of H₂S has been investigated also on rings of bronchial smooth muscle of two rodent species. This study showed that H₂S causes strong relaxation in the isolated bronchus rings from the mouse, but produces only slight relaxation in guinea pig rings.

H₂S content and CSE activity are significantly enhanced also in isolated rat lung submitted to ischemia/reperfusion injury, and a preventive perfusion with H₂S attenuates such an injury, reducing malondyaldehyde (MDA) production and stimulating superoxide dismutase and catalase activity (Fu, 2008).

Concerning the endogenous CSE/H₂S pathway, it seems to play a relevant role in pulmonary hypertension (PH). In particular, this pathway has been found to be down-regulated in hypoxic PH (HPH), resulting in a decreased endogenous H₂S production in rat lung tissues due to oxidative stress. In particular, both the gene expression of CSE and the activity of this enzyme were suppressed in lung tissues during HPH, but the exogenous supply of H₂S resulted in enhancing CSE

activity, upregulating CSE gene expression in lung tissue and lessening pulmonary vascular structure remodeling during HPH (Zhang, 2003). After the treatment with exogenous H₂S, HPH was attenuated, through a direct scavenging of oxidized glutathione (GSSG), an increased total antioxidant capacity (Wei, 2008) and the inhibitory effect of H₂S on pulmonary vascular inflammation, associated with a high I-B (inhibitor of NF- κ B) expression and a down-regulation of NF- κ B p65 expression (Jin, 2008).

Furthermore, The CSE/H₂S pathway seems to exert beneficial roles also in the two most important obstructive airway diseases, such as asthma and chronic obstructive pulmonary disease (COPD). In an ovalbumin-induced asthmatic rat model and in human asthmatic patients, the levels of endogenous H₂S, whose anti-inflammatory effects are related to the inhibition of iNOS activity and decrease with the progression of disease severity (Fan, 2009). Consistently, increased levels of serum H₂S in milder COPD may play a useful role in airway protection, antagonizing oxidative stress and airway inflammation and preventing the progress of COPD.

1.4.4. Reproductive system

Recent studies focused on the effects of exogenous H₂S on mammalian reproductive systems. The powerful vasorelaxant effect of H₂S on the penile artery suggests an important physiological role of H₂S in the erectile response of human corpus cavernosum (Di Villa Bianca, 2009).

Specifically, NaHS (0.1–1 mM) relaxed the precontracted human corpus cavernosum strips *in vitro*, independent of the presence of endothelium or the

function of endothelial NOS (eNOS). The relaxant effect of NaHS depends on the nature of the stimuli that were used to precontract the tissue strips.

1.4.5. Central Nervous System

As an almost ubiquitous bioactive molecule, H₂S exerts important regulatory effects in several biological systems. For instance, it is pivotally involved in the control of important functions in the CNS. A high expression of CBS in the rat hippocampus and cerebellum was observed (Abe, 1996).

In CNS neurons, H₂S enhances cAMP production, thus leading to an increased sensitivity of NMDA receptors to glutamate (Kimura, 2000).

This sensitization of NMDA receptors, elicited by quite high concentrations of H₂S (50–160 μM), contributes to the induction of hippocampal long-term potentiation, a process of synaptic plasticity involved in the mechanisms of learning and memory (Kimura, 2005). Increased production of cAMP activates protein kinase A which regulates brain function through intracellular protein phosphorylation, but this is not the only intracellular signalling in which H₂S seems to be involved.

In fact, H₂S may enhance reducing activity and protect neurons against oxidative stress via activation of upstream receptor tyrosine kinase (Tan, 2010).

Finally, recent findings reported that H₂S inhibits lipopolysaccharide(LPS)-induced NO production in microglia via inhibition of p38-MAPK (Hu, 2010) and that MAPKs regulate cellular activities, such as apoptosis, differentiation, metabolism, etc (Roux, 2004). These data suggest a role for H₂S in the treatment of cerebral ischemia and neuro-inflammatory diseases.

2. Aim of project

Retrospective analysis of the literature on biological effects of H₂S suggests two approaches for studying physio-pathological conditions in which it is involved and for the developing therapies based on its activities:

- use of H₂S in the gaseous state, or "sulfur-precursors" or "prodrugs" capable of releasing, directly or via interaction with specific enzymes, hydrogen sulfide;
- use of CBS/CSE inhibitors, leading to blockade of endogenous production of H₂S.

The aim of my PhD project is design, synthesis and structural characterization of three different series of compounds:

1. CBS/CSE substrates a/o inhibitors, crucial to study the pathophysiological implications of H₂S;
2. hydrogen sulfide-releasing hybrids, containing pharmacologically active compounds and molecules able to release H₂S, that could enhance therapeutic activity;
3. novel compounds able to release H₂S, non enzymatically, with slow kinetic of release, mimicking the physiological conditions.

Because of the unavailability of a pharmacophoric model as a lead for rational design of targeted enzyme substrates and inhibitors we preliminarily selected and tested commercially available cysteine surrogates. The catalytic profiles of recombinant CBS and CSE were assessed in the presence of the

following selected compounds: L-(S-carbamoyl)-cysteine; L-2-oxothiazolidin-4-carboxylic acid; L-3-(2-aminoethylthio)-2-aminopropanoic acid; L-thiazolidine-4-carboxylic acid; D,L-penicillamine.

On the basis of the obtained results, new compounds were designed; they were characterized by the introduction of a propargyl group in α -carboxyl position, aiming to obtain novel molecular entities embodying the structural features of both cysteine and the well known CSE inhibitor, DL-propargylglycine (PGG). In order to consider the small size of the active site channel, containing several patches of hydrophobic residues, we decided to introduce a butyl group in α -carboxyl position, to facilitate the access to the enzyme active site.

The structural modifications were also extended to aromatic scaffolds, to weaken π -stacking interaction between PLP and Tyr114, two important components of the active site (**Table 1**).

Further development of my PhD project is related to new classes of hydrogen sulfide-releasing moieties combined with pharmacologically active compounds. In particular, my attention has been paid to the synthesis of hydrogen sulfide-releasing hybrids, such as glucocorticoids- H_2S donors.

With regard to glucocorticoids, the choice is derived from the analysis of a recent *in vivo* study that investigated the effects of a H_2S donor (NaHS) on airways in balb/c mice sensitized with ovalbumin (OVA) (Roviezzo et al., submitted). In this study, aerosolized NaHS blunted OVA-induced airway hyperresponsiveness: these data suggest that combined early treatment with H_2S donors in association with glucocorticoids might improve asthma symptoms by inhibiting classical inflammatory signals and by acting, at the same time, on

airway myofibroblasts, perhaps delaying the onset of sub-epithelial fibrosis and the secretion of inflammatory factors and contributing to bronchodilation.

Considering the vast potential of hydrogen sulfide in asthma therapy, we have supposed that combined treatment with glucocorticoids and H₂S-releasing moieties could represent an effective therapeutic strategy for asthma care.

Starting from this consideration, glucocorticoids-H₂S donors have been designed: two most commonly used corticosteroids, dexamethasone and beclomethasone, were condensed with different H₂S-releasing compounds, such as 5-(*p*-hydroxyphenyl)-1,2-dithione-3-thione (ADT-OH) and 4-hydroxythiobenzamide (TBZ) (**Table 2**).

Concerning the third class of compounds, H₂S-releasing capacity is a pharmacologically relevant feature, already attributed to naturally occurring compounds, such as the diallyl polysulfides of garlic and our attention was thus devoted to the synthesis of ureic derivatives, as well as 1,2,4-thiadiazolidine-3,5-diones, representing a potential innovative scaffold for the release of H₂S (**Table 3**). These derivatives, in analogy with the N-(benzoylthio)benzamide compounds, recently reported in the literature, were evaluated according to their ability to release H₂S following the cleavage of the NH-S bond.

Table 1

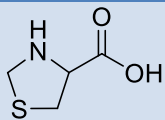
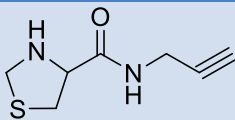
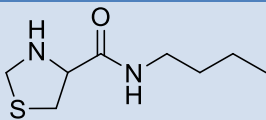
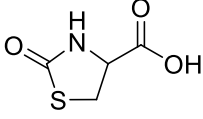
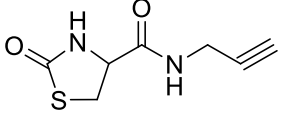
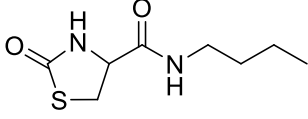
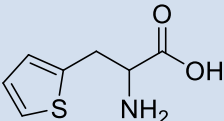
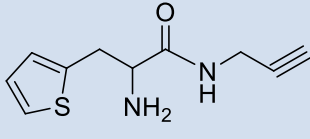
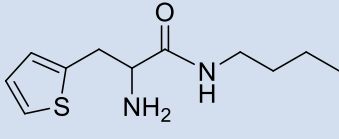
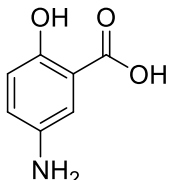
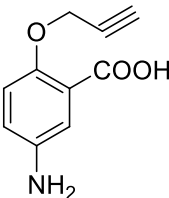
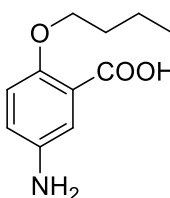
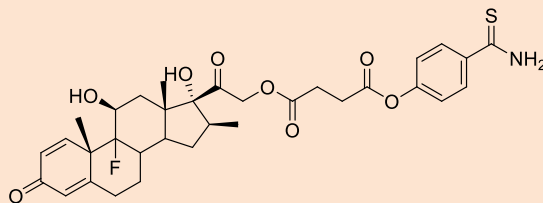
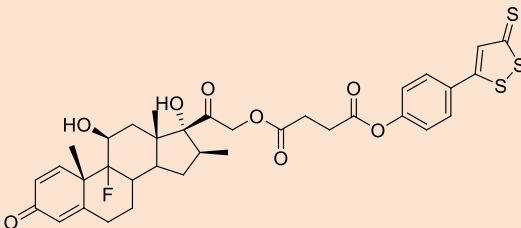
 1	 Ia	 Ib
 2	 IIa	 IIb
 3	 IIIa	 IIIb
 4	 IVa	 IVb

Table 2

Dexamethasone-H₂S donors

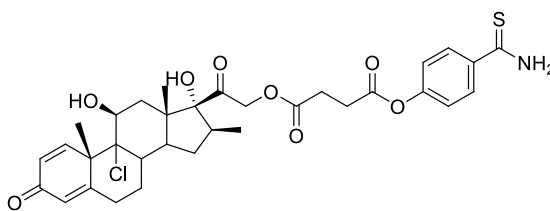


FAS-I

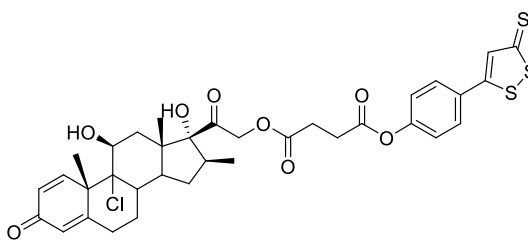


FAS-II

Beclomethasone-H₂S donors

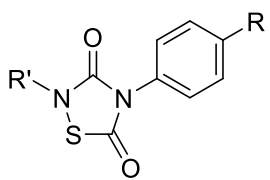
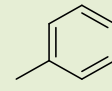
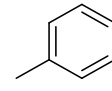
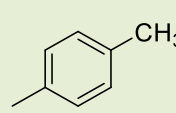
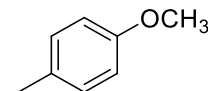
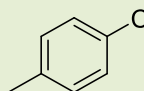
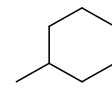
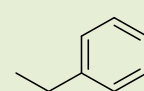


FAS-III



FAS-IV

Table 3

	R	R'	
	-H		THIA I
	-OCH ₃		THIA II
	-OCH ₃		THIA III
	-OCH ₃		THIA IV
	-OCH ₃		THIA V
	-OCH ₃		THIA VI
	-OCH ₃		THIA VII

3. Materials and methods

3.1. Chemistry

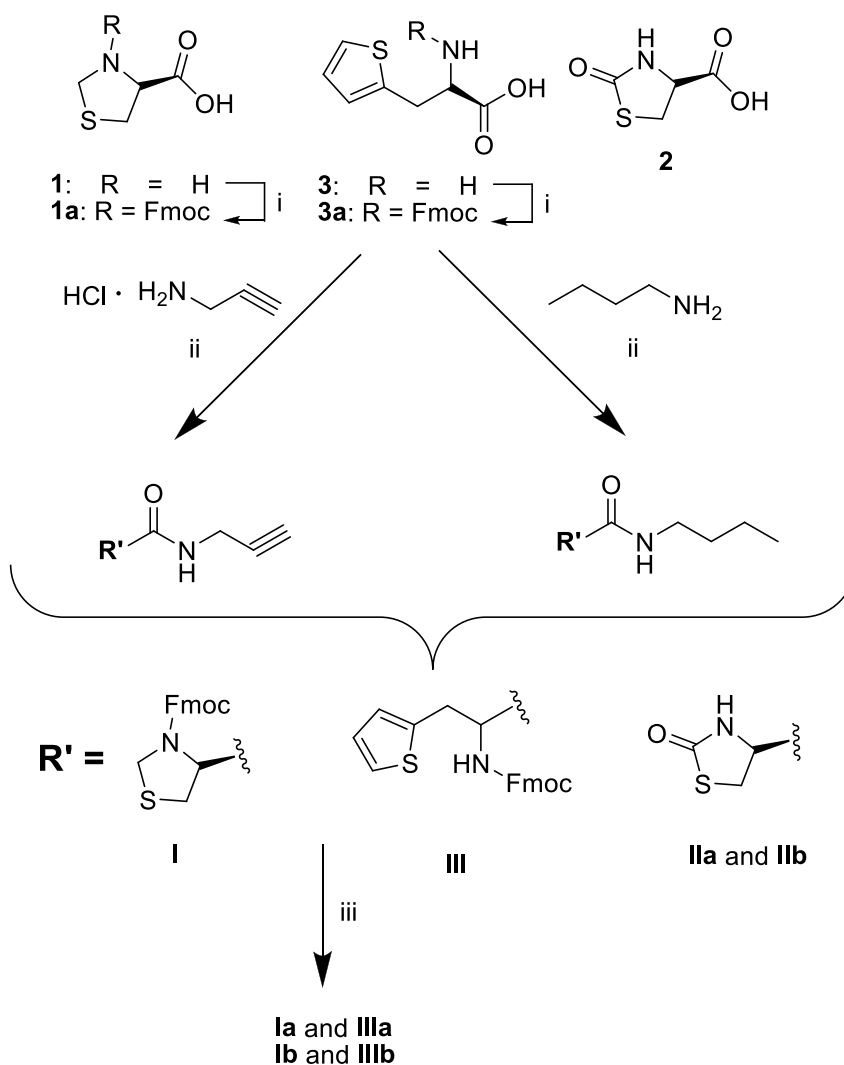
The synthetic route for the preparation of propargylamide (**Ia-IIIa**) and butylamide (**Ib-IIIb**) derivatives is reported in **Scheme 1**. The carboxylic acid was treated with N-(9-fluorenylmethoxycarbonyloxy) succinimide to protect the amine group, if needed. The coupling reaction of N-protected carboxylic acid with opportune amine, propargylamine hydrochloride or butylamine, was performed in the presence of TBTU, HOBt and N,N-diisopropylethylamine (DIPEA), leading to the formation of an amide bond. Fmoc deprotection, when necessary, was carried out using a solution of 33% DIEA in tetrahydrofuran, obtaining compounds **Ia-IIIa** and **Ib-IIIb**, respectively.

The general strategy for the synthesis of compounds **IVa-IVb** is summarized in **Scheme 2**, as follows: protection of amine and carboxyl groups; ether formation using the conventional Williamson synthesis, by treatment with a strong base, NaH or Na₂CO₃, and propargyl bromide or butyl bromide, respectively, performed in anhydrous CH₃CN; subsequent Boc deprotection and methyl ester hydrolysis, providing the final compounds **IVa** and **IVb**.

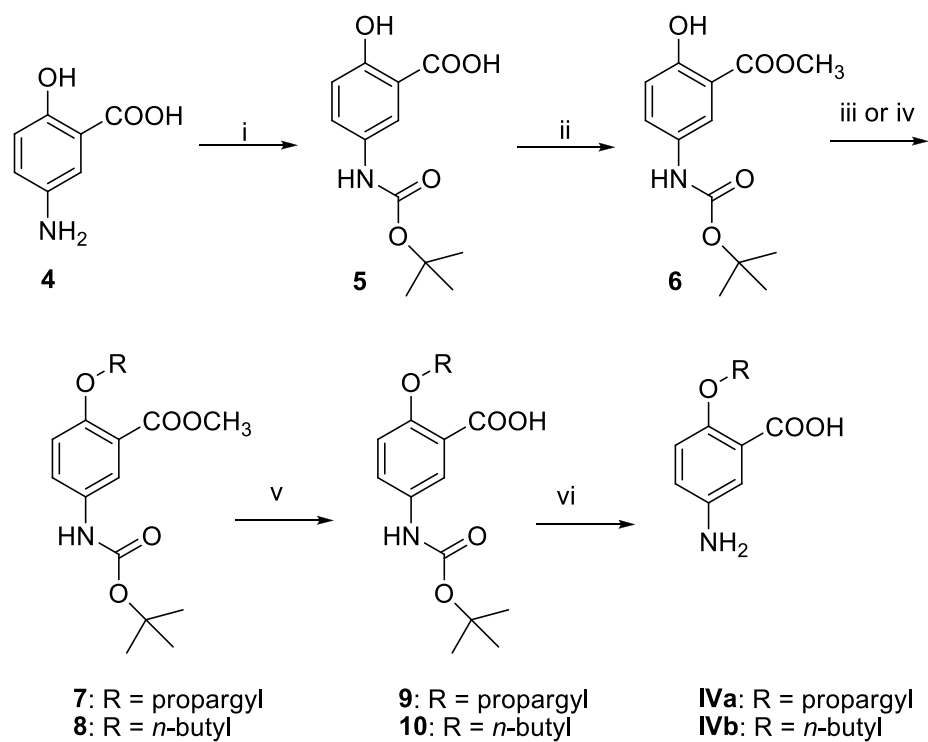
Scheme 3 depicts the synthetic pathways employed to prepare glucocorticoids-H₂S donors. Glucocorticoids, dexamethasone or beclomethasone, were converted to the corresponding 21-succinate by treatment with succinic anhydride in the presence of catalytic amount of DMAP in anhydrous pyridine. Coupling reaction of succinate derivative with H₂S releasing chemical moieties, such as ADT-OH or 4-hydroxythiobenzamide (TBZ), was performed in the

presence of EDC and DMAP, leading to the formation of glucocorticoids derivatives (**FAS I-IV**).

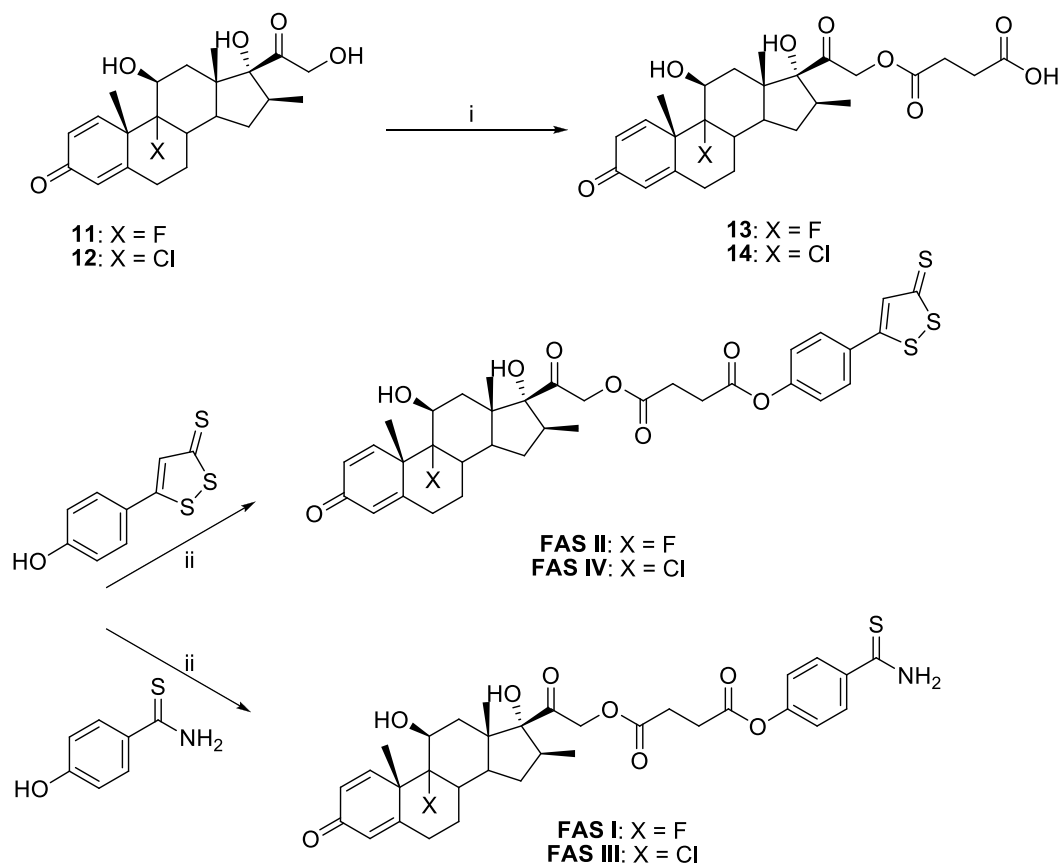
The synthetic strategy employed for the preparation of the 1,2,4-thiadiazolidin-3,5-dionesis summarized in **Scheme 4**. The compounds (**THIA I-VII**) were synthesized through oxidative condensation of isothiocyanates with isocyanates in the presence of SO_2Cl_2 as the oxidizing agent.



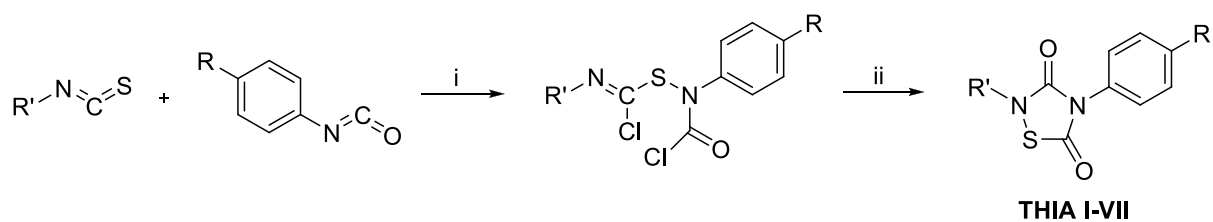
Scheme 1- **i)** Na_2CO_3 9% /Fmoc-OSu/dioxane; **ii)** TBTU/HOBt/DIPEA; **iii)** 33% DIEA in THF.



Scheme 2- **i)** di-*t*-butyl dicarbonate/triethylamine/H₂O/dioxane; **ii)** DCC/MeOH; **iii)** potassium carbonate/acetonitrile; propargylamine hydrochloride; **iv)** sodium hydride/anhydrous acetonitrile; butylamine; **vi)** 1N sodium hydroxide solution/ethanol; **vii)** 40% trifluoroacetic acid in dichloromethane solution.



Scheme 3- i) succinic anhydride/DMAP/anhydrous pyridine; **ii)** EDC/DMAP



Scheme 4- i) SOCl_2 /diethyl ether; **ii)** H_2O , reflux

3.2. Experimental procedures

All reagents were commercial products purchased from Sigma Aldrich. Melting points, determined using a Buchi Melting Point B-540 instrument, are uncorrected and represent values obtained on recrystallized or chromatographically purified material. ¹H-NMR spectra were recorded on Varian Mercury Plus 400 MHz instrument. Unless otherwise stated, all spectra were recorded in DMSO. Chemical shifts are reported in ppm using Me₄Si as internal standard. The following abbreviations are used to describe peak patterns when appropriate: s (singlet), d (doublet), t (triplet), q (quartet), qt (quintet), dd (double doublet), m (multiplet). Mass spectra of the final products were performed on API 2000 Applied Biosystem mass spectrometer. Elemental analyses were carried out on a Carlo Erba model 1106; analyses indicated by the symbols of the elements were within ±0.4% of the theoretical values. All reactions were followed by TLC, carried out on Merck silica gel 60 F254 plates with fluorescent indicator and the plates were visualized with UV light (254 nm). Preparative chromatographic purifications were performed using silica gel column (Kieselgel 60). Solutions were dried over Na₂SO₄ and concentrated with a Buchi R-114 rotary evaporator at low pressure.

3.2.1. Cysteine surrogates: propargylamide and *n*-butylamide derivatives (**Ia-IIIa** and **Ib-IIIb**)

3.2.1.1. 3-(((9H-fluoren-9-yl)methoxy)carbonyl)thiazolidine-4-carboxylic acid (**Ia**). The thiazolidine-4-carboxylic acid (**1**, 1g, 7.5mmol) in Na₂CO₃ 9% (10 mL) was cooled in ice water and mechanically stirred. Then a solution of Fmoc-OSu

(2.5g, 7.5mmol) and dioxane (20 mL) was added dropwise and the mixture was stirred for 2.5 hours at room temperature. The solvent was evaporated, the aqueous residue acidified with 1N HCl and the product extracted with ethyl acetate. The organic phase was then dried on anhydrous Na₂SO₄ and filtered, and the solvent was evaporated. The product was crystallized from diethyl ether, yielding 2.5 g of 3-(((9H-fluoren-9-yl)methoxy)carbonyl)thiazolidine-4-carboxylic acid (**1a**, 94%) as a solid.

3.2.1.2. N-(prop-2-yn-1-yl)thiazolidine-4-carboxamide and N-butylthiazolidine-4-carboxamide (Ia and Ib). The intermediate 3-(((9H-fluoren-9-yl)methoxy)carbonyl)thiazolidine-4-carboxylic acid (**1a**, 1g, 2.8mmol) was dissolved in DMF (30mL) and coupled to the opportune amine, propargylamine hydrochloride (0.258g, 2.8mmol) or butylamine (0.205g, 2.8mmol), in the presence of DIPEA (0.536mL, 3.1mmol), using HOBt (0.472g, 3.1mmol) and TBTU (0.988g, 3.1mmol) as the coupling reagents. This reaction was carried out at room temperature with stirring overnight. The solvent was evaporated, and the crude material was then dissolved in ethyl acetate (150mL) and washed with 5% citric acid (3 x 50mL), 10% NaHCO₃ (3 x 50mL) and brine (50mL). The organic layer was dried on anhydrous Na₂SO₄ and filtered, and the solvent was evaporated. After chromatography on a silica gel column (eluent, 7:3 ethyl acetate/hexane) 0.86 g and 0.82 g of intermediates **I** were obtained (82% for the propargylamide derivative and 75% for the *n*-butylamide derivative, respectively) as solids.

Fmoc deprotection of intermediates **I** was performed using a 33% diethylamine solution in tetrahydrofuran and the mixture was stirred for 2.5 hours at room temperature. Afterward the solvent was concentrated in vacuo and the obtained residue was purified by column chromatography (dichloromethane/methanol 9.5:0.5 (v/v)). The combined and evaporated product fractions were crystallized from hexane, to give the final compounds N-(prop-2-yn-1-yl)thiazolidin-4-carboxamide **Ia** and N-butylthiazolidine-4-carboxamide **Ib** as white solids (obtained yields 72% and 70% respectively).

N-(prop-2-yn-1-yl)thiazolidine-4-carboxamide (**Ia**) mp 126–127 °C; ¹H NMR (400 MHz, DMSO-d₆) δ 3.13 (s, 1H, CCH), 3.10–3.18 (dd, 1H, CH₂CH thiaz, J=6.65), 3.39–3.43 (dd, 1H, CH₂CH thiaz, J=6.65), 3.88 (s, 2H, NHCH₂), 3.96 (d, 1H, SCH₂NH, J=9.90), 4.13 (t, 1H, CH₂CH thiaz), 4.24 (d, 1H, SCH₂NH, J=9.90), 8.29 (s, 1H, NH), 8.99 (s, 1H, NH); ¹³C NMR (400 MHz, DMSO-d₆) δ 29.0, 32.9, 61.8, 74.0, 74.6, 81.3, 170.1; ESI-HRMS (M + H)⁺ m/z calcd 170.23 for C₇H₁₀N₂OS; found 171.

N-butylthiazolidine-4-carboxamide (**Ib**) mp 126–127 °C; ¹H NMR (400 MHz, DMSO-d₆) δ 0.91 (t, 3H, CH₃, J=6.96, J=7.33), 1.30–1.36 (m, 2H, CH₂CH₃), 1.46–1.51 (qt, 2H, CH₂CH₂CH₃, J=6.65, J=7.04, J=7.43, J=7.04), 3.10–3.18 (dd, 1H, CH₂CH thiaz, J=6.65), 3.25 (t, 2H, CH₂CH₂CH₂CH), 3.39–3.43 (dd, 1H, CH₂CH thiaz, J=6.65), 3.96 (d, 1H, SCH₂NH, J=9.90), 4.13 (t, 1H, CH₂CH thiaz), 4.24 (d, 1H, SCH₂NH, J=9.90), 8.29 (s, 1H, NH), 8.99 (s, 1H, NH); ¹³C NMR (400 MHz, DMSO-d₆) δ 14.1, 19.9, 31.5, 32.8, 38.9, 61.8, 74.6, 170.1; ESI-HRMS (M + H)⁺ m/z calcd 188.29 for C₈H₁₆N₂OS; found 189.

3.2.1.3. *2-oxo-N-(prop-2-yn-1-yl)thiazolidine-4-carboxamide* and *N-butyl-2-oxothiazolidine-4-carboxamide (IIa and IIb)*. A mixture of 2-oxo-N-thiazolidine-4-carboxylic acid **2** (1g, 6.8mmol), the opportune amine, propargylamine hydrochloride (0.622g, 6.8mmol) or butylamine (0.497g, 6.8mmol), HOBt (1.15g, 7.5mmol), TBTU (2.40g, 7.5mmol) and DIPEA (1.30mL, 7.5mmol) in DMF (20mL) was stirred overnight at room temperature. The solvent was concentrated to dryness and the crude mixture was purified by silica gel column chromatography using ethyl acetate/hexane 7:3 (v/v) as eluent. The crude product was recrystallized from hexane, yielding 0.96 g of 2-oxo-N-(prop-2-yn-1-yl)thiazolidine-4-carboxamide **IIa** (76%) and 0.94 g of N-butyl-2-oxothiazolidine-4-carboxamide **IIb** (69%), respectively.

2-oxo-N-(prop-2-yn-1-yl)thiazolidine-4-carboxamide (IIa) mp 131.5–132.4 °C; ¹H NMR (400 MHz, DMSO-d₆) δ 3.13 (s, 1H, CCH), 3.31 (t, 2H, CH₂), 3.62-3.68 (dd, 2H, CH₂ thiaz, J=8.61), 3.88 (s, 2H, NHCH₂), 4.27 (t, 1H, CH₂CH thiaz), 8.27 (s, 1H, NH), 8.53 (s, 1H, NH); ¹³C NMR (400 MHz, DMSO-d₆) δ 29.0, 32.9, 56.8, 74.0, 81.3, 170.6, 174.0; ESI-HRMS (M + H)⁺ m/z calcd 184.22 for C₇H₈N₂O₂S; found 184.9.

N-butyl-2-oxothiazolidine-4-carboxamide (IIb) mp 83.2-83.7 °C; ¹H NMR (400 MHz, DMSO-d₆); δ 0.85 (t, 3H, CH₃, J=7.04, J=7.43), 1.21-1.30 (m, 2H, CH₂CH₃), 1.34-1.41 (qt, 2H, CH₂CH₂CH₃, J=6.65, J=7.04, J=7.43, J= 7.04), 3.04-3.09 (dd, 1H, CH₂CH thiaz, J=6.65), 3.60-3.65 (dd, 1H, CH₂CH thiaz, J= 8.61), 4.22 (t, 1H, CH₂CH thiaz), 7.99 (s, 1H, NH), 8.23 (s, 1H, NH); ¹³C NMR (400

MHz, DMSO-d₆) δ 14.1, 19.9, 31.5, 32.8, 38.9, 56.9, 170.1, 173.7; ESI-HRMS (M + H)⁺ m/z calcd 202.27 for C₈H₁₄N₂O₂S; found 203.0.

3.2.1.4. *2-(((9H-fluoren-9-yl)methoxy)carbonylamino)-3-(thiophen-2-yl)propanoic acid (3a)*. The 2-amino-3-(thiophen-2-yl)propanoic acid (**3**, 1g, 5.8mmol) in Na₂CO₃ 9% (10mL) was cooled in ice water and mechanically stirred. Then a solution of Fmoc-OSu (1.97g, 5.8mmol) and dioxane (20mL) was added dropwise and the mixture was stirred for 2.5 hours at room temperature. The solvent was evaporated, the aqueous residue acidified with 1N HCl and the product extracted with ethyl acetate. The organic phase was then dried on anhydrous Na₂SO₄ and filtered, and the solvent was evaporated. The product was crystallized from diethyl ether, yielding 2.08 g of 2-(((9H-fluoren-9-yl)methoxy)carbonylamino)-3-(thiophen-2-yl)propanoic acid (**3a**; 91%) as a solid.

3.2.1.5. *2-amino-N-(prop-2-yn-1-yl)-3-(thiophen-2-yl)propanamide and 2-amino-N-butyl-3-(thiophen-2-yl)propanamide (IIIa and IIIb)*. The intermediate 2-(((9H-fluoren-9-yl)methoxy)carbonylamino)-3-(thiophen-2-yl)propanoic acid (**3a**, 1.0g, 2.5mmol) was dissolved in DMF (30mL) and coupled to the opportune amine, propargylamine hydrochloride (0.229g, 2.5mmol) or butylamine (0.183g, 2.5mmol), in the presence of DIPEA (0.48mL, 2.8mmol), using HOBt (0.42g, 2.8mmol) and TBTU (0.885g, 2.8mmol) as the coupling reagents. This reaction was carried out at room temperature with stirring overnight. The solvent was evaporated, and the crude material was then dissolved in ethyl acetate (150 mL) and washed with citric acid 5% (3 x 50 mL), NaHCO₃ 10% (3 x 50 mL) and brine (50 mL). The organic layer was dried on anhydrous Na₂SO₄ and filtered, and the

solvent was evaporated. After chromatography on a silica gel column (eluent, 7:3 ethyl acetate/hexane) 0.90 g and 0.98 g of intermediates **III** were obtained (76% for the propargylamide derivative and 87% for the *n*-butylamide derivative, respectively) as solids. A solution of 33% diethylamine solution in tetrahydrofuran was used during deprotection of Fmoc group of intermediates **III**. The mixture was stirred for 2.5 hours at room temperature. Afterward the solvent was concentrated *in vacuo* and the obtained residue was purified by column chromatography (dichloromethane/methanol 9.5:0.5 (v/v)). The combined and evaporated product fractions were crystallized from hexane, to give the final compounds N-(prop-2-yn-1-yl)thiazolidin-4-carboxamide **IIIa** and 2-amino-N-butyl-3-(thiophen-2-yl)propanamide **IIIb** as white solids (yield: 68% and 75%, respectively).

2-amino-N-(prop-2-yn-1-yl)-3-(thiophen-2-yl)propanamide (IIIa). mp 196.2-196.3°C; ¹H NMR (400 MHz, DMSO-d₆) δ 3.18 (s, 1H), 3.27-3.31 (dd, 2H, CH₂CH, J=6.06), 3.90 (s, 2H, NHCH₂), 3.95 (t, 1H, CHCO, J=6.09), 6.94-6.97 (m, 2H, H-thioph), 7.40 (d, 1H, H-thioph, J=3.9), 8.38 (s, 2H, NH), 9.05 (s, 1H, NH₂); ¹³C NMR (400 MHz, DMSO-d₆) δ 28.9, 31.4, 53.9, 74.6, 80.7, 126.4, 127.9, 128.4, 136.4, 168.0; ESI-HRMS (M + H)⁺ m/z calcd 208.28 for C₁₀H₁₂N₂OS; found 209.2.

2-amino-N-butyl-3-(thiophen-2-yl)propanamide (IIIb). mp 172.9-173.3°C; ¹H NMR (400 MHz, DMSO-d₆) δ 0.85 (t, 3H, CH₃, J=7.04, J=7.43), 1.21-1.30 (m, 2H, CH₂CH₃), 1.34-1.41 (qt, 2H, CH₂CH₂CH₃, J=6.65, J=7.04, J=7.43, J= 7.04), 3.20 (d, 2H, NHCH₂ J= 6.03), 3.27-3.31 (dd, 2H, CH₂CH, J=6.06), 3.95 (t, 1H,

CHCO, J=6.09), 6.94-6.97 (m, 2H, H-thioph), 7.40 (d, 1H, H-thioph, J=3.9), 8.38 (s, 2H, NH), 9.05 (s, 1H, NH₂); ¹³C NMR (400 MHz, DMSO-d₆) δ 14.1, 19.9, 31.4, 38.9, 53.9, 56.9, 126.4, 127.9, 128.4, 136.4, 168.0; ESI-HRMS (M + H)⁺ m/z calcd 226.34 for C₁₁H₁₈N₂OS; found 227.0.

3.2.1.6. Methyl 5-(tert-butoxycarbonylamino)-2-hydroxybenzoate (6). To a solution of 5-amino-salicylic acid (**4**, 2g, 13.0mmol) in 25 ml of dioxane and 12.5 mL of water, triethylamine (2.6mL, 19.5mmol) and di-*tert*-butyl-dicarbonate (4.2g, 19.5mmol) were added with stirring at 0° C for 1/2 h. The reaction mixture was stirred mechanically for 24 h at room temperature. After evaporation of the solvent, 3N HCl (15mL) was added dropwise to the residue. The precipitate is filtered, washed with water, dried and recrystallized from diethyl ether. 5-(*tert*-butoxycarbonylamino)-2-hydroxybenzoic acid was obtained (**5**) (3.28g, 100 % yield) and the powder (**5**, 3g, 11.8mmol) was dissolved in anhydrous methanol. To the solution, cooled to 0 °C, dicyclohexylcarbodiimide (2.4g, 11.8mmol) was added and the mixture was stirred at room temperature for 3h. The solvent was evaporated, the residue was taken up in ethyl acetate and dicyclohexylurea (DCU) was filtered. After chromatography on a silica gel column (eluent, 7:3 ethyl acetate/hexane) 2.3 g of **6** was obtained (73%) as a white solid.

3.2.1.7. 5-amino-2-(prop-2-ynoxy)benzoic acid (IVa). Intermediate **6** (1g, 4.0mmol) in anhydrous acetonitrile was treated with potassium carbonate (0.475g, 4.0mmol) and then propargyl bromide (solution 80% wt. in toluene) (0.446mL, 4.0mmol) was added slowly into the flask. The reaction mixture was stirred under reflux overnight. After this period, carbonate was filtered and solvent concentrated

in vacuo. The residue was purified by column chromatography (3:7 ethyl acetate/hexane (v/v)). The combined and evaporated product fractions were crystallized from diethyl ether/hexane, affording 0.734g (62% yield) of methyl 5-(*tert*-butoxycarbonylamino)-2-(prop-2-ynyloxy)benzoate (**7**).

To a solution of obtained compound (**7**, 0.734g, 2.5mmol) in ethanol, sodium hydroxide was added and the mixture was mechanically stirred at room temperature for 2 hours. The solvent was removed *in vacuo* and residue was slightly acidified with 1N hydrochloric acid. The aqueous solution was extracted with ethyl acetate and the organic phase was dried over anhydrous Na₂SO₄, filtered and evaporated to dryness to afford 0.734 g of compound **9** as a white powder (100% yield).

The crude intermediate (**9**, 0.734g, 2.5mmol) was treated with a solution of 40 % TFA in DCM. After 2 h the solvent was removed to obtain the crude product. The residue was loaded on a silica gel open column and eluted with ethyl acetate/hexane (7:3 v/v). The combined and evaporated fractions were crystallized from hexane to yield 0.386 g (87%) of pure product **IVa**. mp 220.0-220.4°C; ¹H NMR (400 MHz, DMSO-d₆); δ 3.48 (s, 1H, CH), 4.63 (s, 2H, CH₂), 6.69 (d, 1H, J=8.43, Ar-H), 6.89 (d, 1H, J=8.43, Ar-H), 6.91 (s, 1H, Ar-H); ¹³C NMR (400 MHz, DMSO-d₆) δ 58.43 78.69, 80.50, 116.55, 118.35, 118.88,123.74, 143.42, 148.11, 168.04; ESI-HRMS (M + H)⁺ m/z calcd 191.18 for C₁₀H₉NO₃; found 192.

3.2.1.8. 5-amino-2-butoxybenzoic acid (**IVb**). Intermediate **6** (1g, 4.0mmol) in anhydrous acetonitrile was treated with sodium hydride (0.097g, 4.0mmol) and then 1-butyl bromide (0.410 mL, 4.0mmol) was added slowly into the flask. The

reaction mixture was stirred under reflux overnight. The solvent was concentrated *in vacuo* and the crude material was then dissolved in ethyl acetate (150 mL) and washed with citric acid 5% (3 x 50 mL), NaHCO₃ 10% (3 x 50 mL) and brine (50 mL). The organic layer was dried on anhydrous Na₂SO₄ and filtered, and the solvent was evaporated. The residue was purified by column chromatography (2:8 diethyl ether/hexane (v/v)). The combined and evaporated product fractions were crystallized from diethyl ether/hexane, affording 0.957 g (74% yield) of methyl 2-butoxy-5-(*tert*-butoxycarbonylamino)benzoate (**8**).

To a solution of the obtained compound (**8**, 0.957g, 2.74mmol) in ethanol, sodium hydroxide was added and the mixture was mechanically stirred at room temperature for 2 hours. The solvent was removed *in vacuo* and residue was slightly acidified with 1N hydrochloric acid. The aqueous solution was extracted with ethyl acetate and the organic phase was dried over anhydrous Na₂SO₄, filtered and evaporated to dryness to afford 0.908 g of 2-butoxy-5-(*tert*-butoxycarbonylamino)benzoic acid (**10**) as a white powder (99% yield).

The crude intermediate (**10**, 0.908g, 2.9mmol) was treated with a solution of 40 % TFA in DCM. After 2 h the solvent was removed to obtain the crude product. The residue was loaded on a silica gel open column and eluted with ethyl acetate/hexane (7:3 v/v). The combined and evaporated fractions were crystallized from hexane to yield 0.543 g (90%) of pure product **IVb**. mp 213.0-213.1°C; ¹H NMR (400 MHz, DMSO-d₆); δ 0.89 (t, 3H, J=6.96, J=7.33, CH₃), 1.40-1.45 (m, 2H, CH₂CH₃), 1.65-1.68 (qt, 2H, CH₂CH₂CH₃), 4.0 (t, 2H, J= 5.86, J=6.23, OCH₂), 7.16 (d, 1H, J=9.16, Ar-H), 7.39 (d, 1H, J=8.43, Ar-H), 7.55 (s, 1H, Ar-H); ¹³C NMR (400 MHz, DMSO-d₆) δ 14.33, 19.28, 31.31, 69.143, 115.47, 122.96,

125.07, 127.45, 130.11, 156.84, 167.16; ESI-HRMS (M + H)⁺ m/z calcd 209.24 for C₁₁H₁₅NO₃; found 210.

3.2.2. Synthesis of glucocorticoids-H₂S donors (FAS I-IV)

3.2.2.1. *Dexamethasone succinate (13)*. 1.0g (2.55mmol) of dexamethasone **11** was dissolved in anhydrous pyridine (30mL) and 0.77g (7.65mmol) of succinic anhydride and 0.1eq DMAP were then added. After being stirred overnight at room temperature, the mixture was evaporated under reduced pressure. The resulting residue was then treated with 20 mL of water and the mixture was stirred for 20 min and then centrifuged. The obtained precipitate was washed again with H₂O and filtered. White powder of the product **13** (1.12g) was obtained in a yield of 89%. mp 188-189 °C

3.2.2.2. *Dexamethasone-succinate-TBZ (FAS I)*. To a solution of **13** (1g, 2.0mmol) in anhydrous tetrahydrofuran (30mL), 4-hydroxythiobenzamide (0.613g, 4.0mmol) and DMAP (0.024g, 0.2mmol) were added. The reaction mixture was kept on ice bath stirring under nitrogen for 10' and EDC (0.575g, 3.0mmol) was then added. After the addition, the ice bath was removed and the mixture was stirred under nitrogen atmosphere for 3 hour. The solvent was evaporated and the residue was purified by column chromatography on silica (ethyl acetate: hexane, 6:4). The obtained product **FAS I** was recrystallized from hexane, yielding 0.98g (78 %) of product as a colorless solid. mp 144.5–146.1 °C¹H NMR (DMSO-d₆) δ 0.78 (d, 3H, J=7.04), 0.88 (s, H), 1.05-1.10 (m, 1H), 1.48 (s, 3H), 1.53-1.79 (m, 4H), 1.88 (s, 3H), 2.09-2.18 (m, 1H), 2.26-2.40 (m,

2H), 2.58-2.61 (m, 3H), 2.79 (t, 2H, J=6.65, J=5.48), 2.82-2.91 (m, 1H), 2.87 (t, 2H, J=5.87, J=6.26), 5.16 (s, 2H), 5.99 (s, 1H), 6.21 (d, 1H, J=10.17), 7.14 (d, 1H, Ar-H, J=8.61), 7.28 (d, 1H, Ar-H, J=10.17), 7.91 (d, 2H, Ar-H, J=8.61), 9.50 (s, 1H, NH), 9.87 (s, 1H, NH); ^{13}C NMR (DMSO- d_6) δ 15.56, 16.70, 23.45, 27.96, 28.87, 29.36, 30.09, 32.35, 35.86, 36.13, 43.75, 48.21, 48.43, 68.70, 71.30, 90.94, 100.10, 121.61, 124.54, 127.18, 129.43, 137.52, 153.04, 153.10, 167.81, 170.92, 171.81, 185.73, 199.48, 205.11. ESI-HRMS (M + H) $^+$ m/z calcd 627.72 for $\text{C}_{35}\text{H}_{38}\text{FNO}_8\text{S}$; found 628.0.

3.2.2.3. Dexamethasone-succinate-ADT (FAS II). The desired product **FAS II** has been obtained following the same procedure above reported for **FAS I** starting from **13** (1g, 2.0mmol) and 5-(*p*-hydroxyphenyl)-1,2-dithione-3-thione (ADT-OH) (0.904g, 4.0mmol). ADT-OH was prepared from anethole and sulphur in dimethylformamide. Yield: 1.13g (81 %) of product **FAS II** as a colorless solid. mp 134.8–135.1 °C ^1H NMR (DMSO- d_6) δ 0.78 (d, 3H, J=7.04), 0.88 (s, H), 1.05-1.10 (m, 1H), 1.48 (s, 3H), 1.53-1.79 (m, 4H), 1.88 (s, 3H), 2.09-2.18 (m, 1H), 2.26-2.40 (m, 2H), 2.58-2.61 (m, 3H), 2.80 (t, 2H, J=6.65, J=5.48), 2.82-2.91 (m, 1H), 2.89 (t, 2H, J=5.87, J=6.26), 5.40 (s, 2H), 5.47 (d, 1H, J=10.17), 5.73 (s, 1H), 5.96 (s, 1H), 6.21 (d, 1H, J=10.17), 7.14 (d, 2H, Ar-H, J=8.61), 7.80 (s, 1H), 7.95 (d, 2H, Ar-H, J=8.61); ^{13}C NMR (DMSO- d_6) δ 15.57, 16.70, 23.40, 27.72, 28.88, 29.41, 30.71, 32.35, 34.13, 35.87, 36.12, 43.75, 48.27, 48.44, 68.71, 70.76, 71.12, 90.94, 123.49, 124.56, 129.12, 129.28, 129.45, 136.26, 153.18, 153.85, 167.50, 170.85, 171.83, 173.15, 185.72, 205.13. ESI-HRMS (M + H) $^+$ m/z calcd 700.86 for $\text{C}_{35}\text{H}_{37}\text{FNO}_8\text{S}_3$; found 700.

3.2.2.4. *Beclomethasone succinate (14)*. The desired product **14** has been obtained following the same procedure previously reported for compound **13** starting from 1.0 g (2.45mmol) of beclomethasone **12**, 0.73g (7.35mmol) of succinic anhydride and 0.1eq DMAP. Yield: 1.15g (**14**, 92%). mp 180–182.5 °C

3.2.2.5. *Beclomethasone-succinate-TBZ (FAS III)*. The desired product **FAS III** has been obtained following the same procedure above reported for **FAS I** starting from **14** (1g, 2.0mmol) and 4-hydroxythiobenzamide (0.613g, 4.0mmol). Yield: 0.87g (67 %) of **FAS III** as a colorless solid. mp 114.7–115.2 °C ¹H NMR (DMSO-d₆) δ 0.92 (s, 3H), 1.01 (d, 3H, J=7.04), 1.05-1.10 (m, 1H), 1.48 (s, 3H), 1.53-1.79 (m, 4H), 1.88 (s, 3H), 2.09-2.18 (m, 1H), 2.26-2.40 (m, 2H), 2.58-2.61 (m, 3H), 2.79 (t, 2H, J=6.65, J=5.48), 2.82-2.91 (m, 1H), 2.87 (t, 2H, J=5.87, J=6.26), 5.16 (s, 2H), 5.99 (s, 1H), 6.21 (d, 1H, J=10.17), 7.14 (d, 2H, Ar-H, J=8.61), 7.28 (d, 1H, J=10.17), 7.91 (d, 2H, Ar-H, J=8.61), 9.50 (s, 1H, NH), 9.87 (s, 1H, NH); ¹³C NMR (DMSO-d₆) δ 17.66, 20.20, 24.87, 28.04, 28.96, 29.40, 30.38, 34.50, 35.93, 43.26, 47.32, 49.33, 50.17, 70.02, 74.54, 86.01, 88.32, 121.64, 124.45, 129.03, 129.17, 137.52, 153.07, 153.24, 167.22, 170.95, 171.79, 185.69, 199.49, 205.81. ESI-HRMS (M + H)⁺ m/z calcd 644.17 for C₃₃H₃₈ClO₈S; found 643.8.

3.2.2.6. *Beclomethasone-succinate-ADT (FAS IV)*. The desired product **FAS IV** has been obtained following the same procedure above reported for **FAS I** starting from **14** (1g, 2.0mmol) and 5-(*p*-hydroxyphenyl)-1,2-dithione-3-thione (0.904g, 4.0mmol). Yield: 1.1g (78 %) of **FAS IV** as a colorless solid. mp 127.7–128.5 °C ¹H NMR (DMSO-d₆) δ 0.92 (s, 3H), 1.01 (d, 3H, J=7.04), 1.05-1.10 (m, 1H),

1.48 (s, 3H), 1.53-1.79 (m, 4H), 1.88 (s, 3H), 2.09-2.18 (m, 1H), 2.26-2.40 (m, 2H), 2.58-2.61 (m, 3H), 2.80 (t, 2H, J=6.65, J=5.48), 2.82-2.91 (m, 1H), 2.89 (t, 2H, J=5.87, J=6.26), 5.40 (s, 2H), 5.47 (d, 1H, J=10.17), 5.73 (s, 1H), 5.96 (s, 1H), 6.21 (d, 1H, J=10.17), 7.14 (d, 2H, Ar-H, J=8.61), 7.80 (s, 1H), 7.95 (d, 2H, Ar-H, J=8.61); ¹³C NMR (DMSO-d₆) δ 15.57, 16.70, 23.40, 27.72, 28.88, 29.41, 30.71, 32.35, 34.13, 35.87, 36.12, 43.75, 48.27, 48.44, 68.71, 70.76, 71.12, 90.94, 123.49, 124.56, 129.12, 129.28, 129.45, 136.26, 153.18, 153.85, 167.50, 170.85, 171.83, 173.15, 185.72, 205.13. ESI-HRMS (M + H)⁺ m/z calcd 717.3 for C₃₅H₃₇ClO₈S₃; found 716.8.

3.2.3. General procedure for the preparation of 1,2,4-thiadiazoline-3,5-diones (THIA I-VII)

A three-necked flask was equipped with a mechanical stirrer and charged with an ice-cold solution of corresponding isothiocyanate (1eq) and isocyanate (1eq) in anhydrous diethyl ether. Sulfuryl chloride (1eq), dissolved in a minimum volume of anhydrous diethyl ether, was added dropwise under inert atmosphere, keeping the mixture at 0 °C. After completion of the addition, the solution was stirred at room temperature for 48 h. The obtained solid was filtered, dissolved in 10 mL of water and vigorously stirred under reflux for 30 minutes. The reaction mixture was gradually cooled to 0 °C and the solid was recrystallized from water, filtered and dried to yield the pure product as a white solid.

3.2.3.1. 2,4-diphenyl-1,2,4-thiadiazoline-3,5-dione (THIA I). Compound **THIA I** was prepared from phenyl-isothiocyanate (1g, 7.4mmol) and phenyl-isocyanate (0.881g, 7.4mmol) according to a procedure similar to that described above.

Yield=74%: mp 119.1–120 °C; ¹H NMR (400 MHz, CDCl₃) δ 7.31 (t, 2H, Ar-H, J=7.04, J=6.65), 7.46 (t, 4H, Ar-H, J=12.52, J=13.78), 7.55 (d, 2H, Ar-H, J=7.82), 7.58 (d, 2H, Ar-H, J=7.43); ¹³C NMR (400 MHz, CDCl₃) δ 123.5, 127.2, 127.4, 129.4, 129.5, 129.6, 132.6, 135.8, 150.4, 164.7; ESI-HRMS (M+H)⁺ m/z calcd 270.31 for C₁₄H₁₀N₂O₂S; found 271.1.

3.2.3.2. 4-(4-methoxyphenyl)-2-phenyl-1,2,4-thiadiazoline-3,5-dione (**THIA II**)

Compound **THIA II** was prepared from phenyl-isothiocyanate (1g, 7.4mmol) and 4-methoxyphenyl-isocyanate (0.958mL, 7.4mmol) according to a procedure similar to that described above. Yield=72%: mp 155.3–155.4 °C; ¹H NMR (400 MHz, CDCl₃) δ 3.83 (s, 3H, OCH₃, J=), 6.95 (d, 2H, Ar-H, J=9.0), 7.43-7.47 (m, 5H, Ar-H), 7.52 (d, 2H, Ar-H, J=7.43); ¹³C NMR (400 MHz, CDCl₃) δ 55.6, 114.8, 126.3, 127.3, 128.1, 129.3, 129.4, 132.7, 150.8, 158.9, 165.0; ESI-HRMS (M+H)⁺ m/z calcd 300.33 for C₁₅H₁₂N₂O₃S; found 301.1.

3.2.3.3. 4-(4-methoxyphenyl)-2-p-tolyl-1,2,4-thiadiazoline-3,5-dione (**THIA III**)

Compound **THIA III** was prepared from p-tolyl-isothiocyanate (1g, 6.7mmol) and 4-methoxyphenyl-isocyanate (0.870mL, 6.7mmol) according to a procedure similar to that described above. Yield=74%: mp 156.3–156.5 °C; ¹H NMR (400 MHz, CDCl₃) δ 2.41 (s, 3H, -CH₃), 3.83 (s, 3H, -OCH₃), 6.95 (d, 2H, Ar-H, J=9.0), 7.31 (d, 4H, Ar-H, J=6.52), 7.45 (d, 2H, Ar-H, J=9.0); ¹³C NMR (400 MHz, CDCl₃) δ 21.2, 55.6, 114.8, 126.2, 127.1, 128.2, 130.1, 139.5, 150.9, 158.8; ESI-HRMS (M+H)⁺ m/z calcd 314.36 for C₁₅H₁₂N₂O₃S; found 315.1.

3.2.3.4. *2,4-bis(4-methoxyphenyl)-1,2,4-thiadiazoline-3,5-dione* (**THIA IV**)

Compound **THIA IV** was prepared from 4-methoxyphenyl-isothiocyanate (1g, 6.1mmol) and 4-methoxyphenyl-isocyanate (0.785mL, 6.1mmol) according to a procedure similar to that described above. Yield=71%: mp 177.8–177.3 °C; ¹H NMR (400 MHz, CDCl₃) δ 3.83 (s, 3H, -OCH₃), 3.84 (s, 3H, -OCH₃), 6.95 (d, 2H, Ar-H, J=7.04), 7.01 (d, 2H, Ar-H, J=7.43), 7.34 (d, 2H, Ar-H, J=6.65), 7.45 (d, 2H, Ar-H, J=7.05); ¹³C NMR (400 MHz, CDCl₃) δ 55.5, 55.6, 114.7, 114.8, 125.3, 126.2, 128.2, 128.6, 151.0, 158.8, 160.0, 165.2; ESI-HRMS (M+H)⁺ m/z calcd 330.36 for C₁₆H₁₄N₂O₄S; found 331.1.

3.2.3.5. *2-(4-chlorophenyl)-4-(4-methoxyphenyl)-1,2,4-thiadiazoline-3,5-dione* (**THIA V**)

Compound **THIA V** was prepared from 4-chlorophenyl-isothiocyanate (1g, 5.9mmol) and 4-methoxyphenyl-isocyanate (0.764mL, 5.9mmol) according to a procedure similar to that described above. Yield=76%: mp 182.7–183.4 °C; ¹H NMR (400 MHz, CDCl₃) δ 3.83 (s, 3H, OCH₃), 6.95 (d, 2H, Ar-H, J=8.61), 7.40 (d, 2H, Ar-H, J=8.61), 7.44 (d, 2H, Ar-H, J=7.04), 7.49 (d, 2H, Ar-H, J=8.61); ¹³C NMR (400 MHz, CDCl₃) δ 55.6, 114.8, 126.4, 127.8, 128.6, 129.6, 131.1, 135.2, 150.5, 159.0, 164.8; ESI-HRMS (M+H)⁺ m/z calcd 334.78 for C₁₅H₁₁ClN₂O₃S; found 335.8.

3.2.3.6. *2-cyclohexyl-4-(4-methoxyphenyl)-1,2,4-thiadiazoline-3,5-dione* (**THIA VI**)

Compound **THIA VI** was prepared from cyclohexyl-isothiocyanate (1g, 7.1mmol) and 4-methoxyphenyl-isocyanate (0.917mL, 7.1mmol) according to a procedure similar to that described above. Yield=77%: mp 98.8–99.7 °C; ¹H

NMR (400 MHz, CDCl₃) δ 1.18-1.41 (m, 6H, cyclohexane: (CH₂)₃), 1.78-1.89 (q, 2H, cyclohexane: CH₂), 2.25-2.31 (q, 2H, cyclohexane: CH₂), 3.81 (s, 3H, OCH₃), 4.18-4.23 (qt, 1H, cyclohexane-CH), 6.92 (d, 2H, Ar-H, J=11.7), 7.37 (d, 2H, Ar-H, J=8.7); ¹³CNMR(400MHz,CDCl₃)δ 25.2, 26.1, 29.1, 55.0, 55.6, 118.9, 129.5, 132.4, 150.5, 159.0, 164.7; ESI-HRMS (M+H)⁺ m/z calcd 306.38 for C₁₅H₁₈N₂O₃S; found 307.1.

3.2.3.7. 2-benzyl-4-(4-methoxyphenyl)-1,2,4-thiadiazoline-3,5-dione (**THIA VII**)

Compound **THIA VII** was prepared from benzyl-isothiocyanate (1g, 6.7mmol) and 4-methoxyphenyl-isocyanate (0.868mL, 6.7mmol) according to a procedure similar to that described above. Yield=75%: mp 113.7–114.5 °C; ¹H NMR (400 MHz, CDCl₃) δ 3.81 (s, 3H, OCH₃), 4.90 (s, 2H, N-CH₂), 6.92 (d, 2H, OCH₃, J=8.60), 7.24-7.39 (m, 5H, Ar-H); ¹³C NMR (400 MHz, CDCl₃) δ 46.2, 55.6, 114.7, 126.2, 128.1, 128.4, 128.8, 129.1, 135.1, 151.4, 158.8, 165.4; ESI-HRMS (M+H)⁺ m/z calcd 314.36 for C₁₆H₁₄N₂O₃S; found 315.0.

3.3. Pharmacology

3.3.1. Cysteine surrogates: propargylamide and *n*-butylamide derivatives

3.3.1.1. Isolated rat aortic ring assay

CD-1 mice were sacrificed and thoracic aorta was rapidly dissected and cleaned from fat and connective tissue. For endothelium-denuded rings, the endothelial layer was removed by gently rubbing the internal surface of the

vascular lumen. Rings of 1.5–2 mm length were cut and mounted in isolated organ baths filled with gassed Krebs solution (95% O₂ + 5% CO₂) at 37 °C linked to isometric force transducers (Ugo Basile, Comerio, Varese, Italy). The composition of the Krebs solution was as follows (mol/l): NaCl 0.118, KCl 0.0047, MgSO₄ 0.0023, KH₂PO₄ 0.0012, CaCl₂ 0.0025, NaHCO₃ 0.025 and Glucose 0.010. Rings were initially stretched until a resting tension of 1.5 g was reached and allowed to equilibrate for at least 45 min during which tension was adjusted, when necessary, to 1.5 g and bathing solution was periodically changed. In a preliminary study a resting tension of 1.5 g was found to develop the optimal tension to stimulation with contracting agents.

In each experiment, rings were firstly contracted with L-phenylephrine (PE) 3 µmol/l and subsequently with L-phenylephrine (PE) 1 µmol/l until the response were reproducible. To verify the integrity of the endothelium, Ach cumulative concentration-response curve (10nM – 30µM) was performed on PE-contracted rings.

Aortic rings were contracted with PE (1µM), once plateau was reached, a cumulative concentration-response curve to surrogate cysteine or derived compounds (10nM – 300µM) was performed.

In another set of experiments aortic rings were incubated with the cysteine surrogates or with their derivatives at different concentration (1mM or 100µM) for 30 minutes. After that time, rings were contracted with PE (1µM), once reached a plateau, a cumulative concentration-response curve to L-cysteine (1µM- 3 mM) was performed.

All data are presented as means \pm SEM. Statistical analysis was performed by one-way ANOVA followed by Newman–Keuls multiple comparison test. Differences were considered statistically significant when P-value was less than 0.05. GraphPadPrism software (GraphPad Software, Inc., La Jolla, CA, USA) was used for all the statistical analysis.

3.3.1.2. Measurement of H₂S production: methylene blue assay

H₂S determination was performed according to Stipanuk and Beck (Stipanuk and Beck, 1982) with modifications.

Briefly, thoracic aorta was dissected, placed in sterile phosphate buffer solution and cleaned of fat and connective tissue. The aortic rings were homogenized in a lysis buffer (potassium phosphate buffer 100 mM pH=7.4, sodium orthovanadate 10 mM and protease inhibitor) and the protein concentration was determined using Bradford assay (Bio-Rad Laboratories, Milano, Italy). The homogenates were treated with cysteine surrogates and their derived compounds at different concentration for 30 minutes and then added in a reaction mixture (total volume 500 μ l) containing piridoxal-5'-phosphate (2mM, 20 μ l), L-cysteine (10mM, 20 μ l) and saline (30 μ l). The reaction was performed in parafilmed eppendorf tubes and initiated by transferring tubes from ice to a water bath at 37°C. After incubation of 30 minutes, ZnAc (1%, 250 μ l) was added to trap evolved H₂S followed by TCA (10%, 250 μ l). Subsequently, N,N-dimethyl-*p*-phenylenediamine-sulfate (20 μ M, 133 μ l) in 7.2M HCl and FeCl₃ (30 μ M, 133 μ l) in 1.2M HCl were added. After 20 minutes absorbance values were measured at a wavelength of 650 nm. All samples were assayed in duplicate and H₂S

concentration was calculated against a calibration curve of NaHS (3.12-250 μ M). Results were expressed as nmoles per milligram of protein.

3.3.2. Glucocorticoids-H₂S donors

3.3.2.1. Cell cultures and Nitrite determination

The murine monocyte/macrophage J774 cell line was grown in Dulbecco's modified Eagle's medium (DMEM) supplemented with 2 mM glutamine, 25 mM hepes, penicillin (100 units/mL), streptomycin (100 μ g/mL), 10% fetal bovine serum (FBS), and 1.2% sodium pyruvate.

Cells were plated to a seeding density of either 2×10^6 in P60 well plates or 2.5×10^5 in 24 multiwell plates. Cells were pretreated (for 2h) with increasing concentration of the tested compounds and stimulated with LPS from *Escherichia coli*, serotype 0111:B4 (10 μ g/mL). Treatment with tested compounds and/or LPS was carried out under serum-free conditions. The concentrations of the FAS utilized (0.1 and 1 μ g/mL) were chosen according to what was reported in the literature.

Cells were pretreated with tested compounds for 2 hand further incubated for 24 h with LPS (10 μ g/mL). At the end of the incubation, the supernatants were collected for the nitrite measurement.

The nitrite concentration in the samples was measured by the Griess reaction, by adding 100 μ L of Griess reagent (0.1% N-(1-naphthyl)ethylenediamide dihydrochloride in H₂O and 1% sulfanilamide in 5% H₃PO₄; vol. 1:1) to 100 μ L samples. The optical density at 550nm (OD₅₅₀) was measured using an ELISA microplate reader (SLT Lab instruments, Salzburg,

Austria). Nitrite concentration was calculated by comparison with OD₅₅₀ of standard solutions of sodium nitrite prepared in culture medium.

3.3.3. 1,2,4-Thiadiazolidine-3,5-diones

3.3.3.1. Amperometric determination of H₂S

The characterization of the potential H₂S-generating properties of the tested compounds has been carried out by an amperometric approach, using the Apollo-4000 free radical analyzer (WPI) detector and H₂S-selective mini-electrodes.

The experiments have been carried out at room temperature. The H₂S-selective mini-electrode was equilibrated in 10 mL of the assay buffer (NaH₂PO₄·H₂O 1.28 g, Na₂HPO₄·12H₂O 5.97 g, NaCl 43.88 g in 500 mL H₂O), until the recovery of a stable baseline. Then, 100 µL of a DMSO solution of all the tested THIAAs was added (the final concentration of the tested compounds was 1 mM; the final concentration of DMSO in the AB was 1%).

The selected compounds were tested in absence and in presence of L-cysteine and when required by the experimental protocol, L-cysteine (4 mM) was added before the addition of the THIAAs. The H₂S generation was monitored for 20 min. H₂S concentration was determined against a calibration curve obtained plotting amperometric currents (recorded in pA) vs. increasing concentrations of NaHS (1, 3, 5, and 10 µmol/L) at pH 4.0.

3.3.3.2. Isolated rat aortic ring assay

CD-1 mice were sacrificed and thoracic aorta was rapidly dissected and cleaned from fat and connective tissue. For endothelium-denuded rings, the endothelial layer was removed by gently rubbing the internal surface of the

vascular lumen. Rings of 1.5–2 mm length were cut and mounted in isolated organ baths filled with gassed Krebs solution (95% O₂ + 5% CO₂) at 37 °C linked to isometric force transducers (Ugo Basile, Comerio, Varese, Italy). The composition of the Krebs solution was as follows (mol/l): NaCl 0.118, KCl 0.0047, MgSO₄ 0.0023, KH₂PO₄ 0.0012, CaCl₂ 0.0025, NaHCO₃ 0.025 and Glucose 0.010. Rings were initially stretched until a resting tension of 1.5 g was reached and allowed to equilibrate for at least 45 min during which tension was adjusted, when necessary, to 1.5 g and bathing solution was periodically changed. In a preliminary study a resting tension of 1.5 g was found to develop the optimal tension to stimulation with contracting agents.

In each experiment, rings were firstly contracts with L-phenylephrine (PE) 3 µmol/l and subsequently with L-phenylephrine (PE) 1 µmol/l until the response were reproducible. To verify the integrity of the endothelium, Ach cumulative concentration-response curve (10nM – 30µM) was performed on PE-contracted rings.

Aortic rings were contracted with PE (1µM), once plateau was reached, a cumulative concentration-response curve to THIA (10nM – 300µM) was performed. In another set of experiments, rings were denuded of the endothelium and THIA cumulative concentration-response curve was performed (10nM – 300µM).

4. Results and Discussion

4.1. Cysteine surrogates: propargylamide and *n*-butylamide derivatives

In order to evaluate the inhibitory activity of the selected compounds, we firstly tested the commercially available cysteine surrogates on the L-cysteine-induced vasorelaxation in rat aortic rings and compared the results to the effect obtained with synthesized compounds. In physiological conditions, L-cysteine induced vasorelaxation, in a concentration-dependent manner, with a maximum value of $39,8 \pm 5\%$.

The pre-treatment with the compound **II** reduced the L-cysteine-induced vasorelaxation in a concentration-dependent manner. Indeed, the tested compound at the concentration of 1 mM reduced the vasorelaxation significantly and at the concentration of 3 mM achieved the E_{\max} value of $13.7 \pm 6.1\%$ ($n=3;***=p<0,001$). In contrast, the treatment with the compound **II** (**Figure 11**) tested at the concentration of 100 μM did not affect the L-cysteine-induced vasorelaxation (E_{\max} $27,7 \pm 11,1\%$ **II** vs $39,8 \pm 5\%$ **vehicle** respectively; $n=3$).

Figure 12 shows the results obtained with the compound **III**. In particular, this compound, tested at the concentration of 10 mM, significantly reduced the L-cysteine-induced vasorelaxation, (E_{\max} $26 \pm 5\%$ **III** vs $39,8 \pm 5\%$ **vehicle**; $n=4$). This effect was concentration-dependent, in fact, the pre-treatment with the compound **III** at the concentration of 1 μM , did not affect the L-cysteine-induced vasorelaxation (E_{\max} $26 \pm 5\%$ **III** vs $39,8 \pm 5\%$ **vehicle**; $n = 4$).

In contrast, as shown in **figure 10**, the pre-treatment with the compound **I** induced a significant increase of the L-cysteine induced vasorelaxation effect (E_{\max} $74.0 \pm 17.6\%$ **I** vs $39.8 \pm 5\%$ **vehicle**; $n = 4$; $*** = p < 0.001$).

Incubation of aortic rings with the compound **IIa** at the concentration of $100 \mu\text{M}$ (**Figure 14**) completely abrogated the L-cysteine-induced vasorelaxation, achieving the E_{\max} value of $13.7 \pm 6.1\%$ ($n=3$; $***=p<0,001$), but unaffected by **Ia** (**Figure 13**).

A similar pattern of inhibition was obtained with the compound **IIIa** (**Figure 15**). In particular L-cysteine-induced vasorelaxation was reduced by pre-treatment with the compound **IIIa**. However, compared to **IIa**, the compound **IIIa**, even at the highest concentration tested (1mM), was not able to completely abrogate the relaxation (E_{\max} $13,3 \pm 1,8\%$ **IIIa** 1mM ; $24,0 \pm 2,0$ **IIIa** $100 \mu\text{M}$, vs $39,8 \pm 5\%$ vs **vehicle**; $n=3$; * $p < 0,05$; ** $p < 0,01$).

Furthermore, the synthesized compounds were also tested for their potential as vasorelaxing agents on rat aortic rings and these relaxations were compared to those obtained in the presence of L-cysteine (**Figure 16**). Compounds **Ia** and **IIa** have also showed a vasorelaxing ability that was similar or slightly higher than the L-cysteine (E_{\max} $51,3 \pm 14,8\%$ **IIa**; $49 \pm 10,0\%$ **IIIa**; $31 \pm 16,1\%$ vs $38,8 \pm 9,5\%$ **Ia** vs **L-cys**; $n=3$).

In another set of experiments, *n*-butylamide derivatives (**Ib-IIIb**) were tested for their ability to inhibit the L-Cys induced vasorelaxation on rat aortic rings pre-contracted with PE but none of tested compounds affected the vasorelaxation effect (data not shown).

With regard to parsalimide (**IV**) and its derivatives (**IVa** and **IVb**), all of them significantly inhibited L-cysteine induced vasorelaxation (**Figure 17**) and **IV** and **IVb** also showed vasorelaxant activities (**Figure 18**).

Additionally, in order to evaluate a possible involvement of L-Cys/H₂S pathway, the compounds showing the higher inhibitory action, were tested by measuring H₂S production and the methylene blue assay was performed.

Under basal conditions, tissue homogenates produced $1,4 \pm 0,08$ % nmol of H₂S per mg of protein and the addition of exogenous L-Cys boosted the production of H₂S by 2-fold.

Incubation with compounds **II**, **III**, **IIa** and **IIIa** significantly inhibited the increase in H₂S production stimulated with L-Cys. These results confirmed those obtained from *ex vivo* experiments. In fact, as shown in **figure 20**, pre-treatment with the propargylamide derivative compounds (**IIa**, 100 μ M and **IIIa**, 1mM) reduced H₂S production compared to the vehicle (E_{max} $2,7 \pm 0,09$ nmol/mg).

Comparing the compounds **IIa** (E_{max} $2,1 \pm 0,07\%$ nmol/mg protein^{*min-1} (n=4)) and **IIIa** (E_{max} $1,960 \pm 0,06\%$ nmol/mg protein^{*min-1} (n=3)), they showed a comparable inhibitory action on H₂S production, but the effect of the compound **IIa** was obtained with a lower dose (**IIa**, 100 μ M vs **IIIa**, 1mM).

On the basis of the obtained results, we decided to compare the inhibitory activity of the compound **IIa** with the known CSE inhibitor, D,L-propargylglycine (**PGG**) (**Figure 19**).

Incubation of aortic rings with the compound **IIa** completely abrogated the L-cysteine-induced vasorelaxation, achieving the E_{max} value of $3,7 \pm 0,88\%$ (n=3; ***=p<0,001), while **PGG** reduced but not completely abrogated

the L-cysteine-induced vasorelaxation (E_{max} $20,3 \pm 5.2\%$ nmol/mg protein^{*min⁻¹}¹(n=3) vs $45,3 \pm 6.7\%$ nmol/mg protein^{*min⁻¹} vehicle), despite it was tested at an higher concentration (1mM vs 100 μ M; PGG vs IIa).

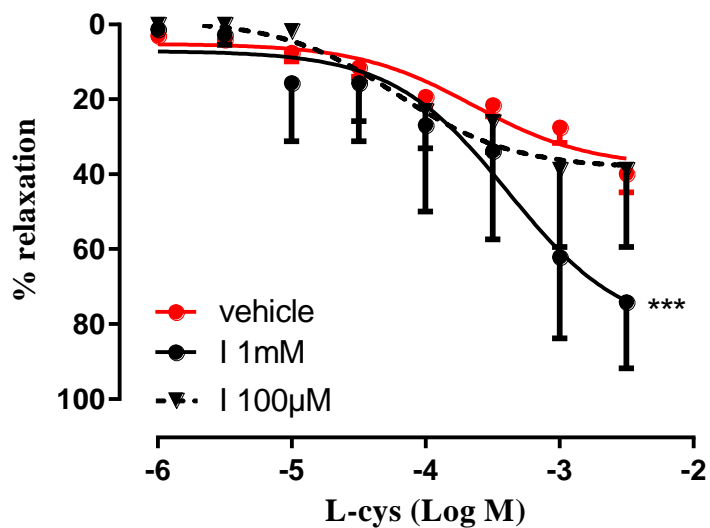


Figure 10- Effect of compound I on L-cysteine-induced vasorelaxation.

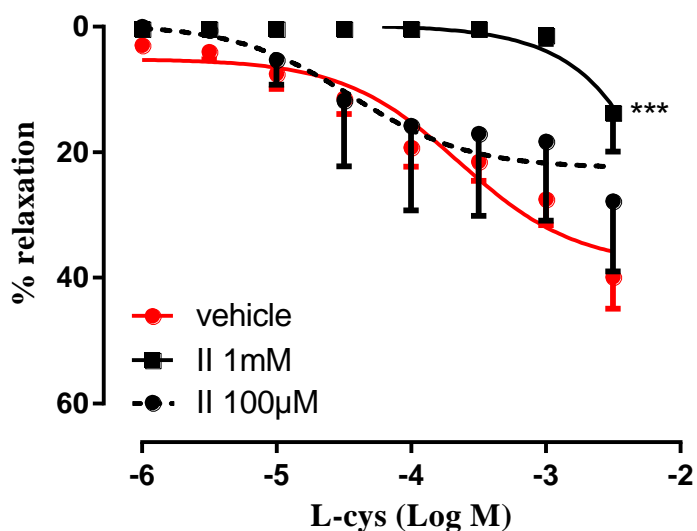


Figure 11- Effect of compound II on L-cysteine-induced vasorelaxation.

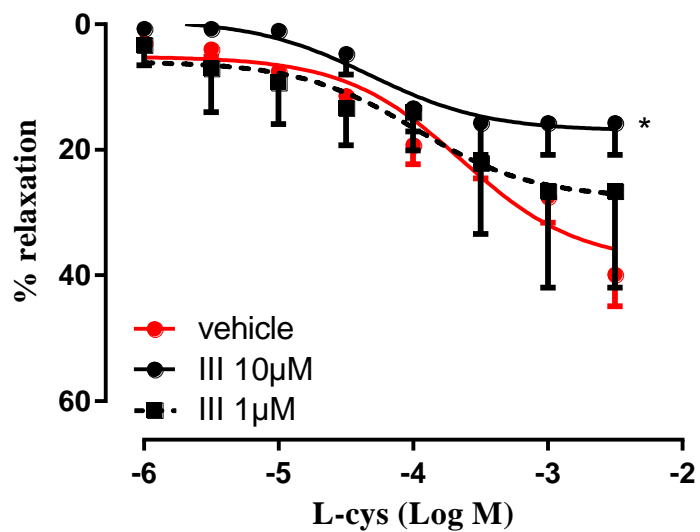


Figure 12- Effect of compound **III** on L-cysteine-induced vasorelaxation.

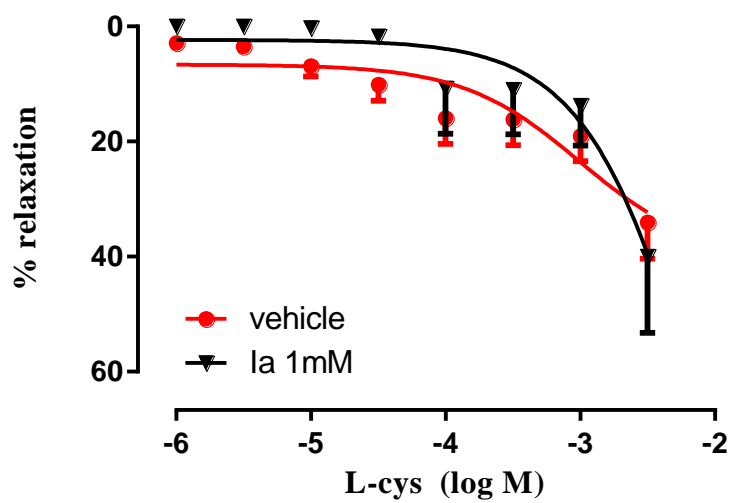


Figure 13- Effect of compound **Ia** on L-cysteine-induced vasorelaxation.

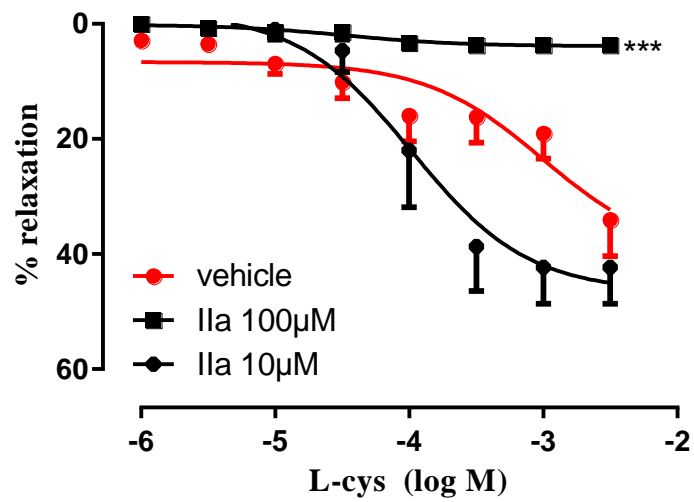


Figure 14- Effect of compound **IIa** on L-cysteine-induced vasorelaxation.

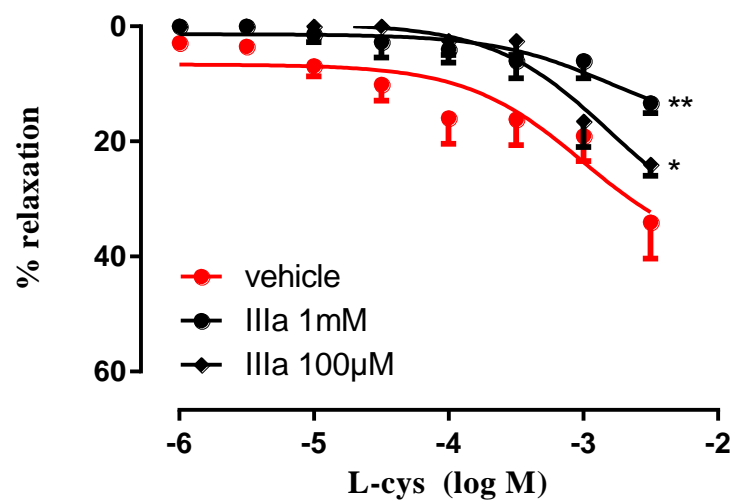


Figure 15- Effect of compound **IIIa** on L-cysteine-induced vasorelaxation.

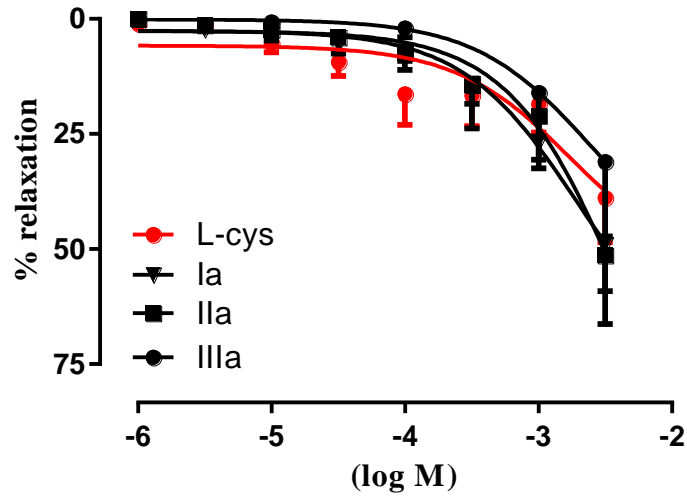


Figure 16- Effect of propargylamide derivatives (**Ia-IIIa**), compared to L-cysteine, on vasorelaxation.

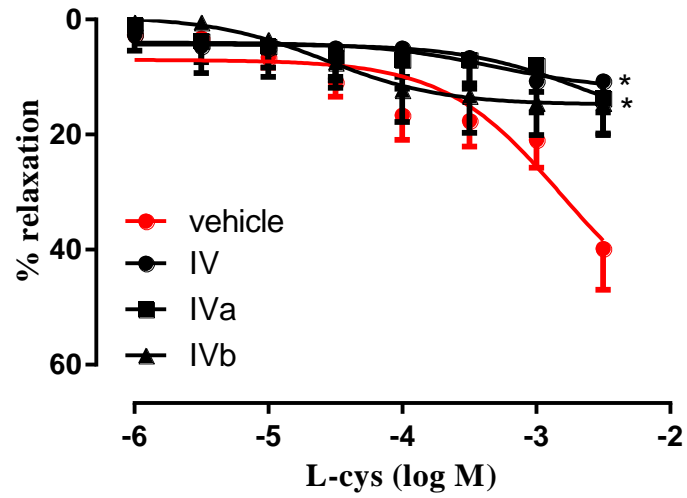


Figure 17- Effect of parsalimide (**IV**) and derivatives (**IVa-IVb**) on L-cysteine-induced vasorelaxation.

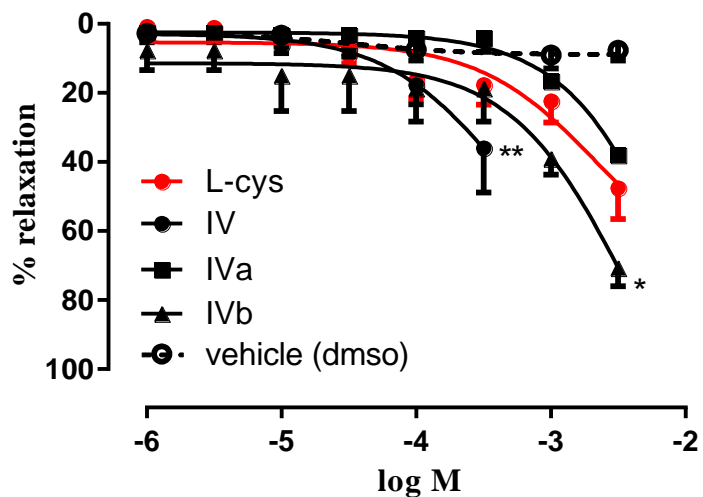


Figure 18- Effect of propargylamide derivatives (**Ia-IIIa**), compared to L-cysteine on vasorelaxation.

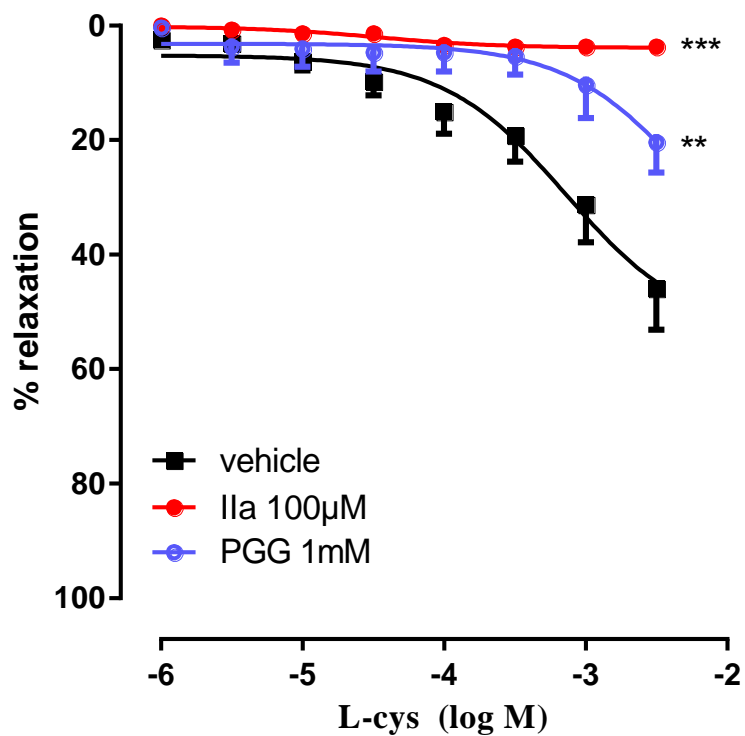


Figure 19- Effect of compound **IIa**, compared to the CSE inhibitor **PGG** on L-cysteine-induced vasorelaxation.

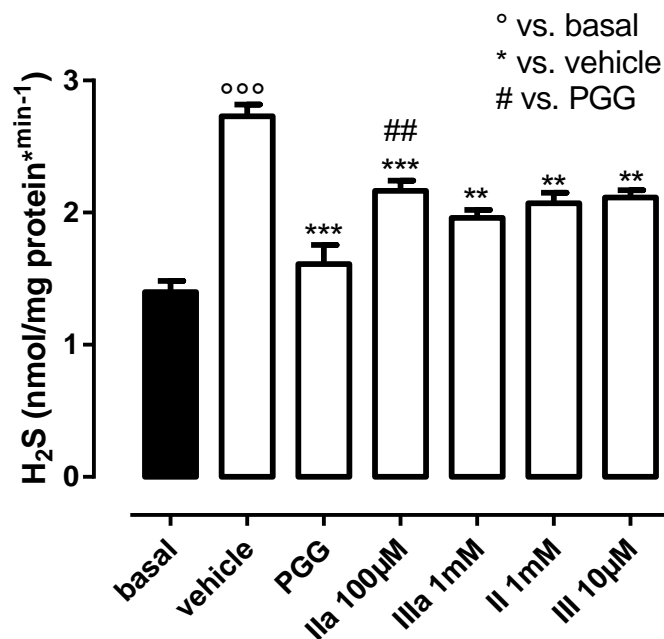


Figure 20- Measurement of H₂S production in rat aortic rings homogenates with **II**, **III**, **IIa** and **IIIa** compounds, compared to **PGG**.

4.2. Glucocorticoids-H₂S donors

Asthma is one of the most common chronic inflammatory disorder of the airways of the lungs. Nitric oxide (NO) is endogenously produced in mammalian airways by nitric oxide synthase (NOS) and is known to regulate many aspects of human asthma, including the modulation of airway and vascular smooth muscle tone and the inflammation. Asthmatic patients show an increased expression of inducible nitric oxide synthase (iNOS) in airway epithelial cells and an increased level of NO in exhaled air. iNOS produces large amounts of NO (Alderton et al., 2001), in response to inflammatory signals, such as cytokines and lipopolysaccharides (LPS).

The glucocorticoids have been reported to inhibit iNOS induction, which may contribute to the inflammation-reducing effects. Specifically, glucocorticoids

(10-250 nM) inhibited the expression of iNOS mRNA and protein dose and time dependently, resulting in decreases in NO production.

On the other hand, a growing number of observations suggest that, similarly to NO, hydrogen sulfide might be of biological relevance as an endogenous gasotransmitter in the pathogenesis of airway diseases, such as COPD and asthma (Chen and Wang, 2012). Endogenous H₂S may exert its anti-inflammatory effect by inhibiting inducible nitric oxide synthase (iNOS)/NO pathway. Cystathionine- γ -lyase is mainly expressed in airway and vascular smooth muscle cells in rat lung tissue.

For these reasons, we tested the synthesized hybrids on J774 macrophages stimulated with LPS (10 μ g/mL), measuring the NO production and comparing obtained data to the pure glucocorticoids (dexamethasone and beclomethasone succinates).

In J774 cells stimulated with LPS, pure glucocorticoids clearly inhibited NO formation in a concentration-dependent manner, as shown in **Figure 21** and **22**, comparing two sets of data at different concentration (log M -7 vs. log M -6).

When succinate glucocorticoids and derivatives were given to cells 2 h before LPS, the inhibitory activity of dexamethasone succinate was lower than its derivatives, glucocorticoid-H₂S donors (**FAS I** and **II**), but this effect did not occur with beclomethasone derivatives. Specifically, pretreatment with **FAS III** and **IV** 2 h before LPS did not induce any inhibition (**Figure 21**).

These data suggested that a pre-incubation of 2 h was not enough to lead to the hydrolysis of ester bond in beclomethasone-hybrids, allowing the release of the pure glucocorticoid and its H₂S donor moieties.

Consequently, another set of experiments was performed and J774 cells were pretreated for a longer time (4h). The obtained data confirmed the enhanced inhibitory activities of dexamethasone-H₂S donors (**FAS I** and **II**), compared to the precursor, dexamethasone succinate (**Figure 22**).

These results supported our hypothesis that the anti-inflammatory effect could be enhanced with hybrids containing glucocorticoids and H₂S releasing moiety, both responsible for inhibitory action on inducible nitric oxide synthase.

In contrast, the effect of beclomethasone succinate on nitrite production, even at the highest concentration used (1μM), resulted equal or greater than that obtained with its derivatives (**FAS IV** and **III**, respectively).

This result can be explained by the presence of a chlorine atom into the 9-position of a pregnane steroid, instead of fluorine, that could have a long range effect on ester bond, slowing down the hydrolysis and the subsequent hydrogen sulfide release.

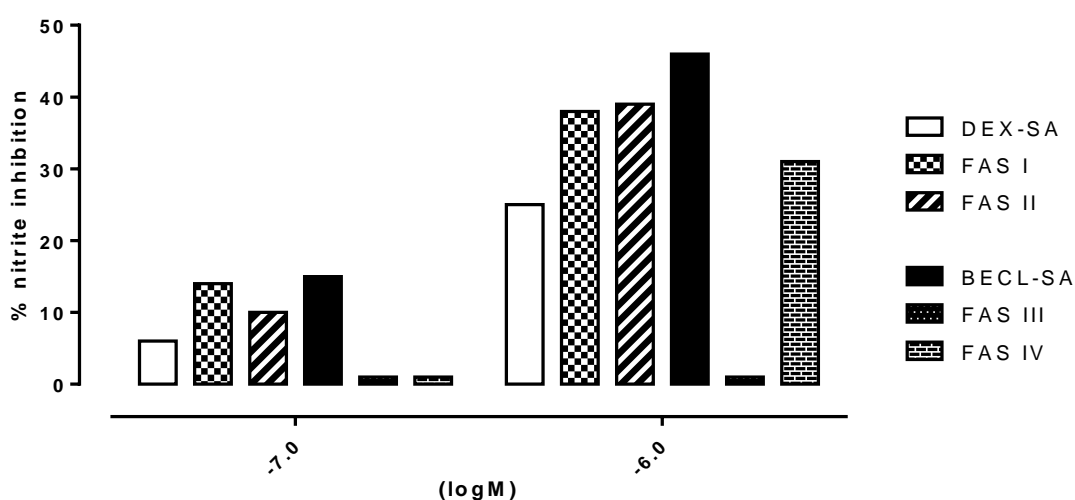


Figure 21 - Effect of glucocorticoids and derivatives on nitrite production. J774 macrophages were pretreated for 2 h with glucocorticoids and derivatives.

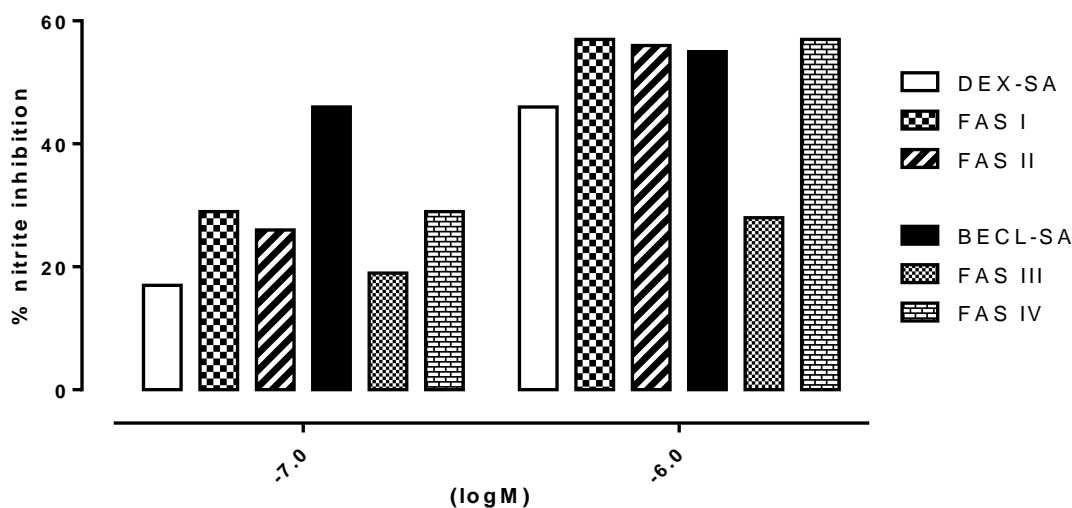


Figure 22 - Effect of glucocorticoids and derivatives on nitrite production. J774 macrophages were pretreated for 4 h with glucocorticoids and derivatives.

4.3. 1,2,4-Thiadiazolidine-3,5-diones

In order to characterize the potential H₂S-releasing properties of 1,2,4-thiadiazolidine-3,5-diones, all compounds were added at 1 mM concentration to the assay buffer. The generation of H₂S was evaluated by an amperometric approach, allowing to have a real-time determination of the H₂S-release and thus to perform a qualitative/quantitative description of the process.

The experiments were also performed in the presence of 4 mM L-cysteine. The incubation of **THIA I-VII** in the assay buffer led to a negligible release of H₂S (data not shown); in contrast, in the presence of L-cysteine, all compounds (**VII** except) exhibited a slow and significant release of H₂S (**Figure 23**).

Noteworthy, the previous amperometric measurements indicated that THIAs ensured a long-lasting release of H₂S, requiring the presence of L-cysteine.

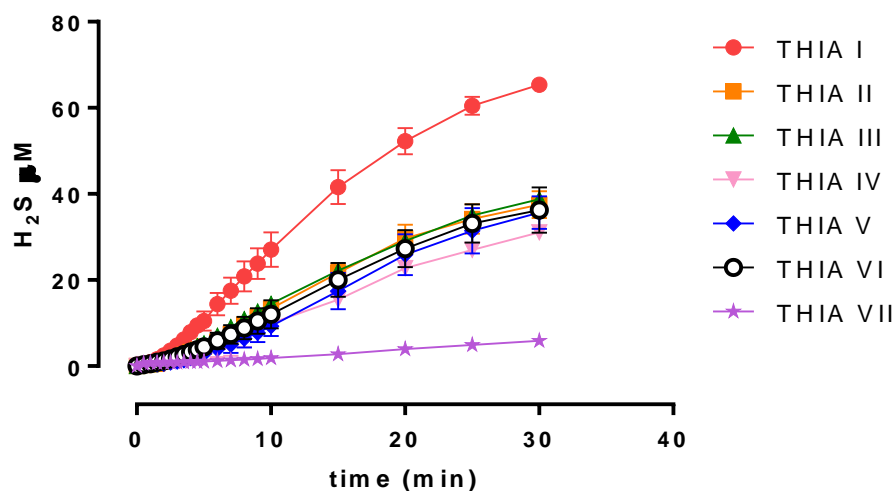


Figure 23 - Amperometric determination of H₂S. Hydrogen sulfide-release from THIAs in the presence of L-cysteine. The curves describe the increase of the H₂S concentration with respect to time, following the incubation of THIA I-VII in the presence of L-cysteine.

Additionally, to prove the nature of 1,2,4 thiadiazolidine 3,5 diones as spontaneously releasing H₂S donors, further pharmacological experiments were performed. In these studies, the endothelium-intact or endothelium-denuded aortic rings were exposed to the **THIA I-VII**.

The tested compounds induced a vasorelaxant effect, irrespective of whether endothelium was present or not. In particular, incubation of aortic rings with **THIA I (Figure 24)**, **II (Figure 25)**, **III (Figure 26)**, **V (Figure 28)** and **VI (Figure 29)** allowed us to obtain the maximum vasorelaxant effect, that was independent of endothelium.

Furthermore, the pre-treatment of endothelium-intact aortic rings with **THIA IV** induced a maximum vasorelaxation, as well as the other compounds of the series, but the response was reduced in endothelium-denuded rings (75%)

(Figure 27). Instead, the removal of the endothelium showed an increase of the vasorelaxing capacity of THIA VII (Figure 30). The obtained results suggested that the presence of endothelium with all their components could affect the release of the hydrogen sulfide.

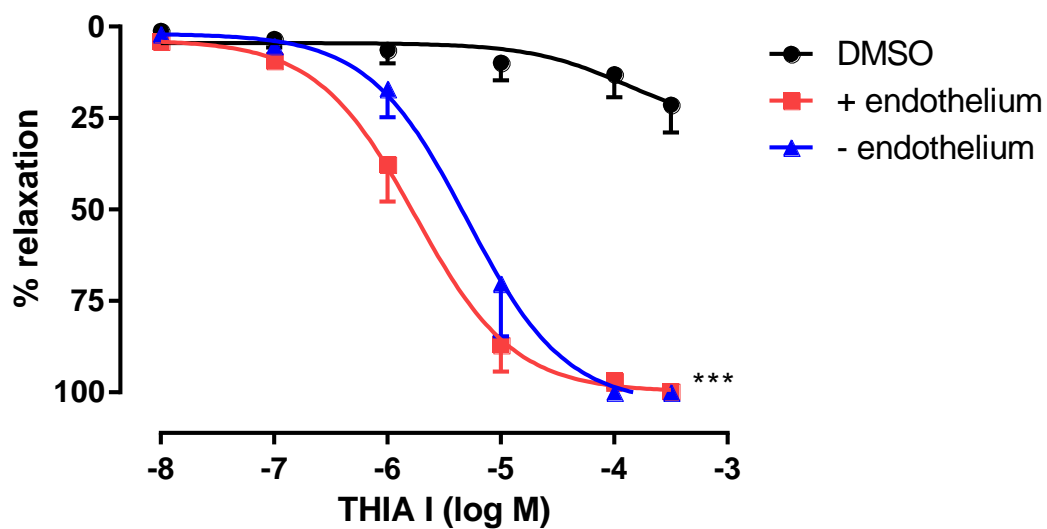


Figure 24 – Effect of THIA I compound on endothelium-denuded and endothelium-intact aortic rings.

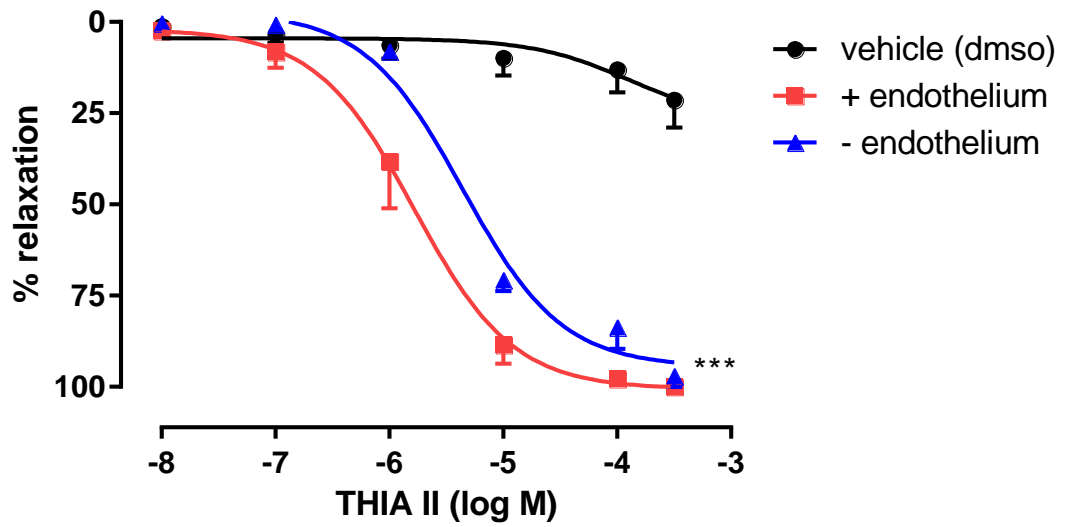


Figure 25 – Effect of THIA II compound on endothelium-denuded and endothelium-intact aortic rings.

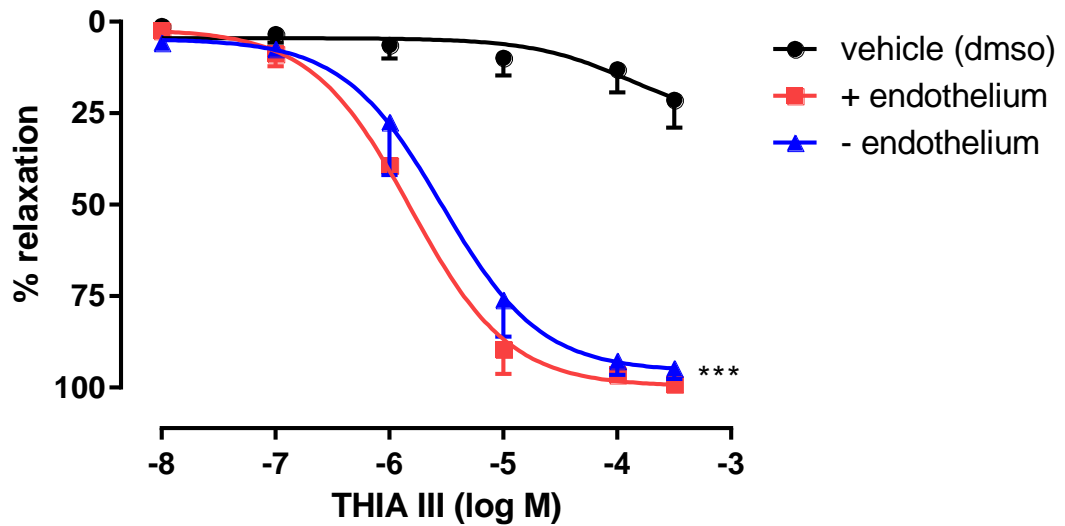


Figure 26 – Effect of THIA III compound on endothelium-denuded and endothelium-intact aortic rings.

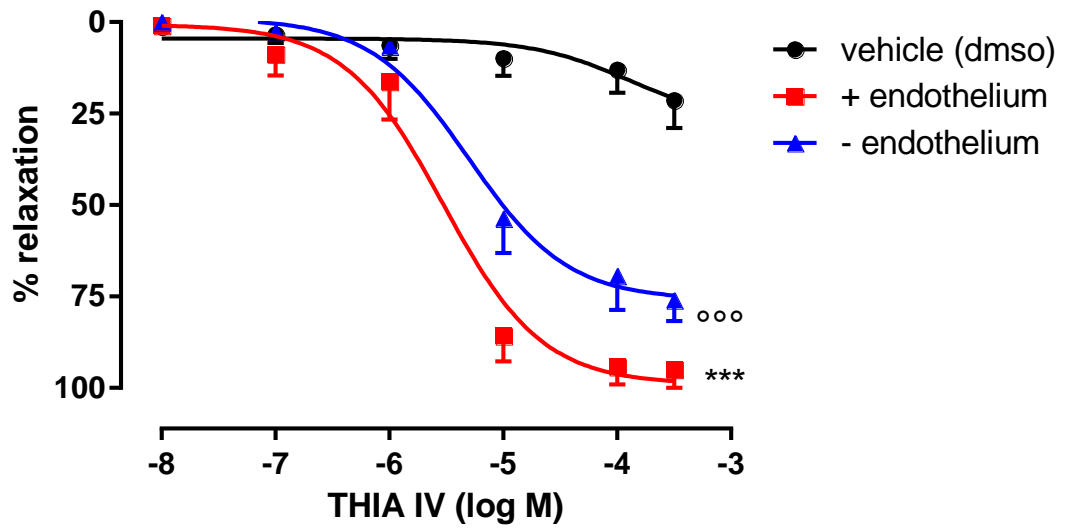


Figure 27 – Effect of **THIA IV** compound on endothelium-denuded and endothelium-intact aortic rings.

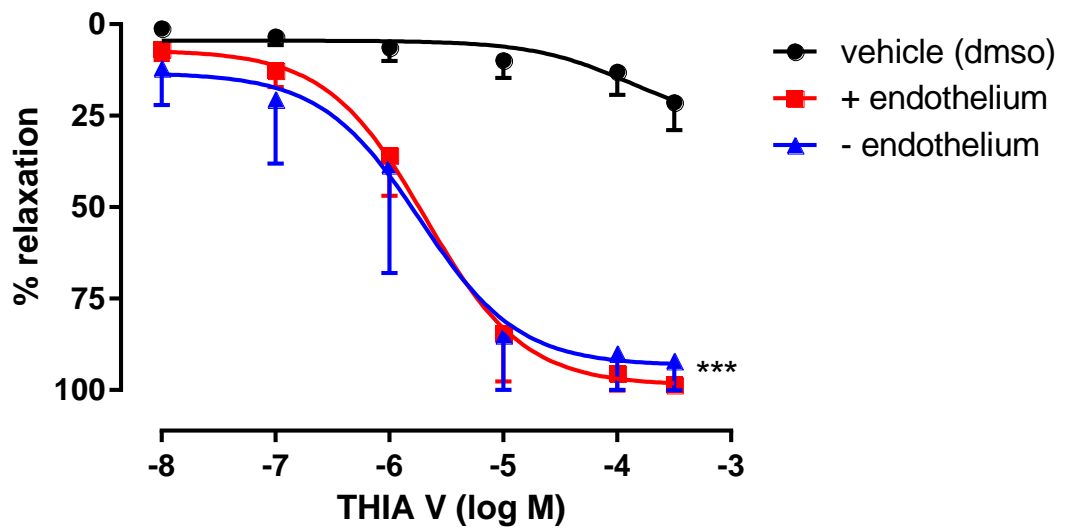


Figure 28 – Effect of **THIA V** compound on endothelium-denuded and endothelium-intact aortic rings.

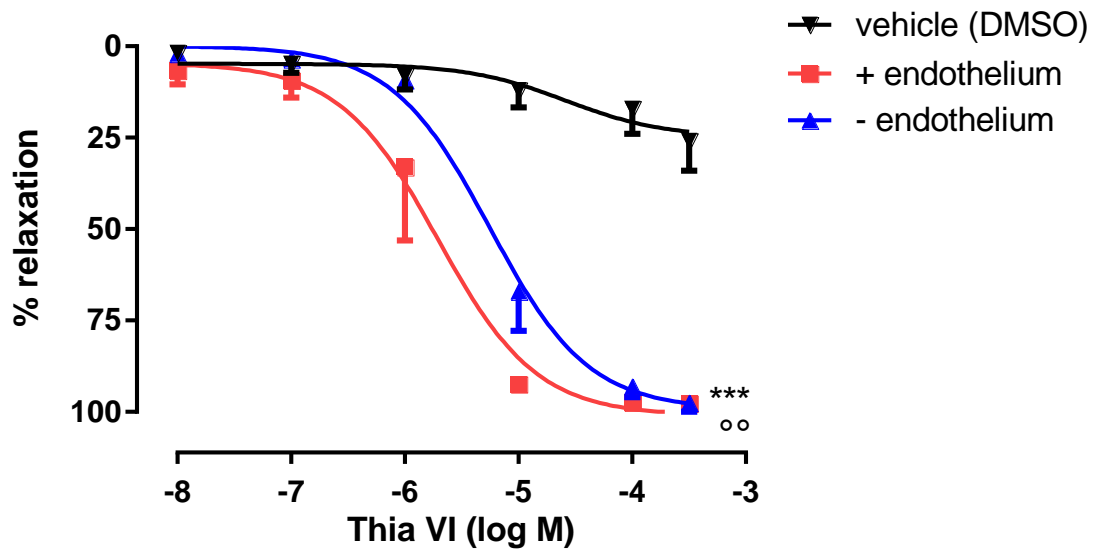


Figure 29 – Effect of THIA VI compound on endothelium-denuded and endothelium-intact aortic rings.

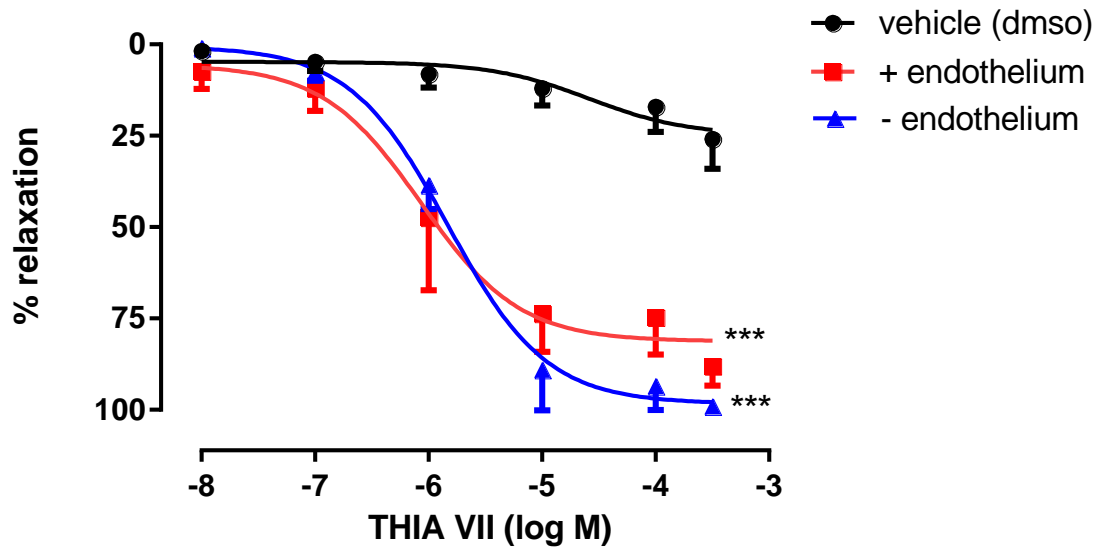


Figure 30 – Effect of THIA VII compound on endothelium-denuded and endothelium-intact aortic rings.

5. NMR-based metabolomics

5.1. Objectives

In order to confirm the promising results obtained in *ex vivo* tissues with the synthesized compound **IIa**, able to completely inhibit L-cysteine-induced vasorelaxation, the effects of the selected compound were further tested on the purified recombinant enzymes.

For this purpose, a metabolomic approach based on nuclear magnetic resonance techniques was used, upon expression, purification and characterization of CBS and CSE enzymes.

5.2. Expression and purification of recombinant CBS and CSE enzymes.

5.2.1. Plasmids, bacterial strains and media

E. coli BL21 (DE3) Codon Plus was used as the host strain to express recombinant human CSE or CBS. CSE cDNA was cloned into pGEX-4T3 and CBS into pGEX-Kg to create N-terminal GSH-S-transferase (GST) fusion proteins. The expression vectors were transformed and plated on LB-agar plates, supplemented with ampicillin ($100 \text{ mg}\cdot\text{mL}^{-1}$).

5.2.2. Bacterial expression of human CBS enzyme

The expression and purification of CBS was performed as described previously with modifications (Huang, 2010).

A colony of the pGEX-Kg/GST-CBS transformed BL21 cells was

inoculated into 100 mL of steam-autoclaved Luria-Bertani (LB) broth supplemented with 100 µg/mL of ampicillin (LB-Amp100), and incubated at 37 °C overnight with vigorous shaking.

A part of starter culture (40 mL) was propagated into 5 L baffled flask, containing 960 mL of LB-Amp100. The mixture was incubated at 37 °C with vigorous shaking until an optical density of 0.3 at 600 nm (OD₆₀₀) was attained, upon which bacterial growth was continued at 30 °C until an OD₆₀₀ of 0.5 was attained.

After the addition of 0.3 mM δ-ALA, IPTG was added at a rate of 0.1 mM to induce the expression of human CBS at 30 °C for 18 h. The cells were harvested by centrifugation in a Beckman Avanti centrifuge J-26XP equipped with a JSP-FIBERLite rotor at 5000 rpm for 40 min at 4 °C. The supernatants were thrown away and the pellets, re-suspended in PBS (140 mM NaCl, 2.7 mM KCl, 10 mM Na₂HPO₄, 1.8 mM KH₂PO₄, pH 7.3), were kept at -20 °C overnight.

5.2.3. Bacterial expression of human CSE enzyme

The expression and purification of CSE was adapted from a previously described (Huang, 2010).

A colony of the pGEX-4T-3/GST-CSE transformed BL21 cells was inoculated into 100 mL of steam-autoclaved Luria-Bertani (LB) broth supplemented with 100 µg/mL of ampicillin (LB-Amp100), and incubated at 37 °C overnight with vigorous shaking.

A part of starter culture (40 mL) was propagated into 5 L baffled flask, containing 960 mL of LB- Amp100. The mixture was incubated at 37 °C with

vigorous shaking until an optical density of 0.3 at 600 nm (OD₆₀₀) was attained,

upon which bacterial growth was continued at 18 °C until an OD₆₀₀ of 0.5 was attained. IPTG was then added at a rate of 0.1 mM to induce the expression of human CSE at 18 °C for 18 h. The cells were harvested by centrifugation in a Beckman Avanti centrifuge J-26XP equipped with a JSP-FIBERLite rotor at 5000 rpm for 40 min at 4 °C.

The supernatants were thrown away and the pellets, re-suspended in PBS (140 mM NaCl, 2.7 mM KCl, 10 mM Na₂HPO₄, 1.8 mM KH₂PO₄, pH 7.3), were kept at -20 °C overnight.

5.2.4. Purification of human enzymes

The bacterial pellets were thawed and re-suspended in lysis buffer containing PBS pH 7.3, 1% Igepal, 5 mM dithiothreitol (DTT), 100 mM PLP, protease inhibitors (Complete EDTA-free tablet), DNase I and Lysozyme. Cell lysis was performed by sonication on ice using the 30% pulsed maximum output of a Brandson Sonifier 250 equipped with a macrotip. The lysates were then cleared by centrifuging at 16000 rpm for 30 min at 4 °C using a Beckman JA20 rotor.

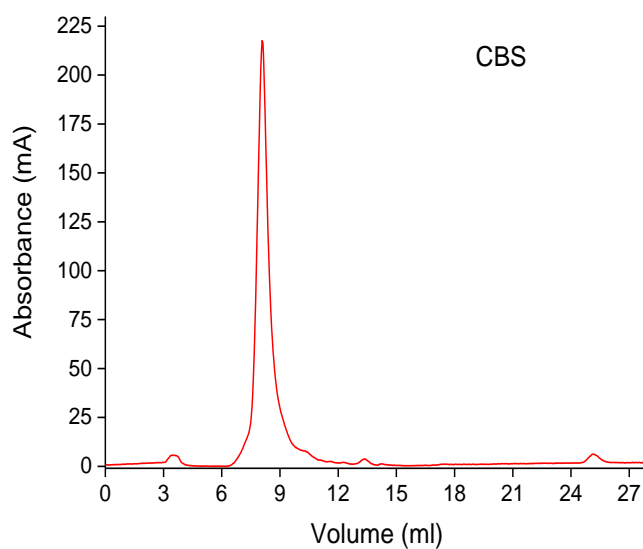
The soluble fractions, containing the GST-CBS and GST-CSE recombinant proteins respectively, were loaded onto a Glutathione sepharose 4B columns previously equilibrated with binding buffer PBS. The columns were sealed and incubated with slight shaking in a cold room (4 °C) for 20 min.

Following that, the flow-throughs were collected, and the beads were washed with five column volumes of binding buffer. Proteins attached to the

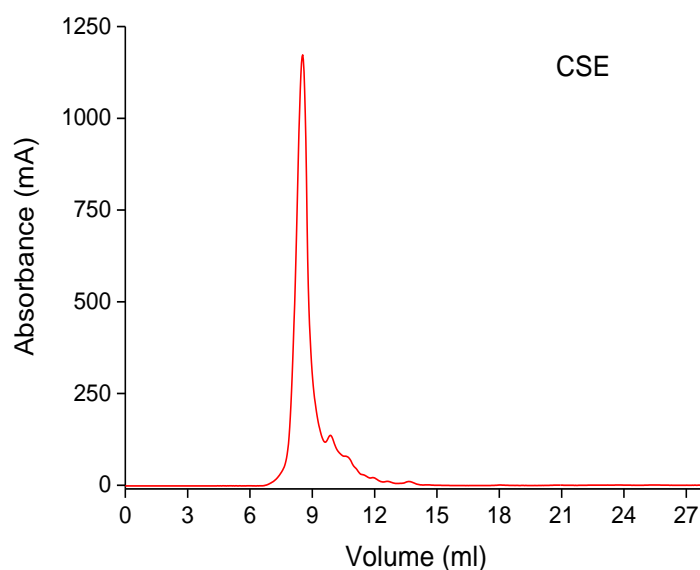
columns were eluted with five column volumes of elution buffer (50 mM Tris–HCl, 10 mM reduced GSH, 5mM DTT, pH 8.0) and then dialyzed and concentrated in 10 mM sodium phosphate buffer pH 8.2 and DTT 1 mM.

This was repeated until minimal protein concentration was detected in the eluates by Bradford assay. The eluates were then pooled together and concentrated using an ultra-centrifugal filter (Millipore Amicon Ultra-4 30000 MWCO) at 4 °C.

The concentrated eluates were subsequently passed through a Superdex-200 column connected to the AKTA purifier FPLC equilibrated with buffer A (10 mM sodium phosphate buffer pH 8.2 and 1 mM DTT) at a flow rate of 1 mL/min (**Figure 31**).



A.



B.

Figure 31 - FPLC chromatography. Gel filtration profile of GST-CBS (A) and GST-CSE (B) proteins.

Fractions containing CBS and CSE respectively were identified by sodium dodecyl sulfate polyacrylamide gel electrophoresis (SDS-PAGE), and then pooled together. Peak fractions corresponding to the target CBS and CSE proteins were pooled together and concentrated to about 5 mg/mL in 10 mM sodium phosphate buffer pH 8.2 and 1 mM DTT using an ultra-centrifugal filter (Millipore Amicon Ultra-4 10000 MWCO) at 4 °C. The proteins were kept at -80 °C for long-term storage.

The purity of the recombinant enzymes was checked by SDS-PAGE on 12% polyacrylamide gels after staining of protein bands with Coomassie dye (**Figure 32**).

GST was not removed from the fusion proteins as it has been previously

reported that the presence of GST does not affect activity. Furthermore, GST did not interfere with the assay, since no H₂S-synthesizing activity was observed in a control activity experiment with GST alone (Huang, 2010).

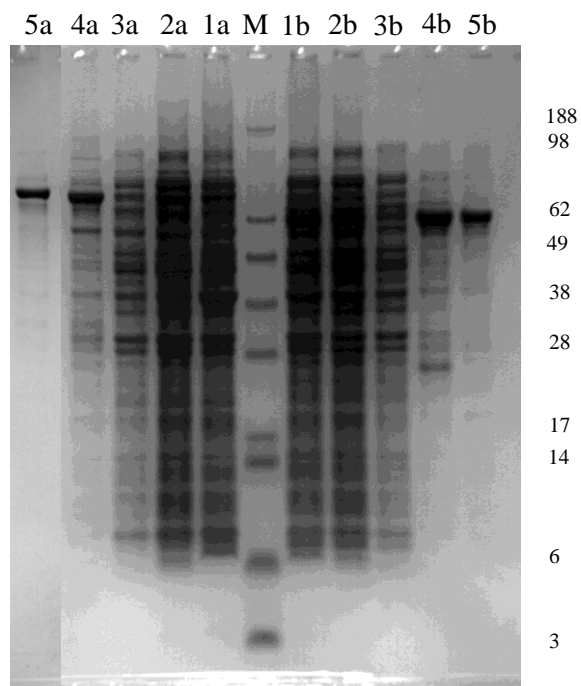


Figure 32 - Representative SDS-PAGE. Fractions after different purification steps of recombinant GST-CBS (**a**) and GST-CSE (**b**) from bacterial cell lysates. Lanes: M, protein marker; 1, cell Lysate before purification; 2. flow through; 3. wash with binding buffer; 4. eluted GST-CBS or GST-CSE; 5. purified proteins after gel filtration.

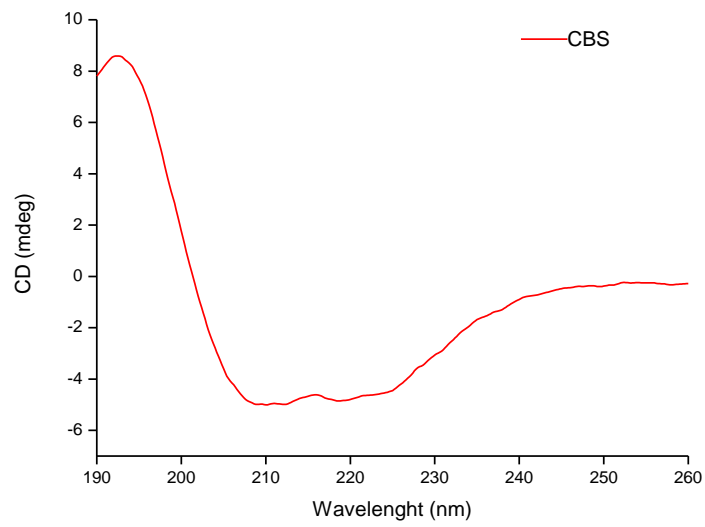
5.3. Structural characterization of recombinant enzymes

5.3.1. Analysis of protein secondary structure via circular dichroism (CD) measurements

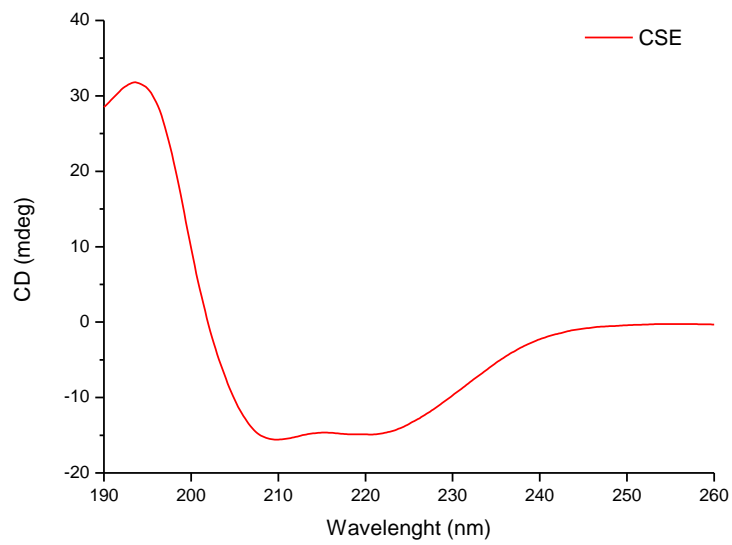
Far-UV CD measurements were performed on a J-715 spectropolarimeter (JASCO, Oklahoma City, OK) equipped with a PTC-348 Peltier temperature control system. The instrument was flushed with nitrogen gas, after which the nitrogen gas flow was maintained at a flow rate of 4 L/min. Samples were prepared using an enzyme concentration of 4 μM in 10 mM sodium phosphate pH 8.2 buffer. The spectra were recorded at different time points using quartz cuvettes (Hellma, Plainview, NY) with path-lengths of 1 mm.

Baseline correction was performed by subtraction of the appropriate buffer spectrum. The recorded CD spectra resulted from averaging five separate wavelength scans on independent protein preparations to ensure reproducibility of the results. The parameters were scanned wavelength from 260 nm to 190 nm, scanning speed 200 nm/min, data pitch 0.2 nm, 2 nm slit width, temperature 37 °C for each protein (**Figure 33**).

CD intensities are presented as the CD absorption coefficient calculated using the molar concentration of the proteins ($\Delta\epsilon_{\text{M}}$). Far-UV CD spectral decomposition to obtain the secondary structure content was achieved with the CONTIN, SELCON, and CDSSTR methods (**Figure 34**).

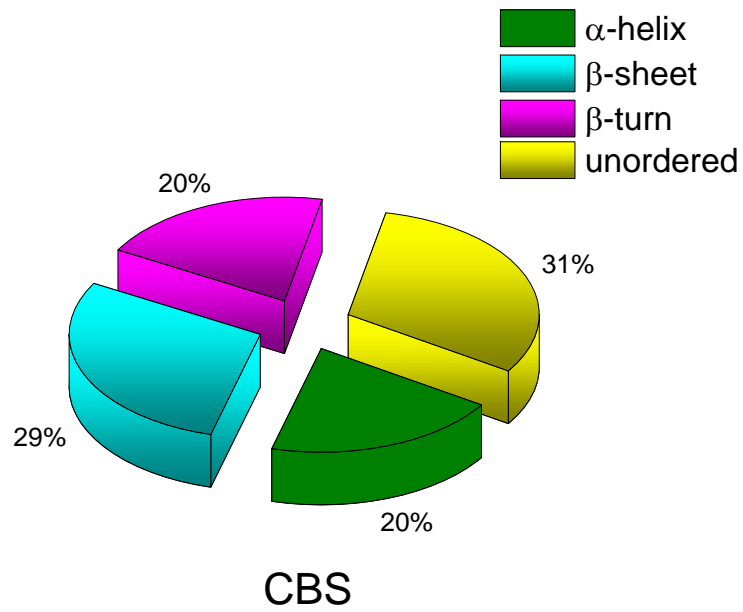


A.

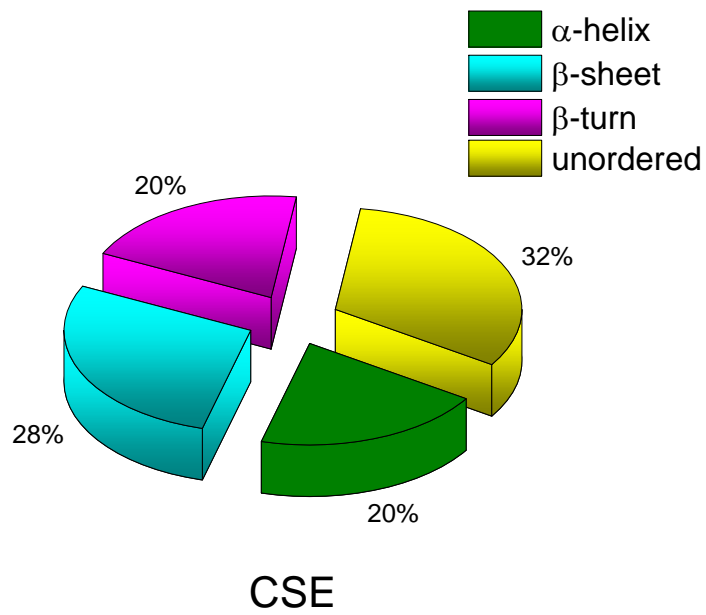


B.

Figure 33 - Circular dichroism. Far-UV CD spectra of GST-CBS (**A**) and GST-CSE (**B**) in 10 mM sodium phosphate pH 8.2



A.



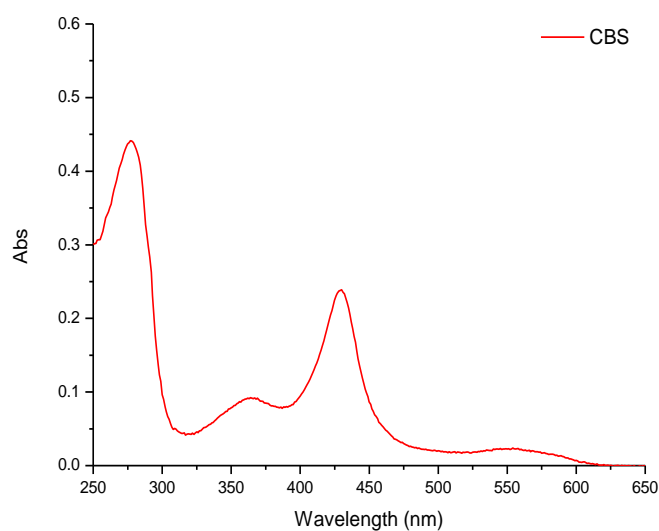
B.

Figure 34 - Circular dichroism, the secondary structure content. Proportion of α -helices, β -sheets, turns and unordered regions of GST-CBS (A) and GST-CSE (B) achieved with the CONTIN, SELCON, and CDSSTR methods.

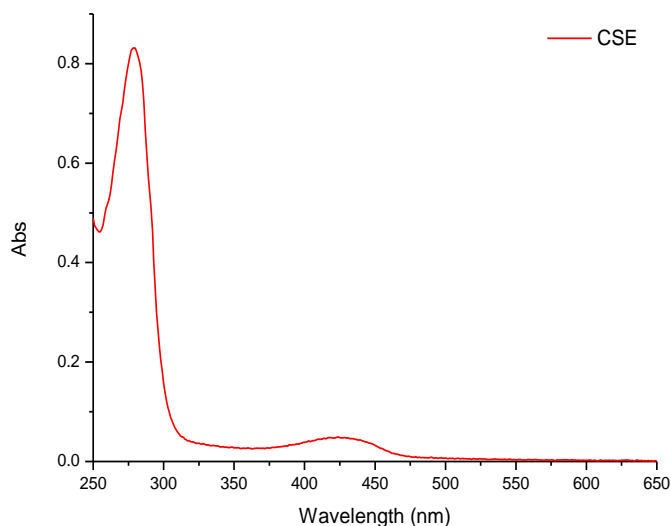
5.3.2. UV-vis Spectroscopy Analysis of recombinant enzymes CBS and CSE

Absorbance spectroscopy was carried out on a Varian Cary 50 Bio UV-Visible Spectrophotometer. The analyzed samples were dissolved in 10 mM sodium phosphate pH 8.2.

Measurements were performed in a 1 cm cuvette cell and monitored spectroscopically from 650nm to 250 nm. The absorption spectrum of human CBS exhibited a peak at 430 nm (**Figure 35A**) suggesting the presence of haem in the recombinant protein. As shown in **Figure 35B**, the purified CSE enzyme displayed the characteristic 427 nm absorbance peak which corresponded to the Schiff-base linkage between PLP and Lys-212.



A.



B.

Figure 35 - Absorption spectroscopy. UV-vis absorption spectra of purified CBS (A) and CSE (B) enzymes in 10 mM phosphate buffer pH = 8.2.

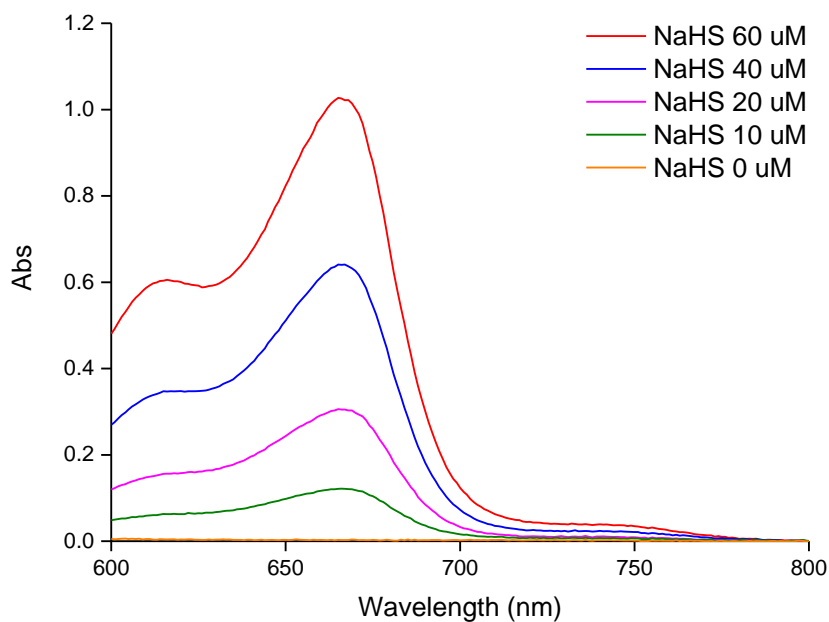
5.3.3. Kinetics of H₂S production from purified recombinant human CBS and CSE

5.3.3.1. Determination of H₂S standard curve

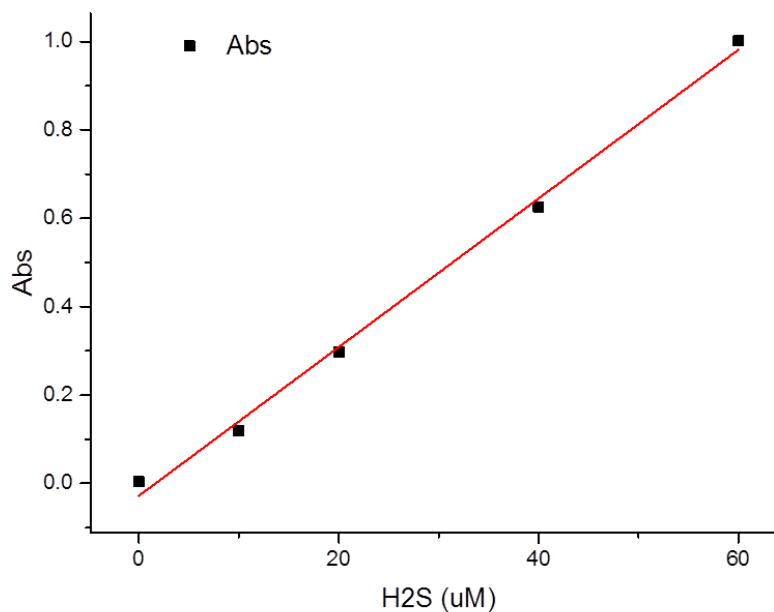
A mixture of 0.85 % w/v ZnAc and 3 % w/v NaOH (100 μ L) was added to various H₂S standards (0-60 μ M, 100 μ L) prepared in 50 mM sodium phosphate pH 8.2 buffer containing 0.5 mM PLP, 20 mM NaCl and 0.1 mM DTT. TCA (10 % w/v, 100 μ L) was added and the tubes were then treated with NNDPD (20 mM, 42.9 μ L) and FeCl₃ (30

mM, 42.9 μ L). After a short spin, 300 μ L of the supernatant was removed for absorbance measurements at 670 nm.

The calibration curve was generated by plotting the average A_{670} value against the amount of H_2S present for each standard (**Figure 36**).



A.



B.

Figure 36 - H₂S standard curve. A. UV-vis spectra of H₂S standards using the methylene blue assay. **B.** Calibration curve of the spectrophotometric detection of hydrogen sulfide.

5.3.3.2. Enzyme activities

In order to verify the catalytic activities of the purified enzymes, hydrogen sulfide production was measured by the methylene blue method. The assay was performed according to Stipanuk and Beck (1982) with some modifications.

Each reaction mixture consisted of 5 µg of the purified enzyme, saline (10 µL), and L-cysteine (27.5 mM, 10 µL), dissolved in 10mM sodium phosphate pH 8.2 buffer to a final volume of 100 µL. For the CBS enzyme, the reaction mixture contained the same as for the CSE plus 27.5 mM homocysteine (10 µL).

The Eppendorf tubes were parafilmed tightly, gently vortexed, and then incubated in a 37 °C water bath. After 60 min of incubation, the evolved H₂S was

trapped via addition of ZnAc (1 % w/v, 100 μ L) and proteins were precipitated via addition of TCA (10 % w/v, 100 μ L).

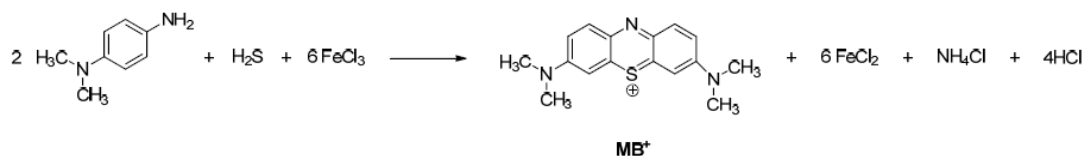
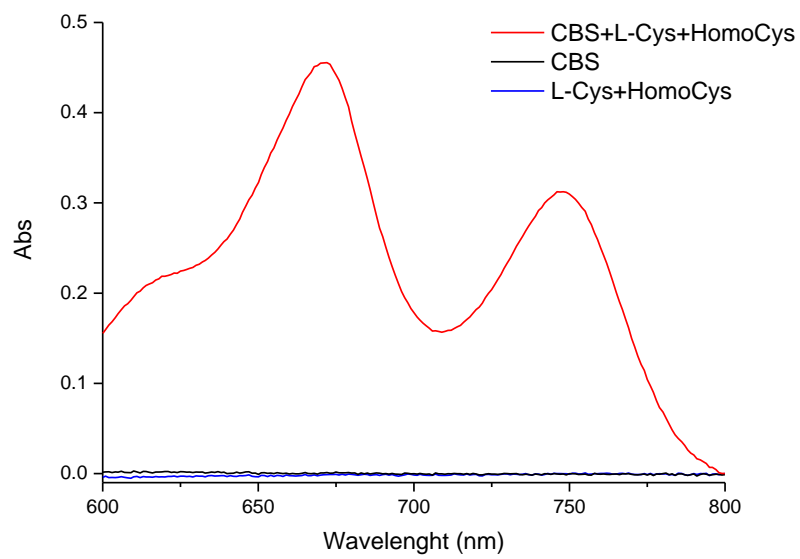


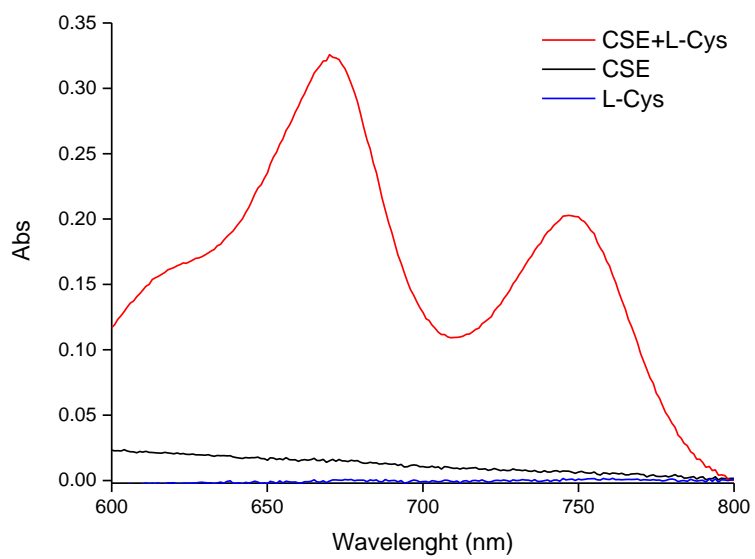
Figure 37 - Reaction of methylene blue assay

Subsequently, N,N-dimethyl-p-phenylenediamine-sulfate in 7.2 M HCl was immediately followed by addition of FeCl₃ in 1.2 M HCl, for development of methylene blue, according to the reaction equation shown above (**Figure 37**).

The amount of H₂S produced was then determined via absorbance measurements of the centrifugal supernatants. The absorbance of the resulting solution was measured at 655 nm (**Figure 38**).



A.



B.

Figure 38 - Spectrophotometric method using methylene blue assay.
 Measurement of H₂S producing CBS (A) and CSE enzymes (B).

5.4. Enzyme Kinetics: NMR spectroscopy

Metabolomics Nuclear Magnetic Resonance technique was used to study the kinetics of two main enzymes involved in trans-sulfuration pathway. Specifically, CBS converts L-cysteine and L-Homocysteine into L-cystathionine (**Figure 39A**) and CSE enzyme utilizes L-cysteine as a substrate in an α,β -elimination reaction to produce H_2S , pyruvate and ammonia (**Figure 39B**). NMR spectra were acquired to follow the disappearance of the L-Cysteine peaks over time, monitoring its conversion in cystathionine or pyruvate, the final products of CBS and CSE enzymes, respectively.

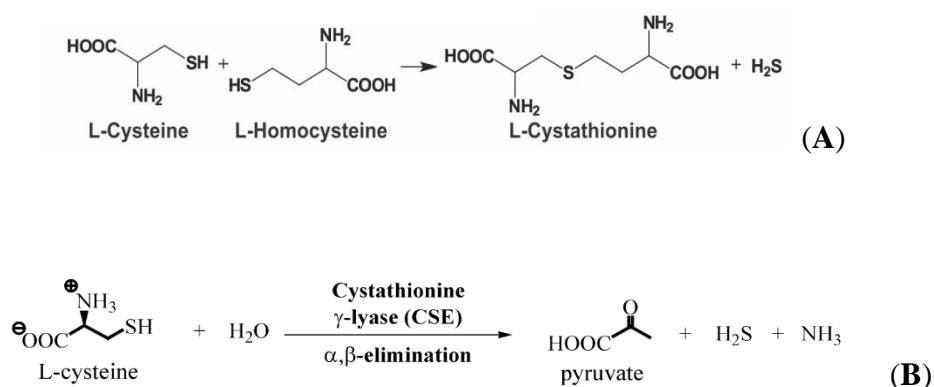


Figure 39- Enzyme kinetics. Reactions catalyzed by cystathionine beta synthase (A) and cystathionine gamma lyase (B).

5.4.1. Sample preparation

All reaction components were prepared in 10 mM sodium phosphate pH 8.2. A standard assay in a 5 mm glass tube was composed of the enzyme substrate, $^{15}\text{N},^{13}\text{C}$ -L-Cysteine (125 μL , 1 mM), L-Homocysteine (125 μL , 1 mM) (added

only for CBS timecourse as co-substrate), DTT (0.5 μL , 1M), D_2O (50 μL), enzyme (100 μL , 110 μM) and filled to a final volume of 500 μL with 10 mM sodium phosphate buffer pH 8.2 in a 5 mm NMR tube. In order to verify the enzyme kinetics in the presence of the potential inhibitor, all components above were put into a different tube, preincubating the selected compound **IIa** (125 μL , 2.5 mM) with each enzyme. Similarly, another sample was prepared using the known CSE inhibitor, D,L-propargylglycine (PGG) (125 μL , 2.5 mM), instead of the compound **IIa**.

5.4.2. NMR measurements

NMR experiments were performed at 300 K on a Bruker AVANCE spectrometer operating at 800 MHz with TCI Cryoprobes. Initially, the isolated enzyme or the enzyme pre-incubated with the tested compounds was excluded from the sample as a control. This blank was used to tune the spectrometer, acquire a lock signal and shim the instrument before the reaction was started by removing the tube from the instrument, adding the enzyme (100 μL , 110 μM), mixing several times by inverting the tube and re-inserting the tube in the instrument. Data acquisition was initiated once a stable lock signal was achieved.

The same set of experiments was carried out in the absence and in the presence of tested compound (compound **IIa** and **PGG**, separately), pre-incubated with each enzyme.

For each sample, pseudo-2D experiments were collected in which the first increment of a ^{13}C HSQC spectrum was acquired with a 5 minutes repetition time for a total of 60 spectra, using ^{15}N , ^{13}C , L-Cysteine and unlabeled L-Homocysteine

as CBS substrate and ^{15}N , ^{13}C , L-Cysteine as a unique substrate for CSE enzyme. Furthermore, 2D ^1H , ^{13}C HSQC spectra were acquired before and after the enzyme reaction was completed.

5.5. Results and Discussion II

Pseudo 2D spectra allowed us to follow ^{15}N , ^{13}C , L-Cysteine conversion into the final products. Two dimensional ^{13}C HSQC spectra were collected before and after each experiment to further confirm the completeness of the reactions.

The time course for CBS production of L-Cystathionine is presented in **Figure 40**. As shown, ^{15}N , ^{13}C , L-Cysteine peaks ($^1\text{H-NMR}$ δ 3.05, C_βH_2 ; 3.90, C_αH) were gradually decreasing until completely disappearance, while the product was growing up. Cystathionine peaks ($^1\text{H-NMR}$ δ 3.97, 3.15, 3.10) were not all detected, because of the unlabeled homocysteine contribution.

With regard to the time course of CSE, **Figure 41** clearly shows that ^{15}N , ^{13}C , L-Cysteine peaks ($^1\text{H-NMR}$ δ 3.05, C_βH_2 ; 3.90, C_αH) decrease in size until completely disappearance, whereas the product pyruvate increase ($^1\text{H-NMR}$ δ 2.4, CH_3).

Another set of experiments was carried out in the presence of compound **II**, pre-incubated with each enzyme. When compound **IIa** was incubated with CBS enzyme, there was no kinetic modification, with the complete conversion of L-Cysteine into L-cystathionine (**Figure 42**). **Figure 48** shows 3D graphics derived from all acquired 1D ^{13}C HSQC spectra over time during CBS time course (**A**) and the kinetics in the presence of compound **IIa** (**B**); comparison of the resulting graphics showed no significant differences.

Conversely, the tested compound was able to inhibit the production of pyruvate catalyzed by CSE (**Figure 43**), proving to be a CSE selective inhibitor, as well as the known CSE inhibitor, D,L-propargylglycine (**PGG**). It is clearly evident in the **Figure 49** representing 3D graphics derived from all acquired 1D ^{13}C HSQC spectra over time during CSE timecourse (**A**) and the kinetics in the presence of compound **IIa** (**B**).

To verify if it is a competitive reaction, at the end of the CSE time course with compound **IIa**, an excess of L-cysteine was added and the experiment was carried out again. As shown in **Figure 50**, the cysteine peaks were not decreased, demonstrating that the enzyme was not able to continue its work anymore and that it was a noncompetitive inhibition.

When **PGG** was used in the enzyme reaction, the pyruvate peak did not increase, as expected. Surprisingly, the L-cysteine peaks decreased and new product peaks, at 3.92, 3.40, 3.25 ppm, different from pyruvate, appeared and progressively increased (**Figure 44**).

Most likely the new peaks represent the cystine. A possible explanation is that the cystine was formed enzymatically and not chemically, because in the reducing environment for the presence of dithiothreitol (DTT), it would not be possible the cysteine oxidation and consequent formation of the disulfide bond, unless enzyme activity.

To further verify the completeness of the reaction, two dimensional ^{13}C HSQC spectra, acquired before and after each time course, were overlapped. **Figure 45** shows the cysteine peaks (blue spectrum acquired before the reaction), appeared at 55 ppm in F1 and 3.90 ppm in F2 (C_αH) and at 25 ppm in F1 and 3.05

ppm in F2 ($C_{\beta}H_2$). These peaks are absent in the ^{13}C HSQC spectrum (red), acquired at the end of the reaction, confirming the completeness of reaction. In **Figure 46** ^{13}C HSQC spectrum acquired after CSE time course with compound **IIa**, was shown. The persistence of cysteine peaks at the end of the reaction confirms that compound **IIa** is a selective CSE inhibitor, by blocking the formation of pyruvate with a different mechanism from **PGG** inhibition. When CSE timecourse with **PGG** is completed, ^{13}C HSQC spectrum (shown in **Figure 47**) was acquired. Pyruvate production was blocked (despite a very small amount was formed, as evidenced by the presence of pyruvate peak); however, cysteine peaks were decreased, converting mainly into cystine (peaks at 55 in F1 and 3.92 ppm in F2; 32 ppm in F1 and 3.4 in F2; 32 ppm in F1 and 3.25 ppm in F2). This suggests that both compounds (**IIa** and **PGG**) inhibit CSE production of pyruvate, by acting through two different mechanisms of inhibition: the compound **IIa** prevents the CSE enzyme from binding to its substrate, inhibiting the conversion of L-cysteine into pyruvate; **PGG** also inhibits the formation of pyruvate, but L-cysteine, not able to bind the active site, becomes substrate for another binding site, giving cystine as different product (**Figure 51 A-C**).

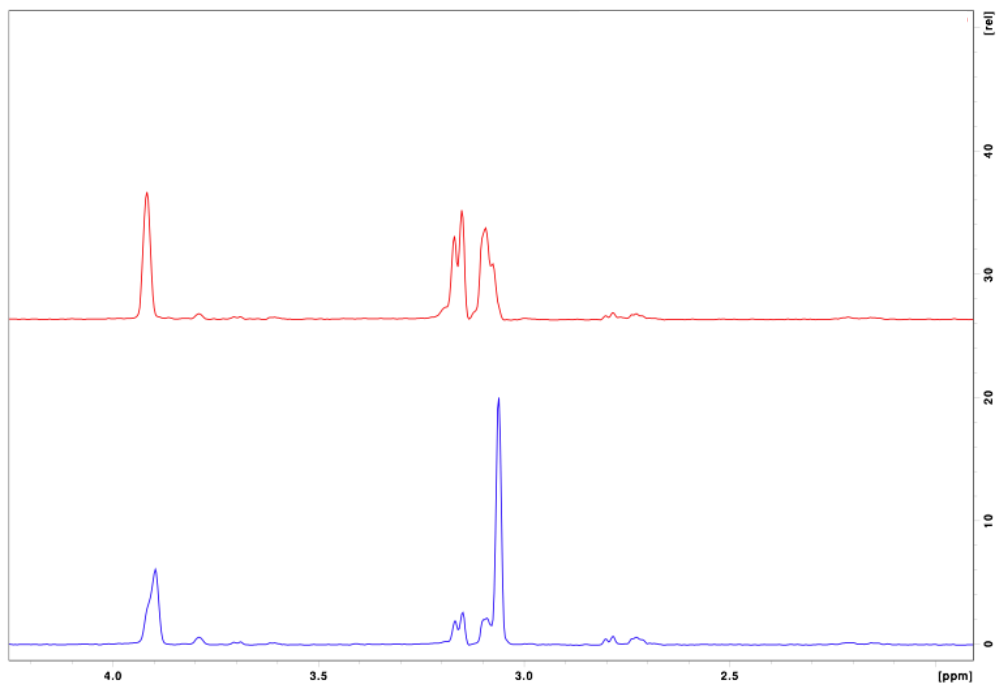


Figure 40 - CBS time course. Real-time monitoring of CBS forward reaction by ^{13}C filtered ^1H NMR. Representative first (blue) and last (red) spectra are shown. Spectra showing CBS conversion of L-cysteine to L-cystathionine. The first spectrum was obtained ~2 min after the addition of enzyme, and subsequently 59 spectra were collected over a 300 min period.

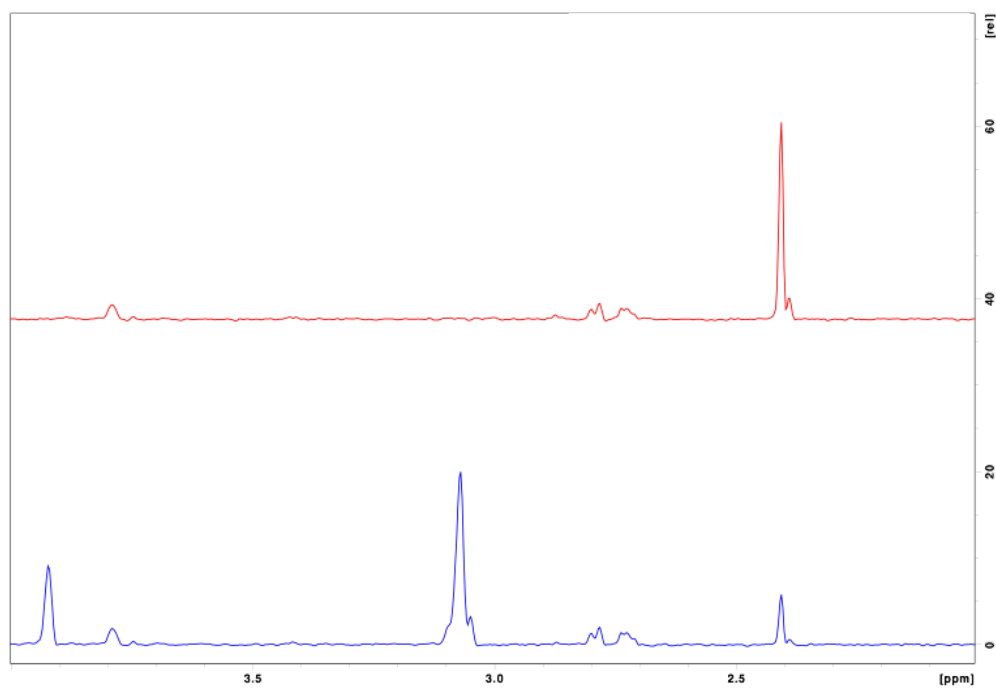


Figure 41 - CSE time course. Real-time monitoring of CSE forward reaction by ^{13}C filtered ^1H NMR. Representative first (blue) and last (red) spectra are shown. Spectra showing CSE conversion of cysteine to pyruvate. The first spectrum was obtained ~2 min after the addition of enzyme, and subsequently 59 spectra were collected over a 300 min period.

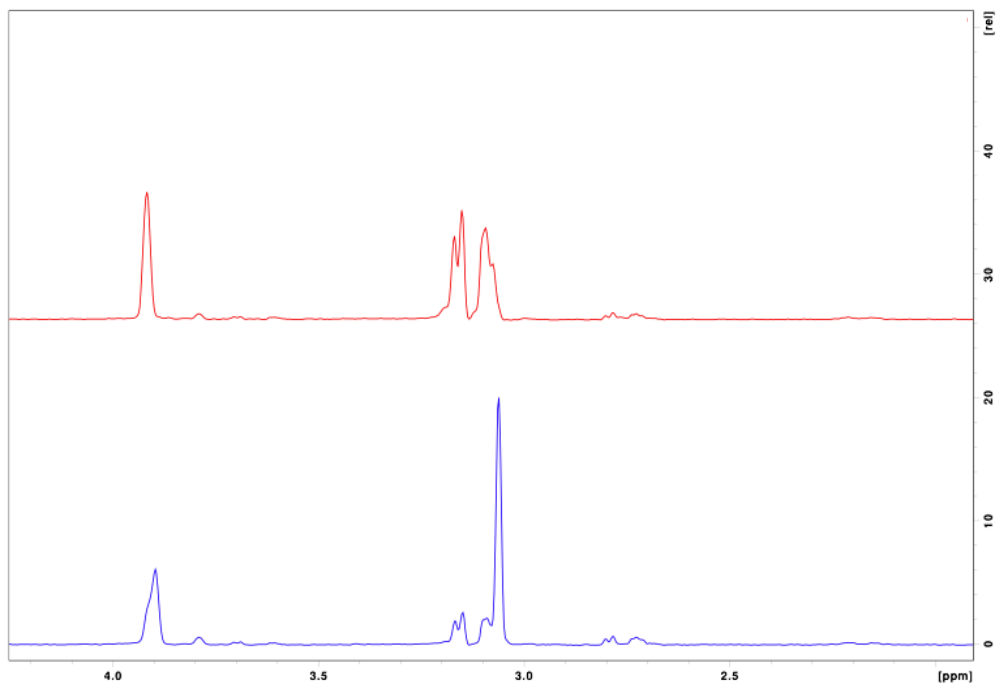


Figure 42 - CBS time course with compound **IIa.** Real-time monitoring of CBS forward reaction by ¹³C filtered ¹H NMR. Representative first (blue) and last (red) spectra are shown. Spectra showing CBS time course in the presence of compound **IIa**. The first spectrum was obtained ~2 min after the addition of enzyme, and subsequently 59 spectra were collected over a 300 min period.

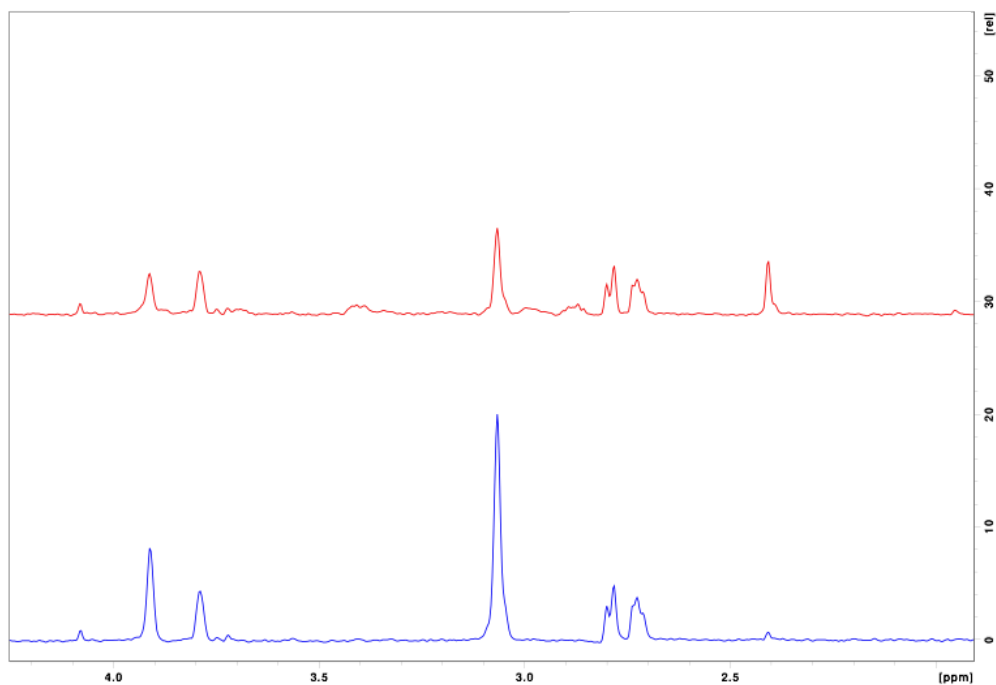


Figure 43 - CSE time course with compound IIa. Real-time monitoring of CBS forward reaction by ^{13}C filtered ^1H NMR. Representative first (blue) and last (red) spectra are shown. Spectra showing CBS time course in the presence of compound **IIa**. The first spectrum was obtained ~2 min after the addition of enzyme, and subsequently 59 spectra were collected over a 300 min period.

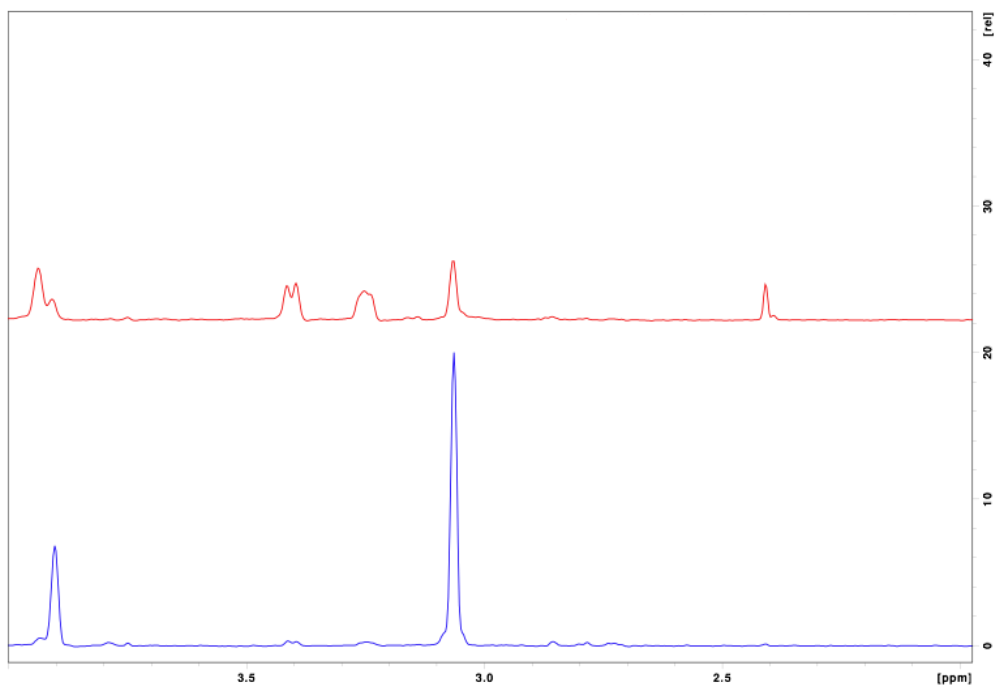


Figure 44 - CSE time course with the inhibitor D,L-propargylglycine. Real-time monitoring of CSE forward reaction by ¹³C filtered ¹H NMR. Representative first (blue) and last (red) spectra are shown. Spectra showing CSE inhibition with D,L-propargylglycine. The first spectrum was obtained ~2 min after the addition of enzyme, and subsequently 59 spectra were collected over a 300 min period.

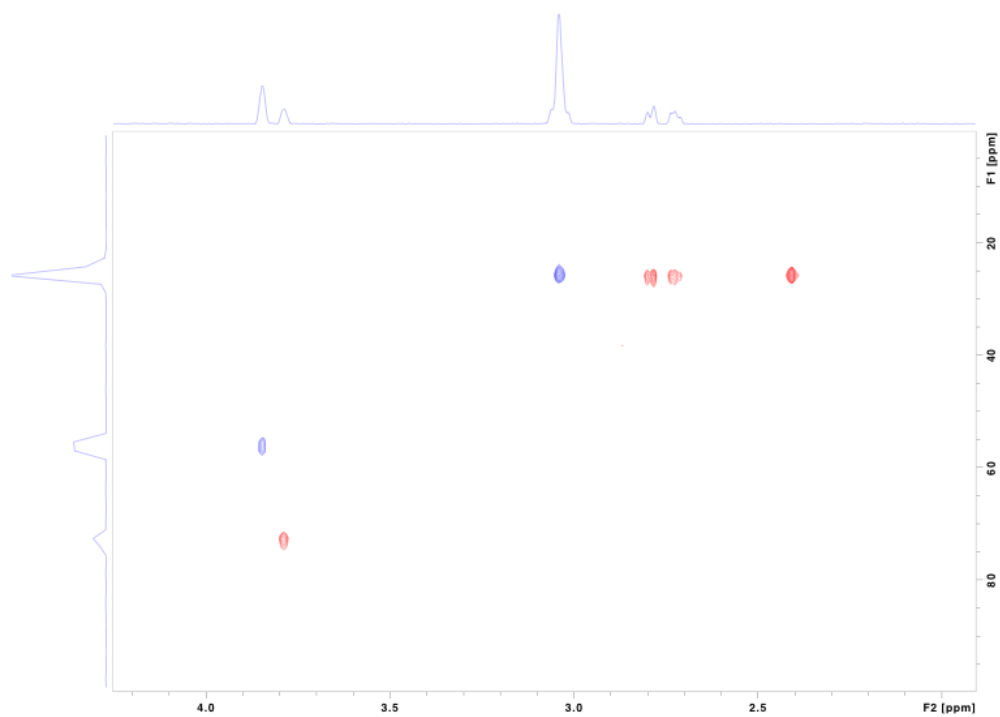


Figure 45 - CSE time course. 2D ¹H, ¹³C-HSQC spectra acquired before (blue peaks) and after (red peaks) the enzyme reaction.

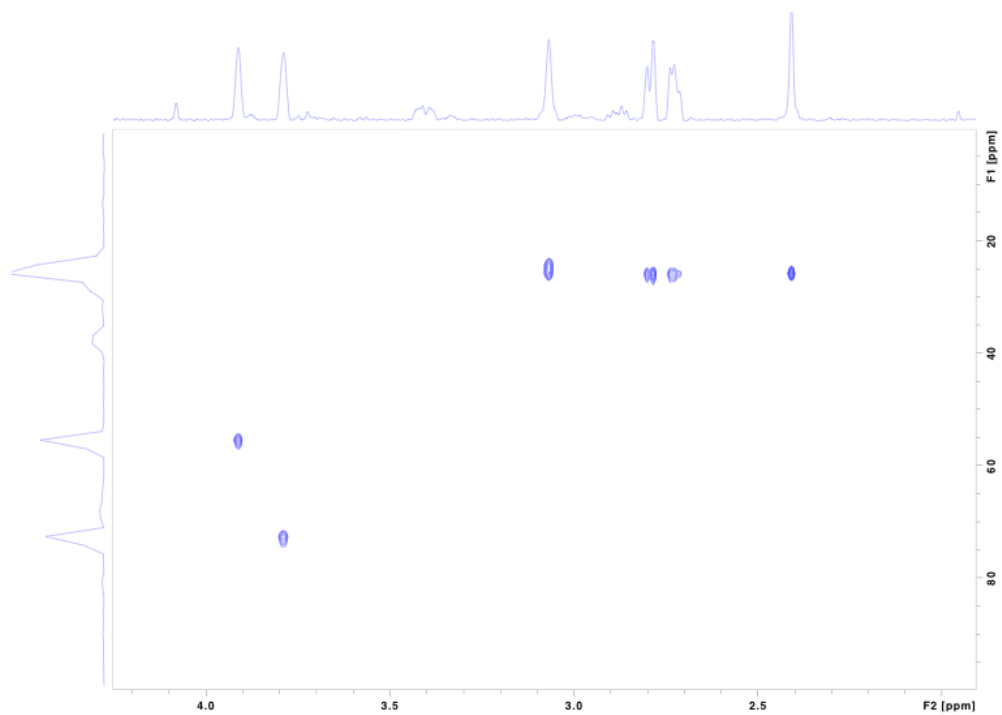


Figure 46 - CSE time course with compound **IIa. 2D ^1H , ^{13}C -HSQC spectrum acquired at the end of the reaction in the presence of compound **IIa**.**

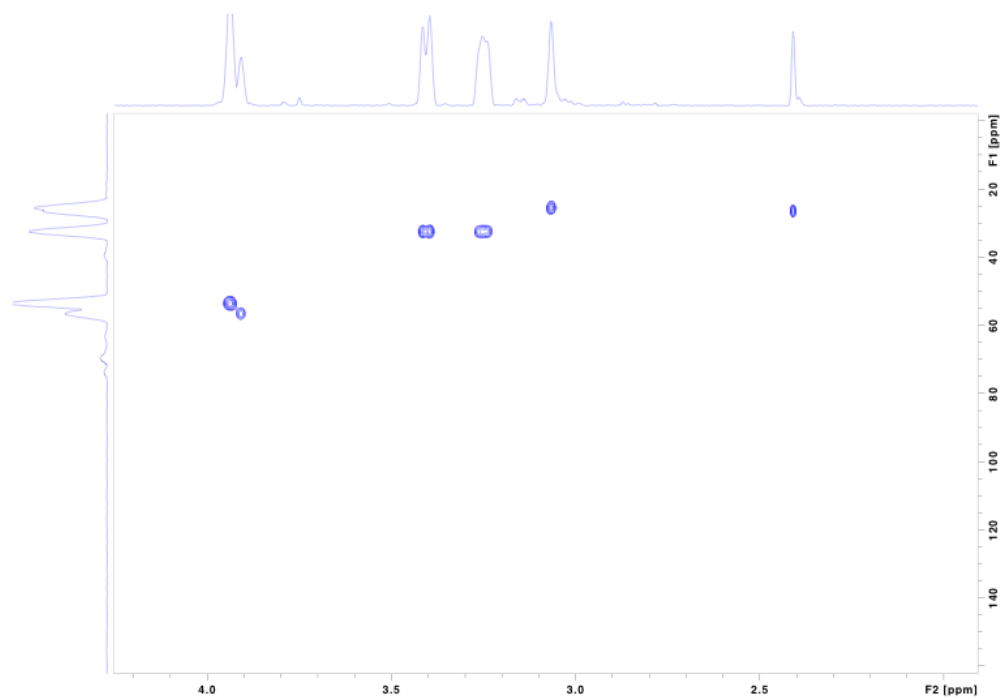
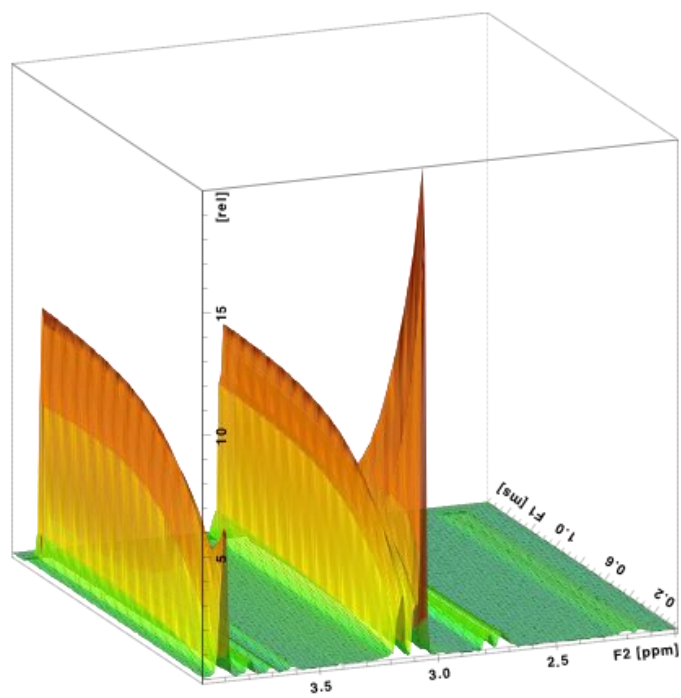
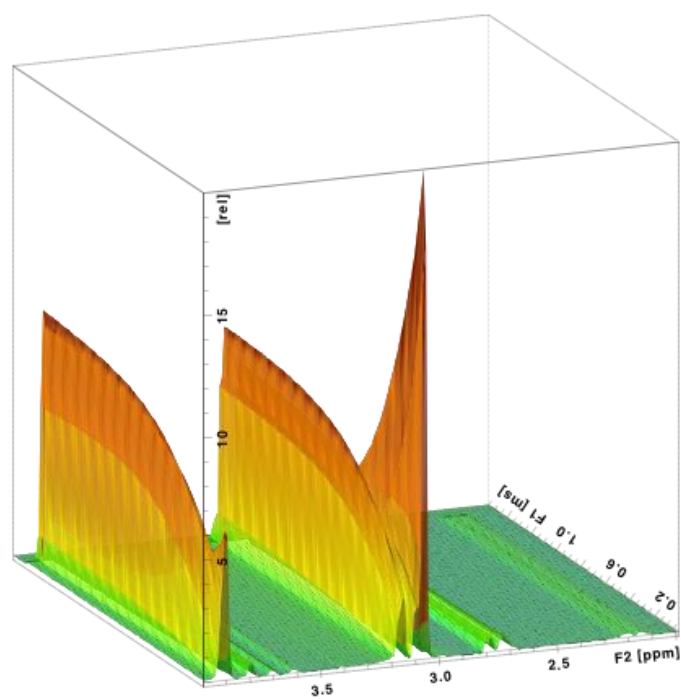


Figure 47 - CSE time course with the inhibitor D,L-propargylglycine. 2D ^1H , ^{13}C -HSQC spectrum acquired at the end of the reaction in the presence of PGG.

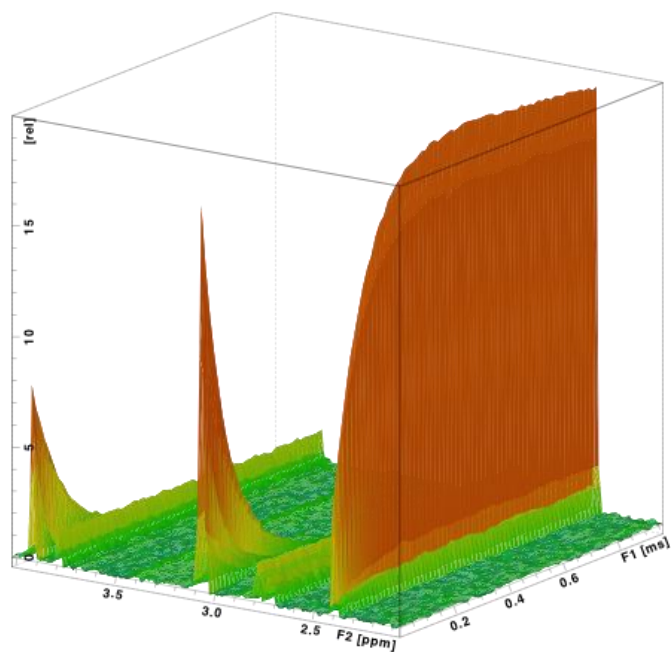


A.

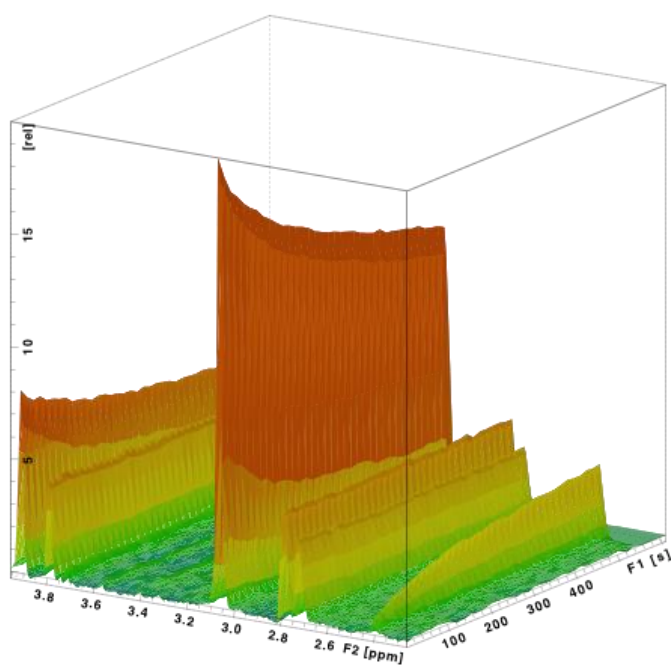


B.

Figure 48 - 3D graphics of CBS time course. A. CBS time course; **B.** CBS time course in the presence of compound **IIa**.

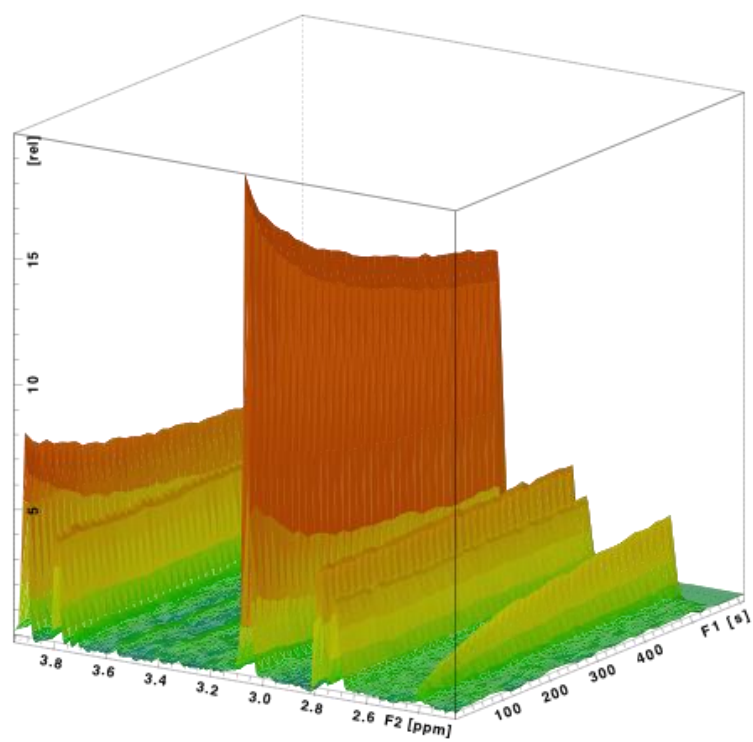


A.

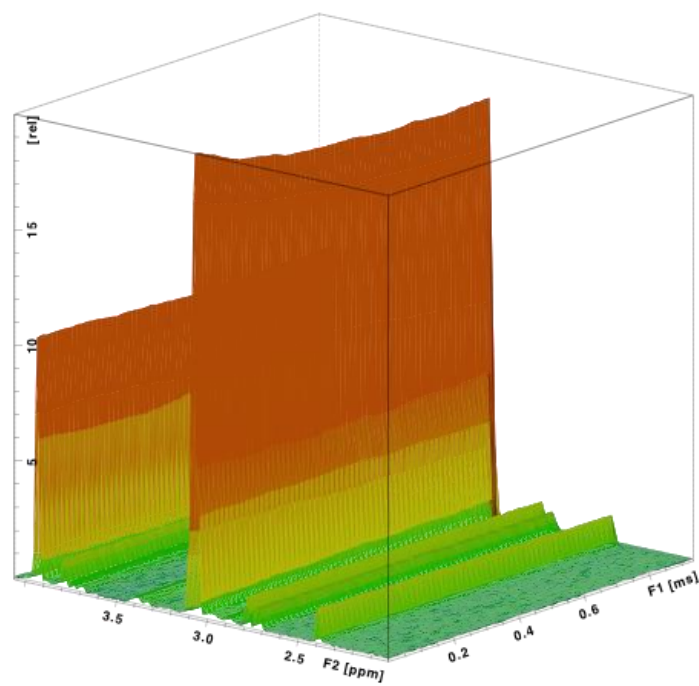


B.

Figure 49 - 3D graphics of CSE time course. A. CSE time course; B. CSE time course in the presence of compound IIa.

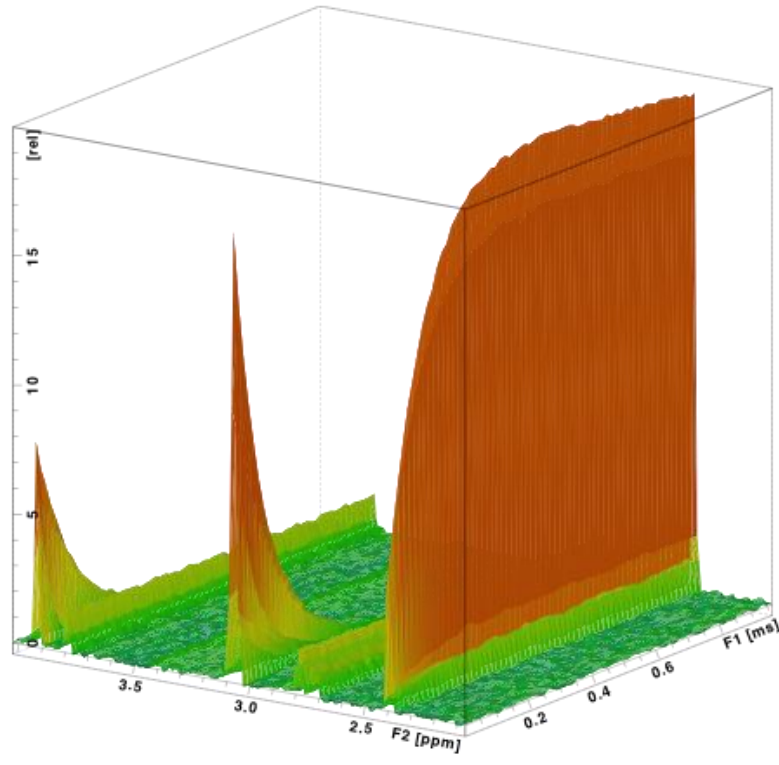


A.

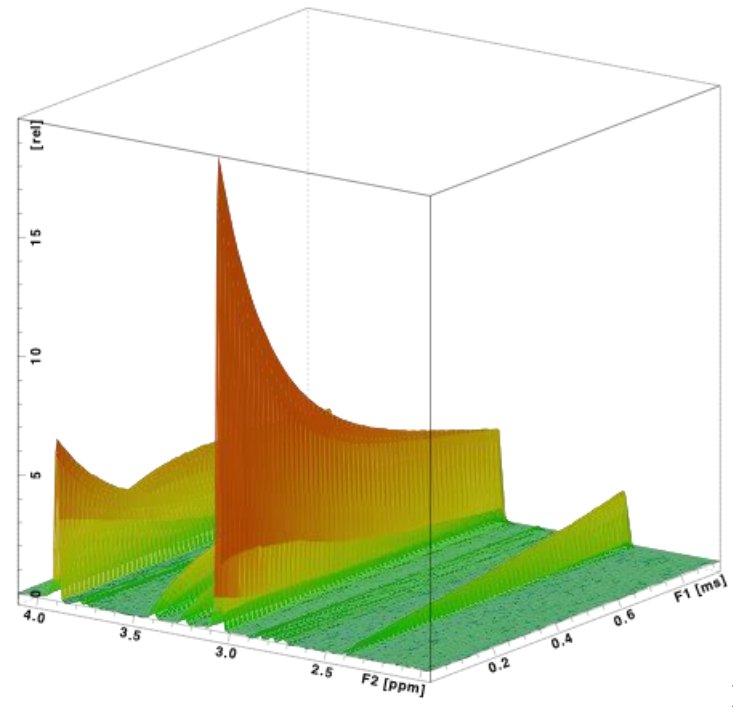


B.

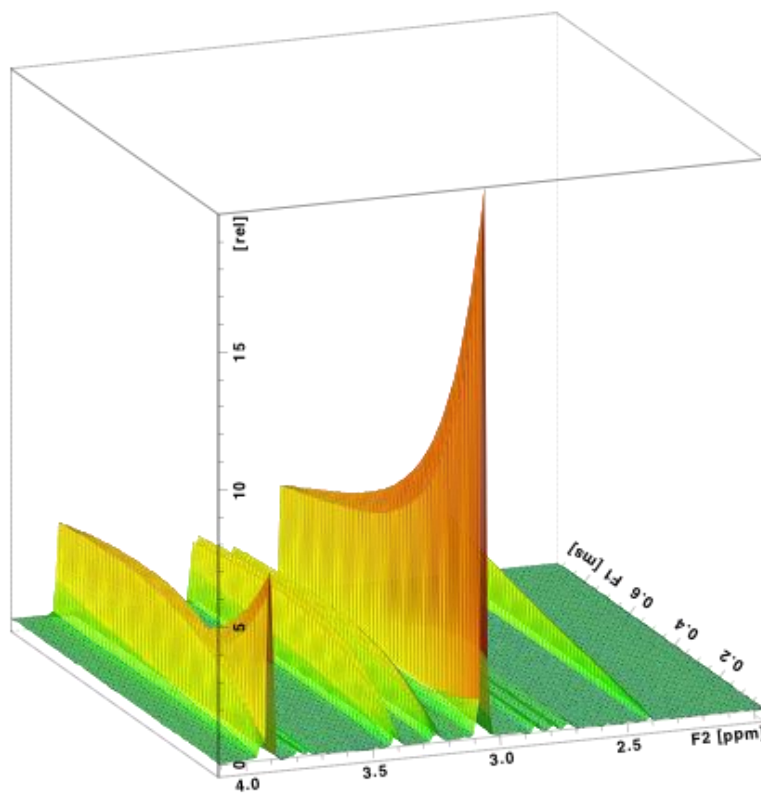
Figure 50 - 3D graphics of CSE time course. A. CSE time course in the presence of compound **IIa**; **B.** CSE time course with L-Cysteine excess.



A.



B.



C.

Figure 51 - 3D graphics of CSE time course. A. CSE time course; **B.** CSE time course in the presence of **PGG**; **C.** Different perspective of CSE time course in the presence of **PGG**.

6. Conclusion

In the last few decades, investigation of the pathophysiological and pharmacological roles of hydrogen sulfide has represented a challenging research field, which is still widely unexplored.

It is noteworthy to highlight that H₂S relevance is constantly growing within scientific environment and it is now accepted as a novel gasotransmitter.

Many researchers are trying to address biological functions of this gaseous mediator but achievements in this field are still lacking of “proof-of-concept”, despite the large body of evidence available in the literature.

Several H₂S donors have been used for basic research and many drug candidates are in development. Among them, there are agents that either directly release H₂S when in solution (NaHS, Na₂S, Lawesson's reagent, GYY4137) or function as a precursor for endogenous H₂S synthesis (N-acetylcysteine, L-cysteine).

Currently, NaHS is the prototypical example of a H₂S-generating agent: it is most widely used H₂S donor for experimental purposes. However, this salt is not suitable for clinical purposes, as the quick release of H₂S may cause adverse effects, such as a rapid and excessive lowering of blood pressure.

Therefore, the design, synthesis and characterization of novel H₂S donors could enormously boost this research field.

In this work, we identified an innovative scaffold for the non-enzymatic release of hydrogen sulphide, acting with a slow release kinetic to emulate which is realized in a physiological context.

Specifically, a small library of 1,2,4 thiazolidine 3,5 diones (**THIA I-VII**, **table 4**) was prepared through suitable synthetic routes and evaluated for their H₂S-releasing properties.

These compounds, exhibiting the kinetic profile of H₂S-releasing agents, may be viewed as both powerful tools for basic studies and new potential pharmacotherapeutic agents for treatment of various diseases.

Another main line of research deals with the synthesis of selective inhibitors. At the present stage the research in this field is impaired by the lack of pharmacological tools such as selective enzymatic inhibitors. In fact, these established inhibitors exhibit low potency, low selectivity and poor cell-membrane permeability.

As such, we aimed to develop more specific and potent inhibitors of CBS and CSE towards H₂S production.

Therefore, in order to develop compounds that selectively regulate enzymatic activity, we preliminarily selected and tested commercially available cysteine surrogates. These molecules were modified with propargyl and *n*-butyl group and the synthetic compounds, obtained in our laboratory, were tested on rat aortic rings.

The compound showing maximal inhibitory effects in this test was an oxothiazolidine derivative, dubbed compound **IIa**. The effects of this compound on the enzyme kinetics was further tested on the purified enzymes using a metabolomic approach based on nuclear magnetic resonance techniques.

These studies clearly showed that compound **IIa** is a potent enzyme inhibitor of CSE, without affecting the CBS kinetics. Comparing its inhibitory

activity with that of the known selective CSE inhibitor, D,L-propargylglycine (**PGG**), a significant difference was revealed: when PGG was used, the enzyme was inhibited from producing pyruvate, ammonia and hydrogen sulphide, but surprisingly, it was still active and gave a new product, using cysteine as substrate. In contrast, the compound **IIa** inhibited the enzyme, keeping the concentration of substrate unaffected.

This finding suggests the possibility of using lower doses of compound **IIa** compared to **PGG**, consequently reducing all possible adverse effects.

The identification of this highly selective CSE inhibitor may help to better define the role of CSE vs CBS in the pathophysiology of the diseases where a role for the H₂S pathway has been proposed.

Furthermore, the development of such agents, particularly water-soluble, will allow us to evaluate the cross-talk of H₂S pathways with other relevant pathways (e.g., NO, COX).

7. Bibliografia

Abe K, Kimura H. *The possible role of hydrogen sulfide as an endogenous neuromodulator*. J. Neurosci 16:1066–1071, 1996.

Alexander FW, Sandmeier E, Mehta PK, Christen P. *Evolutionary relationships among pyridoxal-5'-phosphate-dependent enzymes*. Regio-specific alpha, beta and gamma families, Eur. J. Biochem. 219: 953–960, 1994.

Ali MY, Whiteman M, Low CM, Moore PK, *Hydrogen sulphide reduces insulin secretion from HIT-T15 cells by a K_{ATP} channel-dependent pathway*, J. Endocrinol. 195:105–112, 2007.

Benavides GA, Squadrito GL, Mills RW, Patel HD, Isbell TS, Patel RP, Darley-Usmar VM, Doeller J, Kraus DW. *Hydrogen sulfide mediates the vasoactivity of garlic*. Proc Natl Acad Sci USA 104: 17977–17982, 2007.

Caliendo G, Cirino G, Santagada V and Wallace JL. *Synthesis and Biological Effects of Hydrogen Sulfide (H_2S): Development of H_2S -Releasing Drugs as Pharmaceuticals* J. Med. Chem., 53:6275–6286, 2010.

Chen YH, Wu R, Geng B, Qi YF, Wang PP, Yao WZ, Tang CS. *Endogenous hydrogen sulfide reduces airway inflammation and remodeling in a rat model of asthma*. Cytokine 45: 117–123, 2009.

Cheng Y, Ndisang JF, Tang G, Cao K, Wang R. *Hydrogen sulfide-induced relaxation of resistance mesenteric artery beds of rats*. Am J Physiol Heart Circ Physiol 287:H2316–H2323, 2004.

d'Emmanuele di Villa Bianca R, Sorrentino R, Maffia P, Mirone V, Imbimbo C, Fusco F, De Palma R, Ignarro LJ, Cirino G. *Hydrogen sulfide as a mediator of human corpus cavernosum smooth-muscle relaxation*. Proc Natl Acad Sci USA 106: 4513– 4518, 2009.

DeLano, WL. *The PyMOL Molecular Graphics System*. DeLano Scientific LLC, Palo Alto, CA., 2002.

Fiorucci S, Antonelli E, Distrutti E, Rizzo G, Mencarelli A, Orlandi S, Zanardo R, Renga B, Di Sante M, Morelli A, Cirino G, Wallace JL. *Inhibition of hydrogen sulfide generation contributes to gastric injury caused by anti-inflammatory nonsteroidal drugs*, *Gastroenterology* 129:1210–1224, 2005.

Fu Z, Liu X, Geng B, Fang L, Tang C. *Hydrogen sulfide protects rat lung from ischemia-reperfusion injury*. *Life Sci* 82:1196–1202, 2008.

Hu LF, Wong PT, Moore PK, Bian JS. *Hydrogen sulphide attenuates lipopolysaccharide-induced inflammation by inhibition of p38 mitogen-activated protein kinase in microglia*. *J Neurochem* 100:1121–1128, 2007.

Huang S, Chua JH, Yew WS, Sivaraman J, Moore PK, Tan CH and Deng LW. *Site-Directed Mutagenesis on Human Cystathionine- γ -Lyase Reveals Insights into the Modulation of H₂S Production* *J. Mol. Biol.* 396, 708–718, 2010.

Huang S, Chua JH, Yew WS, Sivaraman J, Moore PK, Tan CH and Deng LW. *Site-directed mutagenesis on human Cystathionine- γ -lyase reveals insights into the modulation of H₂S production*. *J. Mol. Biol.* 396:708–718, 2010.

Jin HF, Liang C, Liang JM, Tang CS, Du JB. *Effects of hydrogen sulphide on vascular inflammation in pulmonary hypertension induced by high pulmonary blood flow: Experiment with rats*. *Zhonghua Yi Xue Za Zhi* 88:2235–2239, 2008.

Kabil O, Banerjee R. *The redox biochemistry of hydrogen sulfide*. *J Biol Chem*; 285:21903–21907, 2010.

Kabil, O, Taoka S, LoBrutto R, Shoemaker R and Banerjee R. *The pyridoxal phosphate binding sites are similar in human heme-dependent and yeast heme-independent cystathionine beta synthases. Evidence from ³¹P NMR and pulsed*

EPR spectroscopy that the heme and the PLP cofactors are not proximal in the human enzyme. J. Biol. Chem. 276:19350–19355, 2001.

Kamoun P. *Endogenous production of hydrogen sulfide in mammals.* Amino Acids 26:243–54, 2004.

Kery V, Poneleit L and Kraus J. *Trypsin cleavage of human cystathionine beta-synthase into an evolutionarily conserved active core: structural and functional consequences.* Arch. Biochem. Biophys 355: 222–232, 1998.

Kimura H, Nagai Y, Umemura K, Kimura Y. *Physiological roles of hydrogen sulfide: Synaptic modulation, neuroprotection, and smooth muscle relaxation.* Antioxid Redox Signal 7:795–803, 2005.

Kimura H. *Hydrogen sulfide induces cyclic AMP and modulates the NMDA receptor.* Biochem Biophys Res Commun 267:129–133, 2000.

Kimura H. *Hydrogen sulfide: its production, release and functions.* Amino Acids 41:113–21, 2011.

Kraus JP, Williamson CL, Firgaira FA, Yang-Feng TL, Münke M, Francke U, Bukovska G and Rosenberg LE. *Cloning and sequencing nanogram amounts of immunopurified mRNA_s: cDNA cloning and chromosomal mapping of cystathionine β -synthase and the β subunit of propionyl CoA carboxylase.* Proc. Natl. Acad. Sci. USA 83: 2047–2051, 1986.

Laggner H, Hermann M, Esterbauer H, Muellner MK, Exner M, Gmeiner BM, Kapiotis S. *The novel gaseous vasorelaxant hydrogen sulphide inhibits angiotensin-converting enzyme activity of endothelial cells.* J. Hypertens 25:2100–2104, 2007.

Lefer DJ. *A new gaseous signaling molecule emerges: Cardioprotective role of hydrogen sulfide.* Proc Natl Acad Sci USA 46:17907–17908, 2007.

Li L, Rose P, Moore PK. *Hydrogen sulfide and cell signaling*, Annu. Rev. Pharmacol. Toxicol. 51:169–187, 2011.

Messerschmidt A, Worbs M, Steegborn C, Wahl MC, Huber R, Laber B and Clausen T. *Determinants of enzymatic specificity in the Cys-Metmetabolism PLP-dependent enzyme family: crystal structure of cystathionine γ -lyase from yeast and intrafamilial structure comparison*. Biol. Chem. 384, 373–386, 2003.

Mikami Y, Shibuya N, Kimura Y, Nagahara N, Ogasawara Y, Kimura H. *Thioredoxin and dihydrolipoic acid are required for 3-mercaptopyruvate sulfurtransferase to produce hydrogen sulfide*. Biochem J 439:479–85, 2011.

Olson KR, Whitfield NL, Bearden SE, St Leger J, Nilson E, Gao Y, et al. *Hypoxic pulmonary vasodilation: a paradigm shift with a hydrogen sulfide mechanism*. Am J Physiol Regul Integr Comp Physiol 298:R51–60, 2010.

Perini R, Fiorucci S, Wallace JL. *Mechanisms of nonsteroidal anti-inflammatory drug-induced gastrointestinal injury and repair: a window of opportunity for cyclooxygenase-inhibiting nitric oxide donors*, Can. J. Gastroenterol 18:229–236, 2004.

Roux PP, Blenis J. *ERK and p38 MAPK-activated protein kinases: A family of protein kinases with diverse biological functions*. Microbiol Mol Biol Rev 68:320–344, 2004.

Roviezzo F, Bertolino A, Sorrentino R, Terlizzi M, Calderone V, Spaziano G, Pinto A, D'Agostino B and Cirino G. *H₂S inhalation prevents mouse airway hyperresponsiveness by regulating mast cells*. Submitted.

Searcy DG, Lee SH. *Sulfur reduction by human erythrocytes*. J Exp Zool 282: 310–322, 1998.

Singh S, Padovani D, Leslie RA, Chiku T, Banerjee R. *Relative contributions of cystathionine beta-synthase and gamma-cystathionase to H₂S biogenesis via alternative trans-sulfuration reactions.* J Biol Chem 284:22457–66, 2009.

Sivarajah A, Collino M, Yasin M, Benetti E, Gallicchio M, Mazzon E, Cuzzocrea S, Fantozzi R, Thiernemann C. *Anti-apoptotic and anti-inflammatory effects of hydrogen sulfide in a rat model of regional myocardial I/R,* Shock 31:267–274, 2009.

Stipanuk MH, Beck PW. *Characterization of the enzymic capacity for cysteine desulphhydration in liver and kidney of the rat.* Biochem J 206: 267–277, 1982.

Stipanuk MH. *Sulfur amino acid metabolism: pathways for production and removal of homocysteine and cysteine.* Annu Rev Nutr;24:539–77, 2004.

Sun Q, Collins R, Huang, S, Holmberg-Schiavone, L, Anand, GS, Tan, CH et al. *Structural basis for the inhibition mechanism of human cystathionine-gamma-lyase: an enzyme responsible for the production of H₂S.* J. Biol. Chem. 284, 3076–3085, 2009.

Szabo C. *Hydrogen sulfide and its therapeutic potential.* Nat. Rev. Drug Discovery, 917–935, 2007.

Szabo C. *Hydrogen sulphide and its therapeutic potential.* Nat Rev Drug Discov 6: 917–935, 2007.

Tan BH, Wong PT-H, Bian JS. *Hydrogen sulphide: A novel signalling molecule in the central nervous system.* Neurochem Int;56:3–10, 2010.

Taoka S, Widjaja L and Banerjee R. *Assignment of enzymatic functions to specific regions of the PLP-dependent heme protein cystathionine β-synthase,* Biochemistry 38:13155–13161, 1999.

Wallace JL, Caliendo G, Santagada V, Cirino G, Fiorucci S. *Gastrointestinal safety and anti-inflammatory effects of a hydrogen sulfide-releasing diclofenac derivative in the rat*. *Gastroenterology* 132:261–271, 2007.

Wang R. *Two's company, three's a crowd: Can H₂S be the third endogenous gaseous transmitter?* *FASEB J.*, 16, 1792–1798, 2002.

Wei HL, Zhang CY, Jin HF, Tang CS, Du JB. *Hydrogen sulphide regulates lung tissue oxidized glutathione and total antioxidant capacity in hypoxic pulmonary hypertensive rats*. *Acta Pharmacol Sin* 29:670–676, 2008.

Whiteman M, Le Trionnaire S, Chopra M, Fox B, Whatmore J. *Emerging role of hydrogen sulfide in health and disease: critical appraisal of biomarkers and pharmacological tools*. *Clin Sci (Lond)* 121: 459–488, 2011.

Yamagata S, Yasugahira T, Okuda Y and Iwama T. *Conversion of the aminocrotonate intermediate limits the rate of γ -elimination reaction catalyzed by L-cystathionine γ -lyase of the yeast *Saccharomyces cerevisiae**. *J. Biochem.* 134, 607–613, 2003.

Yang G, Wu L, Jiang B, Yang W, Qi J, Cao K, Meng Q, Mustafa AK, Mu W, Zhang S, Snyder SH, Wang R. *H₂S as a physiologic vasorelaxant: Hypertension in mice with deletion of cystathionin gamma-lyase*. *Science* 322:587–590, 2008.

Yonezawa D, Sekiguchi F, Miyamoto M, Taniguchi E, Honjo M, Masuko T, Nishikawa H, Kawabata A. *A protective role of hydrogen sulfide against oxidative stress in rat gastric mucosal epithelium*. *Toxicology* 241:11–18, 2007.

Zanardo RC, Brancaleone V, Distrutti E, Fiorucci S, Cirino G, Wallace JL. *Hydrogen sulfide is an endogenous modulator of leukocyte-mediated inflammation*. *FASEB J.* 20:2118–2120, 2006.

Zhang C, Du J, Bu D, Yan H, Tang X, Tang C. *The regulatory effect of hydrogen sulphide on hypoxic pulmonary hypertension in rats*. *Biochem Biophys Res Commun* 302:810–816, 2003.